Induced Superconductivity in Microstructures

PROEFSCHRIFT

ter verkrijging van de graad van Doctor
aan de Rijksuniversiteit te Leiden, op gezag
van de Rector Magnificus Dr. W. A. Wagenaar,
hoogleraar in de faculteit der Sociale Wetenschappen,
volgens besluit van het College van Dekanen
te verdedigen op woensdag 18 juni 1997
te klokke 16.15 uur

door

Joost Adrianus Melsen

geboren te Ossendrecht op 19 januari 1970

Promotiecommissie:

Promotor:	Prof. dr. C. W. J. Beenakker
Referent:	Prof. dr. ir. W. van Saarloos
Overige leden:	Prof. dr. K.-A. Chao (Lunds Universitet, Zweden)
	Prof. dr. L. J. de Jongh
	Prof. dr. J. M. J. van Leeuwen
	Dr. J. Zaanen

Het onderzoek beschreven in dit proefschrift is uitgevoerd als onderdeel van het wetenschappelijke programma van de Nederlandse Organisatie voor Wetenschappelijk Onderzoek (NWO) en de Stichting voor Fundamenteel Onderzoek der Materie (FOM).

The research described in this thesis has been carried out as part of the scientific program of the Netherlands Organization for Scientific Research (NWO) and the Foundation for Fundamental Research on Matter (FOM).

About the cover:
This thesis discusses the anomalous reflection which occurs at the interface between a normal metal and a superconductor. The cover shows a different type of anomalous reflection in the painting *La reproduction interdite* by René Magritte,

Aan mijn ouders

Contents

1 Introduction **7**
1.1 Quantum transport in disordered wires 7
1.1.1 Scattering matrix 8
1.1.2 DMPK equation 9
1.2 Mesoscopic superconductivity 11
1.2.1 Excitation spectrum 11
1.2.2 Andreev reflection 12
1.2.3 Conductance of a normal-metal–superconductor junction . . 13
1.2.4 Induced superconductivity 14
1.2.5 Josephson effect 15
1.3 Quantum chaos 16
1.3.1 Closed systems 16
1.3.2 Open systems 17
1.4 Electrostatic charging effects 18
1.5 This thesis 19

2 Quantum transport through disordered wires with obstacles **27**
2.1 Conductance fluctuations, weak localization, and shot noise for a ballistic constriction in a disordered wire 27
2.1.1 Introduction 27
2.1.2 Mapping of constricted unto unconstricted geometry 29
2.1.3 Many-channel point contact 31
2.1.4 Single-channel point contact 36
2.1.5 Numerical simulations 38
2.2 Conductance fluctuations in a disordered double-barrier junction . 40
2.2.1 Double-barrier junction with strong mode-mixing 43
2.2.2 Effects of strong disorder 46
2.2.3 Numerical simulations 47
Appendix A: Isotropically distributed transfer matrices commute 48
Appendix B: Dyson-Mehta formula for the circular ensemble 49
Appendix C: Moment expansion of the DMPK equation 50

3 Reflectionless tunneling through a double-barrier NS junction **55**
3.1 Introduction 55
3.2 NINIS junction without disorder 56
3.3 Effects of disorder 58
3.4 Conclusions 65

4 Giant backscattering peak in angle-resolved Andreev reflection 69
4.1 Enhanced backscattering 69
4.2 Large magnetoresistance in a point contact 72
4.3 Excess conductance in a Josephson junction 73

5 Induced superconductivity distinguishes chaotic from integrable billiards 79
5.1 Chaotic billiards 80
5.2 Integrable billiards 84
5.3 Partially broken time-reversal symmetry 86
5.4 Conclusion 88

6 Coulomb blockade threshold in inhomogeneous one-dimensional arrays of tunnel junctions 91
6.1 Introduction 91
6.2 Free energy 92
6.3 Threshold voltage 94
6.3.1 No gate coupling 94
6.3.2 Turnstile configuration 95
6.4 Background charge 96

List of publications 107

1 Introduction

Mesoscopic physics is a field within solid-state physics which deals with systems at the borderline between the microscopic and macroscopic world [1–3]. This field started to prosper due to the demand for miniaturized electronic components. The size of integrated circuits has greatly diminished in recent years, and will continue to diminish down to length scales on which quantum-mechanical effects influence the operation of the circuit.

On the (sub-)micrometer scale, the wave nature of the electrons introduces significant corrections to the classical conductivity. Quantum-mechanical interference effects can be experimentally observed in transport experiments on metals small compared to the phase-breaking length. Due to the random impurity potential, one is committed to a statistical description of ensembles of samples. In an experiment, such an ensemble can be realized by varying the external parameters of a single sample, such as magnetic field or gate voltage. (This statement is known as the hypothesis of ergodicity.) A striking example of interference effects are the conductance fluctuations of universal magnitude e^2/h, which have been observed in mesoscopic samples as a function of both magnetic field and gate voltage.

Interference effects are greatly enhanced if the metal is brought into contact with a superconductor. Instead of being a small correction of order e^2/h, quantum interference may change the conductance by an order of magnitude. Mesoscopic superconductivity is a new development within mesoscopic physics, and it is the subject of this thesis.

1.1 Quantum transport in disordered wires

According to Ohm's law, the resistance of a wire increases linearly with its length. This macroscopic law is no longer valid if the length is comparable to or smaller than the phase-breaking length L_ϕ. In that case, phase coherence may be preserved over the whole sample, and interference effects modify the resistance. The phase-breaking length decreases with increasing temperature, so that these interference effects can only be observed at low temperatures (typically below 1 K) and in small structures (typically sub-micron dimensions). In this subsection, we introduce the quantum transport theory which we will use to describe such "mesoscopic" structures.

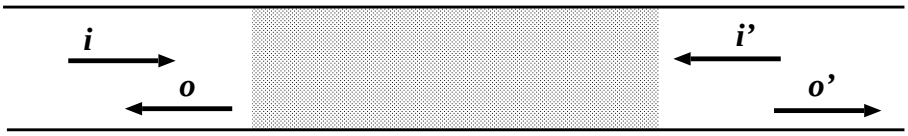

Figure 1-1. The scattering matrix couples incident modes to outgoing modes.

1.1.1 Scattering matrix

The conduction of electrons through a wire can be compared with the propagation of waves in a waveguide. At a given energy E, the confinement in the transverse direction allows for only a discrete set of longitudinal wave vectors, called modes. A propagating mode has a real wave vector. There is a finite number N of propagating modes. For example, in a two-dimensional wire of width W, the propagating modes along the x-axis have wave functions

$$\psi_n^{\pm} = k_n^{-1/2} \sin(n\pi y/W) e^{\pm i k_n x}, \quad n = 1, 2, \ldots, N, \tag{1.1.1}$$

$$k_n = \sqrt{2mE/\hbar^2 - n^2\pi^2/W^2}. \tag{1.1.2}$$

The wave function has been normalized by $1/\sqrt{k_n}$ so that all ψ_n's carry the same current.

The wave function (1.1.1) is valid for a perfectly conducting wire. We want to describe the conduction properties of a disordered wire, containing an impurity potential. We do so by means of the scattering approach pioneered by Landauer [4]. We assume that the disordered wire is coupled to electron reservoirs by two perfectly conducting wires (ideal leads). The propagating modes incident on the disordered region have amplitudes i and i' in the left and right lead (see Figure 1-1). Together, i and i' form a vector of length $2N$. The $2N \times 2N$ scattering matrix S relates the probability amplitudes o and o' of the outgoing modes in the left and right lead to i and i':

$$\begin{pmatrix} o \\ o' \end{pmatrix} = S \begin{pmatrix} i \\ i' \end{pmatrix}, \quad S \equiv \begin{pmatrix} r & t' \\ t & r' \end{pmatrix}. \tag{1.1.3}$$

The scattering matrix consists of four $N \times N$ block matrices which contain the reflection amplitudes r and r' (reflection from left to left and from right to right) and the transmission amplitudes t and t' (transmission from left to right and from right to left). The scattering matrix is unitary ($SS^\dagger = 1$), because of current conservation. The conductance is determined by the Landauer formula,

$$G = G_0 \,\mathrm{Tr}\, tt^\dagger = G_0 \sum_{n=1}^{N} T_n, \quad G_0 = 2e^2/h. \tag{1.1.4}$$

The eigenvalues T_n of $tt^\dagger$ are real numbers between 0 and 1.

1.1.2 DMPK equation

Our interest lies in the statistical properties of the conductance: What is the average conductance and how large is its variance? To that end, we need the distribution function of scattering matrices. This distribution has been determined using methods of random-matrix theory [5,6].

In a wire geometry (length L much greater than width W), the distribution of scattering matrices is isotropic, which means that it depends only on the transmission eigenvalues $T_n (n = 1, 2, \ldots, N)$. The polar decomposition then provides a useful parameterization of the scattering matrix,

$$S = \begin{pmatrix} U & 0 \\ 0 & V \end{pmatrix} \begin{pmatrix} -i\sqrt{1-\mathbf{T}} & \sqrt{\mathbf{T}} \\ \sqrt{\mathbf{T}} & -i\sqrt{1-\mathbf{T}} \end{pmatrix} \begin{pmatrix} U' & 0 \\ 0 & V' \end{pmatrix}, \tag{1.1.5}$$

where $\mathbf{T} = \mathrm{diag}(T_1, T_2, \ldots, T_N)$. The $N \times N$ unitary matrices U, U', V, V' are uniformly distributed in the unitary group. In the presence of time-reversal symmetry (in the absence of a magnetic field or magnetic impurities), the scattering matrix is symmetric, $S = S^{\mathrm{T}}$, so we have $U' = U^{\mathrm{T}}$ and $V' = V^{\mathrm{T}}$. In the presence of a magnetic field, the four matrices U, U', V, V' are independent.

The distribution of the transmission eigenvalues remains to be determined. A scaling equation for this distribution has been derived by Dorokhov [7] and by Mello, Pereyra, and Kumar [8]. By computing the change in S under an incremental increase in L, they obtained a Fokker-Planck equation under the assumption that the mean free path l is much greater than the Fermi wavelength λ_{F}. This equation is called the DMPK equation, and is usually written in terms of the variable $\lambda_n \equiv (1 - T_n)/T_n$:

$$\tfrac{1}{2} l(\beta N + 2 - \beta) \frac{\partial P(\{\lambda_n\}, L)}{\partial L} = \sum_{n=1}^{N} \frac{\partial}{\partial \lambda_n} \lambda_n (1 + \lambda_n) J \frac{\partial}{\partial \lambda_n} \frac{P}{J}, \tag{1.1.6}$$

$$J = \prod_{i=1}^{N} \prod_{j=i+1}^{N} |\lambda_i - \lambda_j|^{\beta}. \tag{1.1.7}$$

The integer $\beta = 1(2)$ in the presence (absence) of time-reversal symmetry.[1] An exact solution of the DMPK equation is known for $\beta = 2$ [9]. Perturbative solutions for all β can be used in the metallic regime $L \ll Nl$.

The conductance is an example of a linear statistic, which is a quantity of the form: $A = \sum_{n=1}^{N} a(T_n)$. In order to calculate the average $\langle A \rangle$ and the variance $\mathrm{Var}\, A = \langle A^2 \rangle - \langle A \rangle^2$ of the linear statistic A, the eigenvalue density $\langle \rho(T) \rangle$ and the two-point correlation function $K(T, T')$ are required. These are defined in terms of the microscopic eigenvalue density $\rho(T) = \sum_{n=1}^{N} \delta(T - T_n)$ through

$$\langle \rho(T) \rangle = \int_0^1 \mathrm{d}T_1 \cdots \int_0^1 \mathrm{d}T_N \, \rho(T) P(\{T_n\}), \tag{1.1.8}$$

[1] The value $\beta = 4$ is taken on in systems with spin-orbit scattering in zero magnetic field. We will not consider that case in this thesis.

$$K(T,T') = \langle\rho(T)\rangle\langle\rho(T')\rangle - \langle\rho(T)\rho(T')\rangle. \tag{1.1.9}$$

The average and variance of A are then found from

$$\langle A\rangle = \int_0^1 \mathrm{d}T\,\langle\rho(T)\rangle a(T), \tag{1.1.10}$$

$$\mathrm{Var}\,A = -\int_0^1 \mathrm{d}T \int_0^1 \mathrm{d}T' K(T,T')a(T)a(T'). \tag{1.1.11}$$

An evolution equation for the eigenvalue density in the metallic regime $Nl \gg L$ is obtained after multiplying the DMPK equation (1.1.6) with $\sum_{n=1}^{N}\delta(\lambda-\lambda_n)$ and integrating over $\lambda_1,\lambda_2,\ldots,\lambda_N$. To close the equation, one decomposes $\langle\rho\rangle = \rho_0 + \delta\rho$, with ρ_0 of order N and $\delta\rho$ of order 1, and linearizes. When $L \gg l$, the density $\rho_0(x)$, with $T = 1/\cosh^2 x$, is uniform with a cutoff at $x = L/l$:

$$\rho_0(x) = \frac{Nl}{L}\theta(L/l - x). \tag{1.1.12}$$

The density $\langle\rho(T)\rangle$ is related to $\langle\rho(x)\rangle$ via $\langle\rho(T)\rangle = \langle\rho(x)\rangle \mathrm{d}x/\mathrm{d}T$. Using Eqs. (1.1.10) and (1.1.12) with $a(T) = T$, one recovers the Drude formula for the average conductance,

$$\langle G\rangle = G_0\frac{Nl}{L}. \tag{1.1.13}$$

The first-order correction $\delta\rho$ reads [6]

$$\delta\rho(x) = (1-2/\beta)[\tfrac{1}{4}\delta(x-0^+) + (4x^2+\pi^2)^{-1}], \tag{1.1.14}$$

describing a dip in the density near $x = 0$ ($T = 1$) for $\beta = 1$. It gives rise to a weak-localization correction to the conductance,

$$\langle\delta G\rangle = G_0\frac{\beta-2}{3\beta}, \tag{1.1.15}$$

which is observable as a dip in the conductance as a function of magnetic field around zero field.

The two-point correlation function $K(x,x')$ can be computed similarly [9,10]:

$$K(x,x') = \mathcal{K}(x-x') + \mathcal{K}(x+x') \tag{1.1.16}$$

$$\mathcal{K}(x) = -\frac{1}{2\beta\pi^2}\frac{d^2}{dx^2}\ln[1+(\pi/x)^2]. \tag{1.1.17}$$

Using this expression in Eq. (1.1.11), the variance of the conductance becomes

$$\mathrm{Var}\,G/G_0 = 2/15\beta. \tag{1.1.18}$$

Since the fluctuations in G are independent of the number of modes N in the wire, they are called *universal*.

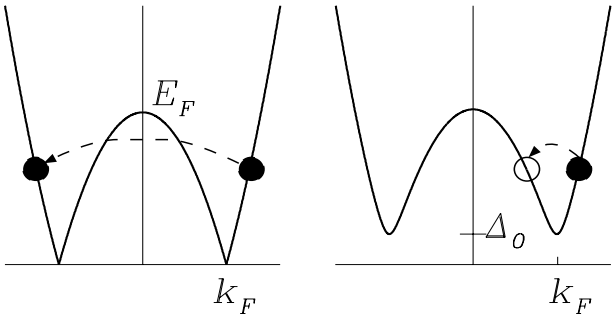

Figure 1-2. The dispersion relation for quasi-particle excitations in a normal metal (left) and in a superconductor with excitation gap Δ_0 (right). The arrows indicate normal reflection (left) and Andreev reflection (right).

1.2 Mesoscopic superconductivity

1.2.1 Excitation spectrum

The quasiparticle excitations of a normal metal consist of electrons (occupied states above the Fermi level) and holes (empty states below the Fermi level). Their dispersion relation is shown in Figure 1-2. In a superconductor, an excited state has both an electron component u and a hole component v. The states (u, v) and their energy E follow from the Bogoliubov-de Gennes equation [11]

$$\begin{pmatrix} H_0 & \Delta \\ \Delta^* & -H_0^* \end{pmatrix} \begin{pmatrix} u \\ v \end{pmatrix} = E \begin{pmatrix} u \\ v \end{pmatrix}, \tag{1.2.1}$$

which is a 2×2 matrix Schrödinger equation. On the diagonal, it contains the normal-state Hamiltonian

$$H_0 = \frac{1}{2m}[\vec{p} + e\vec{A}(\vec{r})]^2 + V(\vec{r}) - E_{\rm F}. \tag{1.2.2}$$

Electrons and holes are coupled by the superconductor pair potential $\Delta(\vec{r})$, which is determined self-consistently according to

$$\Delta(\vec{r}) = g(\vec{r}) \sum_n v_n^*(\vec{r}) u_n(\vec{r}) \tanh\left(\frac{E_n}{2k_{\rm B}T}\right). \tag{1.2.3}$$

Here g is a measure of the strength of the electron-phonon interaction, and the sum is over all eigenstates $E_n > 0$ with a cutoff at the Debije frequency $\omega_{\rm D}$.

In a homogeneous system, the electron-hole states are plane waves and the pair potential is spatially constant. It is given by the BCS equation

$$\Delta_0 = \hbar\omega_{\rm D} \exp(-N(0)g), \tag{1.2.4}$$

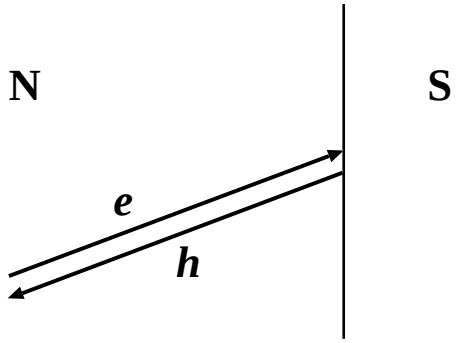

Figure 1-3. An electron (e) incident on the interface between a normal conductor and a superconductor is retroreflected as a hole (h). A Cooper pair is formed at the interface and absorbed in the superconducting condensate.

with $N(0)$ the density of states at the Fermi energy ($E = 0$) in the normal state. The amplitudes u and v are given by

$$\begin{pmatrix} u \\ v \end{pmatrix} = \frac{1}{2\mathcal{V}^{1/2}\sqrt{E^2 - \Delta_0^2/2}} \begin{pmatrix} E \pm \sqrt{E^2 - \Delta_0^2} \\ E \mp \sqrt{E^2 - \Delta_0^2} \end{pmatrix}, \tag{1.2.5}$$

such that $u = v$ when $E = \Delta_0$. The state (u, v) is normalized to unity on the volume $\mathcal{V}$ of the superconductor. For $E \gg \Delta_0$, either u or v goes to zero, corresponding to electron excitations (upper sign) or hole excitations (lower sign). The dispersion relation,

$$E^2 = \left(\frac{\hbar^2 k^2}{2m} - E_F\right)^2 + \Delta_0^2, \tag{1.2.6}$$

is shown in Figure 1-2. The excitation spectrum has a gap of Δ_0 at the Fermi wave vector $k_F = (2mE_F/\hbar^2)^{1/2}$.

1.2.2 Andreev reflection

Andreev reflection [12] is the process that enables charge transport through a junction between a normal conductor and a superconductor (NS junction) at energies below Δ_0: An electron incident from the normal metal at the NS-interface is reflected back as a hole with reversed velocity (See Fig. 1-3). The charge deficit of $2e$ forms a Cooper pair which is absorbed in the superconducting condensate. The process of Andreev reflection can be understood from the Bogoliubov-de Gennes equation, by matching eigenfunctions in the normal metal (where $\Delta = 0$) to decaying solutions in the superconductor (where $\Delta = \Delta_0$). For $E < \Delta_0 \ll E_F$ only states with (nearly) identical wave vectors couple. Consequently, normal reflection ($k \to -k$) is negligible, and reflection of an electron

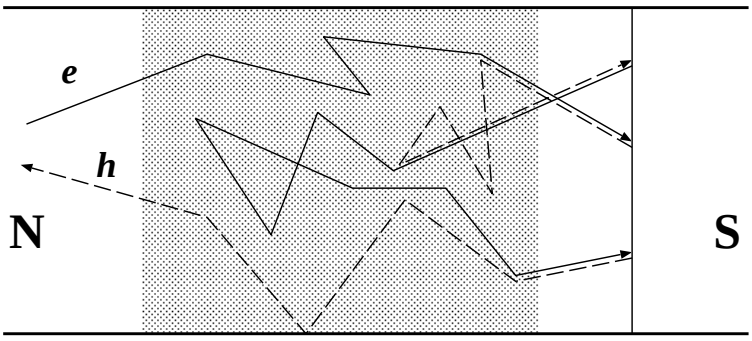

Figure 1-4. Scattering by disorder and Andreev reflection are shown schematically. (Solid lines represent electrons, dashed lines represent holes.) Reflection processes comprising an odd number of Andreev reflections contribute to the current through the NS interface.

as a hole (and vice versa) is the only scattering process allowed, since this can occur at constant k. The Andreev reflected particle acquires a phase shift of $\chi = -\arccos E/\Delta_0$. The difference between normal reflection and Andreev reflection is indicated in hte dispersion relations shown in Fig. 1-2.

1.2.3 Conductance of a normal-metal–superconductor junction

Because the proximity to a superconductor introduces a coupling between the motion of electrons (e) and holes (h) in the normal conductor, the dimension of the scattering matrix is doubled,

$$S = \begin{pmatrix} S_{ee} & S_{eh} \\ S_{he} & S_{hh} \end{pmatrix}. \tag{1.2.7}$$

The scattering theory of an NS junction is reviewed in Ref. [13]. We consider separately the scattering at the NS-interface and the scattering in the normal conducting part of the sample (see Figure 1-4). The scattering matrix $S_{\rm N}$ of the normal part does not couple electrons and holes,

$$S_{\rm N} = \begin{pmatrix} S_0(E) & 0 \\ 0 & S_0^*(-E) \end{pmatrix}, \tag{1.2.8}$$

where S_0 is the scattering matrix associated with the Hamiltonian H_0 of Eq. (1.2.2). In zero magnetic field ($B = 0$) the matrix S_0 is symmetric, so $S_0^* = S_0^\dagger$. The Andreev scattering matrix $S_{\rm A}$ exclusively couples electrons and holes (for $E < \Delta_0$),

$$S_{\rm A} = e^{i\chi} \begin{pmatrix} 0 & 1 \\ 1 & 0 \end{pmatrix}, \quad \chi = \arccos(E/\Delta). \tag{1.2.9}$$

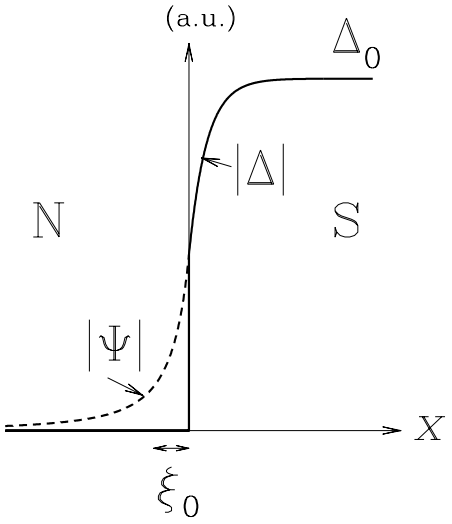

Figure 1-5. The pair potential Δ drops to zero abruptly at the NS interface (solid curve), while the order parameter Ψ extends into the normal metal (dashed curve).

The conductance requires knowledge of S at the Fermi level ($E = 0$). An incident electron contributes to the current if it is reflected as a hole. The reflection matrix r_{he} from electron to hole is a geometrical series of $1, 3, 5, \ldots$ Andreev reflections (see Figure 1-4), which can be summed to yield (for $E = 0$ and $B = 0$)

$$r_{he} = t^\dagger (1 + r' r'^\dagger)^{-1} t. \tag{1.2.10}$$

Just as the normal conductance is given by the Landauer formula $G = G_0 \mathrm{Tr}\, t t^\dagger$, the conductance of an NS-junction is given by $G_{\mathrm{NS}} = 2G_0 \mathrm{Tr}\, r_{he} r_{he}^\dagger$. The extra factor of two is there because Andreev reflection doubles the current (electrons and holes carry current in the same direction). Substitution of Eq. (1.2.10) yields an expression for G_{NS} in terms of the N eigenvalues T_n of $t t^\dagger$,

$$G_{\mathrm{NS}} = \frac{4e^2}{h} \sum_{n=1}^{N} \frac{T_n^2}{(2 - T_n)^2}. \tag{1.2.11}$$

Like the normal-state conductance (1.1.4), G_{NS} is a linear statistic, so its mean and variance are given by Eqs. (1.1.10) and (1.1.11).

1.2.4 Induced superconductivity

In a normal metal without pairing interaction, the interaction parameter g vanishes. Hence, the pair potential Δ drops to zero abruptly at the NS interface (see Figure 1-5). However, the phase coherence of electrons and holes extends into the normal metal, an effect known as the proximity effect. This is described

by the superconductor order-parameter $\Psi(\vec{r}) = \Delta(\vec{r})/g(\vec{r})$, which vanishes if electrons and holes are incoherent. The decay of $|\Psi|$ in the normal metal is algebraic, with a characteristic length scale $\xi_0 = \hbar v_F/\Delta_0$. (In a disordered metal, ξ_0 is to be replaced by $\sqrt{\xi_0 l}$.) Exponential suppression of the order parameter occurs beyond the pair-breaking length $\xi = \hbar v_F/k_B T$, which is $\gg \xi_0$ if $T \ll T_c$. (In a disordered metal, ξ is also to be replaced by $\sqrt{\xi l}$.)

Phase coherence between electrons and holes gives rise to several effects, both in transport and in thermodynamic properties: The conductance, as well as the density of states are modified at low temperatures and low voltages or energies. The typical energy window in which effects can be observed at a distance L from the interface is the Thouless energy $E_T = \hbar v_F \min(l, L)/L^2$, such that $\xi \simeq L$ when $k_B T \simeq E_T$.

1.2.5 Josephson effect

The pair potential $\Delta(\vec{r})$ has an amplitude and a phase. When two superconductors S_1 and S_2 are connected by a normal metal, a current may flow in equilibrium (at zero voltage), if the pair potential in S_1 and S_2 has a different phase. This is known as the Josephson effect. The equilibrium current $I(\phi)$ is a 2π-periodic function of the phase difference $\phi = \phi_1 - \phi_2$ of the superconductor pair potentials. The critical current I_c is the maximum of $I(\phi)$.

The original Josephson effect was predicted for a thin tunnel barrier separating two superconductors, where the separation is $\ll \xi_0$. However, the Josephson effect also exists in SNS structures where the separation of the superconductors is much larger than ξ_0, provided it is smaller than ξ.

Since the supercurrent is an equilibrium quantity, it can be obtained from a thermodynamic relation,

$$I = \frac{2e}{\hbar}\frac{dF}{d\phi}, \tag{1.2.12}$$

where F is the free energy of the junction. The free energy can be obtained from the excitation spectrum by

$$F = -2k_B T \sum_n \ln[2\cosh(E_n/2k_B T)] + \int d\vec{r}\,\frac{|\Delta|^2}{g} + \mathrm{Tr}\, H_0. \tag{1.2.13}$$

The excitation spectrum consists of a discrete part for $E \le \Delta_0$ and a continuous part for $E > \Delta_0$. The discrete spectrum can be found from the condition $Z \equiv \mathrm{Det}[1 - S_A S_N] = 0$, whereas the continuous spectrum has density of states $\rho = -\pi^{-1}\mathrm{Im}\,\partial \ln Z/\partial E$. In order of magnitude, $I_c \simeq (eE_T/\hbar\delta)\min(E_T, \Delta_0)$ at zero temperature, where E_T is the Thouless energy and δ the level spacing of the Josephson junction.

The most important application of the Josephson effect is the superconducting quantum-interference device (SQUID), which consists of a superconducting

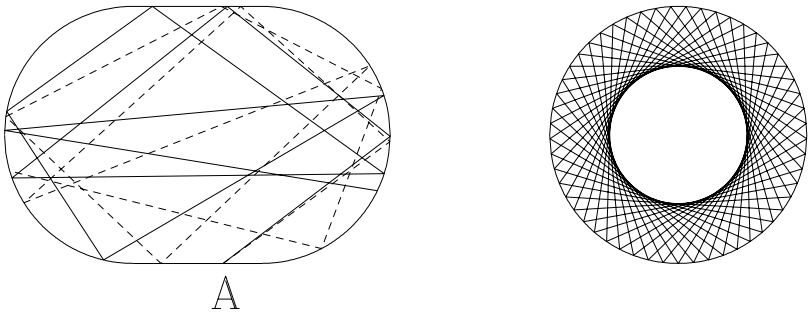

Figure 1-6. Trajectories in a chaotic billiard (left) and an integrable billiard (right). Solid and dashed lines illustrate the divergence of two trajectories in the chaotic billiard, which start in almost the same direction at point A.

ring contacted to two leads. Both branches of the ring contain a Josephson junction. The SQUID is a high-precision magnetometer. It exploits the fact that a modulation on the conductance of the device can be measured with increasing magnetic field, which is due to the modulation of the phase difference ϕ of either Josephson junction by the magnetic flux enclosed by the ring.

1.3 Quantum chaos

1.3.1 Closed systems

In classical mechanics, one can make a clear distinction between integrable and chaotic dynamics by looking at trajectories. A system is called integrable if it has a conserved quantity for each degree of freedom. In the circular billiard of Fig. 1-6, the conserved quantities are the energy and the angle of incidence of a trajectory with the boundary. A chaotic system has no conserved quantities other than the energy, see for example the stadium billiard in Figure 1-6. Chaotic motion is associated with an extreme sensitivity of the trajectories on initial conditions, which is absent for integrable motion.

In quantum mechanics, chaotic and integrable systems can be distinguished from their energy spectrum [14, 15]. Neighboring levels have a distribution of spacings s which vanishes as s^β in a chaotic system. An integrable system, in contrast, has a Poisson distribution of spacings, with a maximum at $s = 0$ (see Figure 1-7).

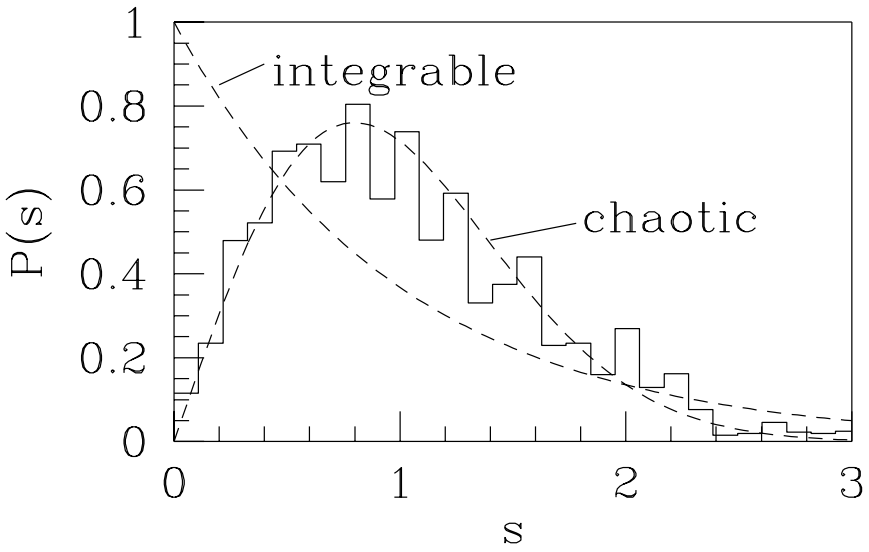

Figure 1-7. Normalized level spacing distributions for chaotic and integrable systems. The dashed lines are the theoretical predictions. The histogram is the experimental result for a chaotic microwave resonator [16].

1.3.2 Open systems

In an open system, chaotic and integrable dynamics is distinghuised by the distribution of dwell times. The dwell time τ of a particle is the time that it spends in the billiard before leaving it. Since the dwell time distributions of both types of billiards differ, this offers a possibility to distinguish billiards with chaotic and integrable dynamics by making weak contacts to them and performing transport experiments. For weak coupling, when the number of collisions of a particle with the boundary before it escapes is very large, the dwell times of particles in a chaotic billiard with nearly identical — but different — initial conditions are uncorrelated. The dwell time distribution is therefore that of stochastic decay, i.e. it is exponential, $P(\tau) \propto \exp(-\tau/\tau_{\rm dwell})$. In an integrable billiard, on the other hand, correlations between initial and final conditions persist. It is possible to "focus" the trajectory of a particle, such that its dwell time is arbitrarily long. This gives rise to an algebraic decay of dwell times, $P(\tau) \propto \tau^{-3}$ [17,18].

The mean dwell time $\tau_{\rm dwell}$ in chaotic and integrable billiards is the same, given by the inverse of the Thouless energy, $\tau_{\rm dwell} \simeq \hbar/E_{\rm T}$. The Thouless energy of a billiard with two narrow openings (containing N modes each) is given by $E_{\rm T} \simeq N\delta$, where δ is the level spacing in the billiard.

A related distribution in a magnetic field is the distribution of fluxes Φ that trajectories enclose. This distribution is exponential for chaotic billiards, $P(\Phi) \propto \exp(-c|\Phi|)$ (c is a constant), and algebraic for integrable billiards, $P(\Phi) \propto |\Phi|^{-2}$.

The shape of the weak-localization peak $\langle \delta G(B) \rangle$ around $B = 0$ is the Fourier transform of the distribution of fluxes [19]. As a result, this shape is different for chaotic and integrable systems. The weak-localization peak has a Lorentzian shape for chaotic billiards, and a triangular shape in integrable billiards. The observation by Chang et al. [20] of this quantum signature of chaos in a semiconducting 2D electron gas has been reproduced in Figure 1-8.

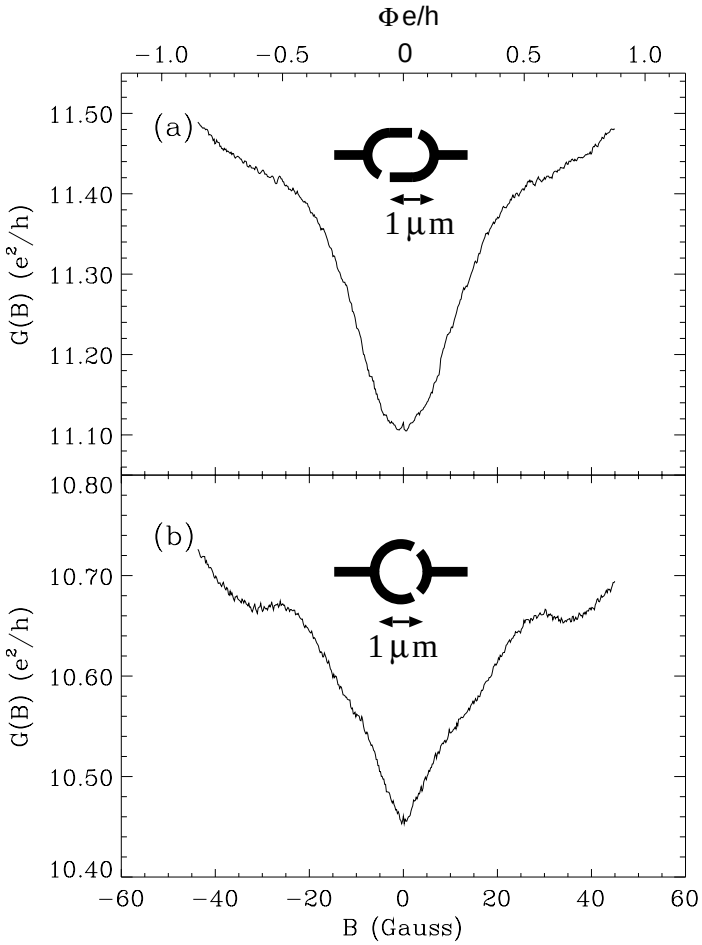

Figure 1-8. Magnetoconductance of ensembles of chaotic billiards (top) and integrable billiards (bottom), confirming the expected Lorentzian and triangular shapes for both types of billiards. The insets show the shape of the billiards, which were fabricated in the 2D electron gas of a GaAs/AlGaAs heterostructure [20].

1.4 Electrostatic charging effects

Coulomb repulsion is important in nearly isolated conducting objects with small electrostatic capacitances. The electrostatic energy that is required to add a

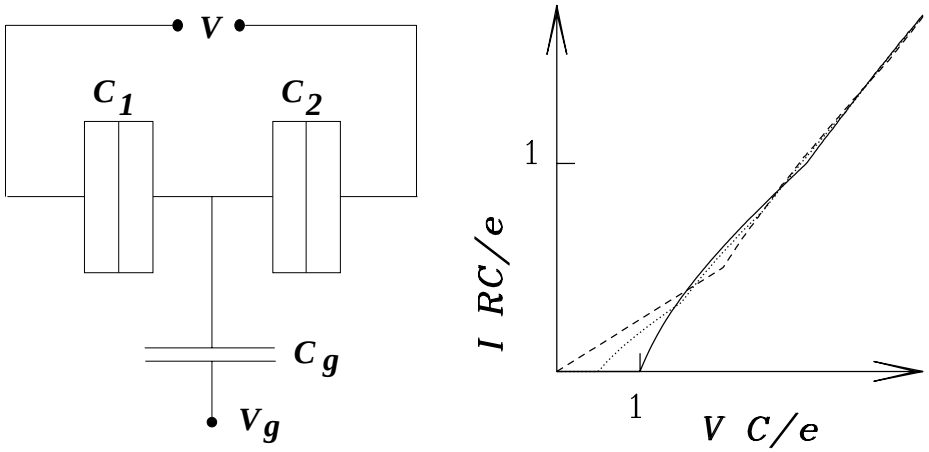

Figure 1-9. The single-electron transistor (left) consists of two tunnel junctions with capacitances C_1, C_2, tunnel resistances R_1, R_2, and a gate capacitance C_g by means of which a fractional charge $C_g V_g$ can be induced on the island. The island has total capacitance $C = C_1 + C_2 + C_g$. The current-voltage characteristic (right) has a threshold which depends on the induced charge. For the curves shown, we have used $C_1 = C_2$, $R_1 = R_2 = R$, and $C_g V_g / e = 0$ (solid line), 0.25 (dotted) and 0.5 (dashed).

charge to a metal particle with capacitance C equals $e^2/2C$. This charging energy becomes an important energy scale if it is of the order of or larger than $k_B T$: Current through the particle is blocked at voltages V below the charging energy, provided that the resistance of the tunnel barriers is greater than h/e^2 (to suppress quantum fluctuations of the charge). This effect is known as the Coulomb blockade [21]. A typical current-voltage characteristic is shown in Figure 1-9.

By means of a gate, an arbitrary charge can be capacitively induced on the particle. This so-called single-electron transistor (see Figure 1-9) is one of the simplest and most studied systems in which the Coulomb blockade can be observed. Using the gate, the threshold voltage for transport through the particle can be tuned to any value between 0 and $e/[2\max(C_1, C_2) + C_g]$. The single-electron transistor can therefore be used as a switch. Other applications of the single-electron tunneling effect are single-electron memory and thermometry.

1.5 This thesis

Quantum transport through disordered wires with obstacles

The DMPK equation (1.1.6) describes how the transmission eigenvalues $T_n = 1/(1 + \lambda_n)$ in a wire change with increasing wire length L. It has been derived under the assumption of weak impurity scattering ($l \gg \lambda_F$). It is not suitable to describe a wire containing obstacles (such as point contacts or tunnel bar-

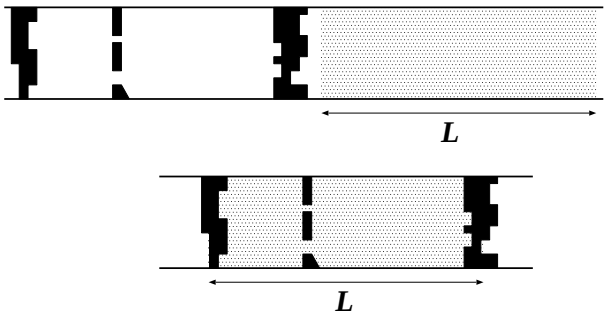

Figure 1-10. Two wires containing disordered regions (dotted) and obstacles (black) in a different sequence. The statistics of the transmission eigenvalues of the two wires is the same.

riers), since these give rise to discontinuities in the evolution of transmission eigenvalues. In Chapter 2, we show that the distribution of transmission eigenvalues is independent of the order of the constituent parts of the sample (disordered regions, point contacts, and tunnel barriers), if each part of the wire has an isotropically distributed scattering matrix. In that case, the disordered wire containing obstacles is equivalent to a ballistic wire containing all the obstacles which is coupled in series to a disordered wire (see Figure 1-10). Putting the disorder behind the obstacles has the technical advantage that the distribution of transmission eigenvalues can be found by integrating the DMPK equation over the disordered region, using the distribution of the ballistic wire with obstacles as the initial condition.

In Section 2.1, we study the conduction through a ballistic point contact in a disordered wire. The point contact is treated as an initial condition on the DMPK equation. The conduction problem is further simplified by mapping this geometry on a wire with identical width to the opening of the point contact, identical length as the original wire, but with an increased mean free path. This mapping allows us to solve the problem of point contact plus disordered wire using known results for a disordered wire alone.

In Section 2.2, the magnitude of the conductance fluctuations of a (disordered) double-barrier junction is calculated. In the limit that the conductance is dominated by the tunnel barriers, the fluctuations have a maximal value of $\mathrm{Var}G/G_0 = 1/4\beta$ for two identical barriers. With increasing disorder, the variance crosses over to the result $2/15\beta$ for a disordered wire without barriers.

In 1991, Kastalsky and coworkers observed that the differential conductance of a Nb-InGaAs junction shows a large and narrow peak around zero voltage [22]. Their result has been reproduced in Figure 1-11. The effect originates from the constructive interference of multiple Andreev reflections [23]. At zero voltage ($E = 0$) and magnetic field ($B = 0$), the phase shift acquired by an electron along a trajectory is exactly cancelled by the phase shift of a hole retracing the trajectory. Therefore, multiple Andreev reflections (as in Figure 1-4) interfere

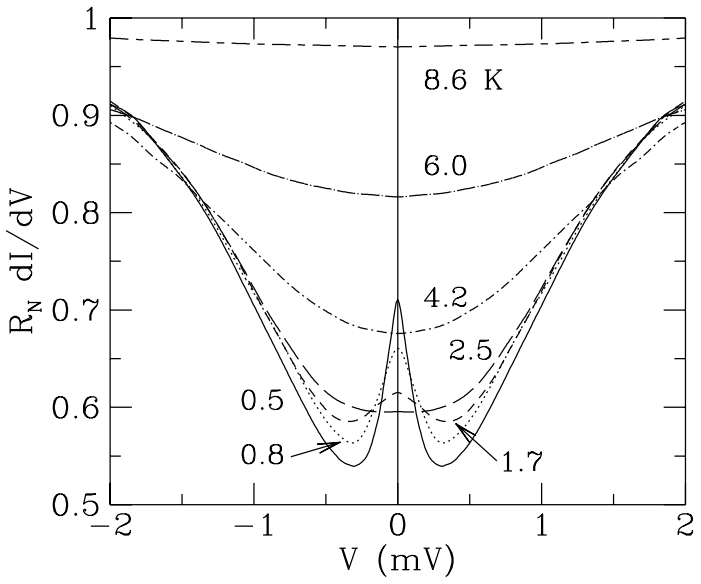

Figure 1-11. Normalized conductance-voltage characteristics of a Nb-InGaAs contact at different temperatures and zero magnetic field [22]. The peak which is observable at low temperatures is due to reflectionless tunneling.

constructively, which greatly increases the current through the junction.

The average conductance $\langle G_{\rm NS}\rangle$ of the NS junction depends on the transparancy Γ of the tunnel barrier at the NS interface, the amount of disorder in the normal metal (characterized by the ratio of its length L and mean free path l), and on the number of modes N in the junction. When phase coherence is destroyed by either a magnetic field or an applied voltage, $\langle G_{\rm NS}\rangle = (2Ne^2/h)(L/l + 2\Gamma^{-2})^{-1}$, which equals the classical resistance. The contribution from the tunnel barrier is quadratic in Γ, since both the incoming electron and the Andreev-reflected hole have to tunnel through the barrier. Upon restoring phase coherence, the conductance crosses over to $\langle G_{\rm NS}\rangle = (2Ne^2/h)(L/l+\Gamma^{-1})^{-1}$ (valid for $\Gamma L/l \gg 1$). Multiple coherent Andreev reflections increase the effective barrier transparancy from Γ^2 to Γ. It is as if, once the electron has tunneled through the barrier, the hole tunnels back without reflections, hence the name *reflectionless tunneling* [13].

Reflectionless tunneling can occur in microstructures where multiple reflection processes with a tunnel barrier determine the conductance. In Chapter 3 of this thesis, we consider the case that a second tunnel barrier instead of disorder causes the multiple reflections. The conductance is $\propto \Gamma$ instead of $\propto \Gamma^2$ if both transparancies are comparable. Studying reflectionless tunneling in a semi-

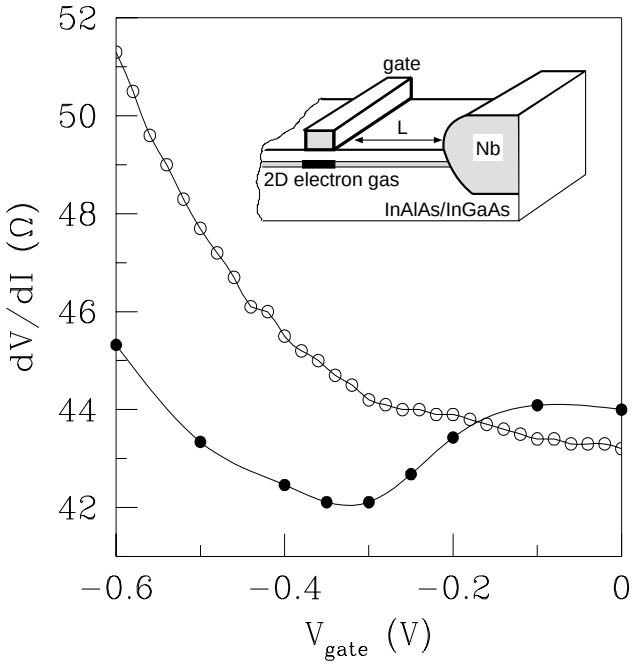

Figure 1-12. Differential resistance of a double-barrier structure in a two-dimensional electron gas (2DEG) formed at a InAlAs/InGaAs heterojunction with a superconducting Nb-contact [24]. The Schottky barrier at the NS interface has fixed transparancy. The gate voltage V_{gate} tunes the transparancy of the second barrier by depleting the 2DEG underneath it. Low gate voltages V_{gate} correspond to low tunnel probabilities.

conducting double-barrier tunneling structure has the advantage that the barrier transparancies can be tuned by means of gates, whereas it is not easy to change the length L or the mean free path l of a disordered NS-junction. This enables a direct observation of the Γ-dependence. A resistance minimum as a function of barrier transparancy has recently been observed by Takayanagi et al. [24] (see Figure 1-12). One notices that the normal-state resistance (open dots) increases monotonically with decreasing gate voltage, whereas the NS-resistance (closed dots) shows a clear minimum.

Giant backscattering peak in angle-resolved Andreev reflection

The weak-localization correction to the conductance of a disordered normal metal is due to coherent backscattering of electrons. In the absence of a magnetic field, time-reversed paths interfere constructively, leading to an average reflection probability $\langle |r_{mn}|^2 \rangle$ into the incoming mode (say n) which is

twice as large as the probability for reflection into any other mode $m \neq n$: $\langle |r_{mn}|^2 \rangle = (1+\delta_{mn})/(N+1)$ plus small corrections of order l/L. If time-reversal symmetry is broken by a magnetic field, coherent backscattering disappears, and $\langle |r_{mn}|^2 \rangle = 1/N$ is the same for $m = n$ and $m \neq n$.

As is shown in Chapter 4, the coherent backscattering is greatly enhanced if the disordered normal metal is backed by a superconductor. The probability of reflection of an electron as a hole into the same mode is Nl/L times more probable than reflection into any other mode. This giant backscattering peak does not give rise to a large magnetoconductance, because the enhancement of $|(r_{he})_{nn}|^2$ is almost completely cancelled by a reduction of $|(r_{he})_{mn}|^2$ for $m \neq n$. The enhanced backscattering can however be observed if we increase the sensitivity to reflection at the angle of incidence. To that end, a point contact is coupled in series to the disordered NS-contact. We then find that a magnetic field can increase the conductance by as much as a factor of two.

Induced superconductivity distinguishes chaotic from integrable billiards

Chaotic and integrable dynamics can be distinguished in the different distribution of spacings of adjacent energy levels (see Figure 1-7). The mean level density $\langle \rho \rangle = \delta^{-1}$, however, is not sensitive to the dynamics of the billiard, because the mean level spacing δ depends only on the available phase space and not on the dynamics within that phase space. In Chapter 5 we will show, that the level density does become a probe for quantum chaos if the billiard is brought into contact with a superconductor: The level density of the billiard has a gap around the Fermi energy if its dynamics is chaotic, whereas it increases linearly with energy if its dynamics is integrable. There is a qualitative explanation in terms of the dwell-time distribution discussed in Section 1.3.2: Long dwell-times correspond to small energies. The asymptotic tails of the dwell-time distributions thus reflect the energy-dependence of the density of states at small energies. The algebraic tail $P(\tau) \propto \tau^{-3}$ of integrable billiards corresponds to a linear density of states, $\langle \rho(E) \rangle \propto E$, whereas the exponential tail for chaotic billiards corresponds to an exponentially small density of states. The relevant energy scale in both cases is the Thouless energy $E_{\rm T}$, such that $\langle \rho(E) \rangle \to 1/\delta$ when $E \gg E_{\rm T}$. The relevance of this signature of quantum chaos lies in the fact that the Thouless energy is a mesoscopic energy scale: It is typically much larger than the microscopic energy scale of δ on which chaotic and integrable billiards differ in normal systems.

The density of states can be measured by tunneling into the particle, since the tunneling conductance is $\propto \rho(eV)$. A difficulty lies in the design and fabrication of the billiards: It is possible to fabricate billiards which are highly regular or highly chaotic, using a 2D electron gas with gates (see Figure 1-8). However, the coupling of a semiconducting 2D electron gas to a superconductor is dif-

ficult because of the appearance of Schottky barriers, which suppress Andreev reflection.

Coulomb blockade threshold in inhomogeneous one-dimensional arrays of tunnel junctions

Operation of electronic devices such as the single-electron transistor in Figure 1-9 requires that one can control charge fluctuations well within the unit charge. This is a major problem in practical designs of single-electron devices containing many elements: Unscreened charges in the environment of the device have the effect of inducing unknown "background charges" on the elements. Moreover, the induced charges may change in time due to charge fluctuations in the environment. In laboratory experiments, one can apply a different gate voltage to each element to compensate for the background charge on all islands in the device, although this is impractical for applications as a transistor. The work described in Chapter 6 is an attempt to treat the effect of background charges in the Coulomb charging of a one-dimensional array of metallic islands. The focus is on the threshold voltage for transport through the array. In contrast to the previously predicted saturation of the threshold voltage with increasing array length at fixed gate coupling for arrays without background charge [25], we find that the expected threshold voltage increases algebraically with the number of islands in the array if background charges are taken into account. The results are consistent with experimental results [26, 27].

References

[1] *Mesoscopic Phenomena in Solids*, edited by B. L. Al'tshuler, P. A. Lee, and R. A. Webb (North-Holland, Amsterdam, 1991).

[2] S. Datta, *Electronic Transport in Mesoscopic Systems* (Cambridge University Press, Cambridge, 1995).

[3] Y. Imry, *Introduction to Mesoscopic Physics* (Oxford University Press, Oxford, 1996).

[4] R. Landauer, IBM J. Res. Dev. **1**, 223 (1957); Philos. Mag. **21**, 863 (1970).

[5] A. D. Stone, P. A. Mello, K. A. Muttalib, and J.-L. Pichard, in Ref. [1].

[6] C. W. J. Beenakker, Rev. Mod. Phys., to be published.

[7] O. N. Dorokhov, Pis'ma Zh. Eksp. Teor. Fiz. **36**, 259 (1982) [JETP Lett. **36**, 318 (1982)].

[8] P. A. Mello, P. Pereyra, and N. Kumar, Ann. Phys. **181**, 290 (1988).

[9] C. W. J. Beenakker and B. Rejaei, Phys. Rev. Lett. **71**, 3689 (1991).

[10] J. T. Chalker and A. M. S. Macêdo, Phys. Rev. Lett. **71**, 3693 (1993).

[11] P. G. de Gennes, *Superconductivity of Metals and Alloys* (Benjamin, New York, 1966).

[12] A. F. Andreev, Zh. Eksp. Teor. Fiz. **46**, 1823 (1964) [Sov. Phys. JETP **19**, 1228 (1964)].

[13] C. W. J. Beenakker, in *Mesoscopic Quantum Physics*, edited by E. Akkermans, G. Montambaux, J.-L. Pichard, and J. Zinn-Justin (North-Holland, Amsterdam, 1995).

[14] *Chaos and Quantum Physics*, edited by M.-J. Giannoni, A. Voros, and J. Zinn-Justin (North-Holland, Amsterdam, 1991).

[15] M. C. Gutzwiller, *Chaos in Classical and Quantum Mechanics* (Springer, New York, 1990).

[16] H.-D. Gräf, H. L. Harney, H. Lengeler, C. H. Lewenkopf, C. Rangacharyulu, A. Richter, P. Schardt, and H. A. Weidenmüller, Phys. Rev. Lett. **69**, 1296 (1992).

[17] W. Bauer and G. F. Bertsch, Phys. Rev. Lett. **65**, 2213 (1990).

[18] H. U. Baranger, R. A. Jalabert, and A. D. Stone, Chaos **3**, 665 (1993).

[19] H. U. Baranger, R. A. Jalabert, and A. D. Stone, Phys. Rev. Lett. **70**, 3876 (1993).

[20] A. M. Chang, H. U. Baranger, L. N. Pfeiffer, and K. W. West, Phys. Rev. Lett. **73**, 2111 (1994).

[21] D. V. Averin and K. K. Likharev, in Ref. [1].

[22] A. Kastalsky, A. W. Kleinsasser, L. H. Greene, R. Bhat, F. P. Milliken, and J. P. Harbison, Phys. Rev. Lett. **67**, 3026 (1991).

[23] B. J. van Wees, P. de Vries, P. Magnée, and T. M. Klapwijk, Phys. Rev. Lett. **69**, 510 (1992).

[24] H. Takayanagi, E. Toyoda, and T. Akazaki, 1996 (unpublished).

[25] N. S. Bakhvalov, G. S. Kazacha, K. K. Likharev, and S. I. Serdyukova, Zh. Eksp. Teor. Fiz. **95**, 1010 (1989) [Sov. Phys. JETP **68**, 581 (1989)]; Physica B **173**, 319 (1991).

[26] P. Delsing, T. Claeson, K. K. Likharev, and L. S. Kuzmin, Phys. Rev. B **42**, 7439 (1990).

[27] A. J. Rimberg, T. R. Ho, and J. Clarke, Phys. Rev. Lett. **74**, 4714 (1995).

2 Quantum transport through disordered wires with obstacles

2.1 Conductance fluctuations, weak localization, and shot noise for a ballistic constriction in a disordered wire

2.1.1 Introduction

The problem addressed in this section is that of phase-coherent electron transport through a ballistic point contact between disordered metals. The geometry is shown schematically in Fig. 2-1. The same problem was studied recently by Maslov, Barnes, and Kirczenow (MBK) [1], to which paper we refer for an extensive introduction and bibliography. The analytical theory of MBK is limited to the case that the mean free path l for elastic impurity scattering is much greater than the total length L of the system. In this "quasi-ballistic" case of $l \gg L$, the backscattering through the point contact by disorder in the wide regions can be treated perturbatively. In the present work we go beyond MBK by solving the problem for arbitrary ratio of l and L, from the quasi-ballistic, through the diffusive, into the localized regime of quantum transport.

Just as in Ref. [1], we model the scattering by the impurities and by the constriction by *independent* and *isotropic* transfer matrices. That is to say, we write the transfer matrix M of the whole system as the product $M = M_2 M_0 M_1$ of the transfer matrices M_1 and M_2 of the two wide disordered regions and the transfer matrix M_0 of the ballistic constriction, and then we assume that the three

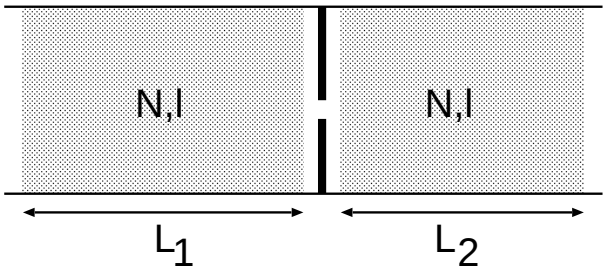

Figure 2-1. Schematic illustration of the point contact geometry, consisting of a ballistic constriction [with conductance $N_0(2e^2/h)$] in a disordered wire [with length $L = L_1 + L_2$, mean free path l, and N transverse modes]. To define a scattering geometry, the disordered regions (dotted) and the point contact (black) are separated by scattering-free segments.

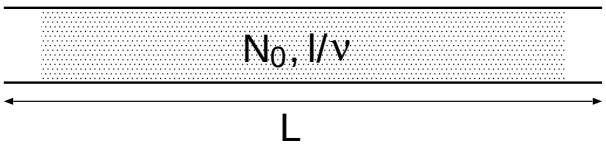

Figure 2-2. Unconstricted geometry, with length L, mean free path l/ν, and N_0 transverse modes. The key result of this section is the equivalence with the constricted geometry of Fig. 2-1, for ν given by Eq. (2.1.1).

transfer matrices are distributed according to independent and isotropic distributions $p_i(M_i)$ $(i = 0, 1, 2)$. [A distribution $p(M)$ is called *isotropic* if it is only a function of the eigenvalues of $MM^\dagger$.] The assumption of three independent transfer matrices requires a spatial separation of scattering by the impurities and by the constriction, which prevents us from treating the effects of impurity scattering on the conductance quantization. (This problem has been treated extensively in the past, cf. Ref. [2] for a recent review.) The isotropy assumption for the transfer matrix M_0 of the constriction is a simple but realistic model of the coupling between wide and narrow regions, which implies that all N transverse modes in the wide regions (of width W) to the left and right of the constriction (of width W_0) are equally coupled to each other [3]. The basic requirement here is that the widening from W_0 to W occurs abruptly and without spatial symmetries.[1] The isotropy assumption for the transfer matrices M_1 and M_2 of the disordered regions (of length L_1 and L_2) requires aspect ratios $L_1/W, L_2/W \gg 1$ corresponding to a wire geometry [4]. Finally, we assume that the impurity scattering is weak in the sense that $l \gg \lambda_F$ (with λ_F the Fermi wavelength). Under these assumptions we can treat the impurity scattering within the framework of the Dorokhov-Mello-Pereyra-Kumar (DMPK) equation [5, 6].

The key result which enables us to go beyond MBK is a mapping between the constricted and unconstricted geometries in Figs. 2-1 and 2-2. The unconstricted geometry of Fig. 2-2 is a disordered wire of length $L = L_1 + L_2$, with N_0 transverse modes and mean free path l/ν. The number N_0 is determined by the quantized conductance $N_0(2e^2/h)$ of the point contact in the constricted geometry. The fraction ν is defined by

$$\nu = \frac{\beta N_0 + 2 - \beta}{\beta N + 2 - \beta}. \tag{2.1.1}$$

(Here $\beta \in \{1, 2, 4\}$ is the Dyson index, which equals 1 in zero magnetic field, 2 in a time-reversal-symmetry breaking magnetic field, and 4 in zero field with strong spin-orbit scattering.) Starting from the DMPK equation, we will deduce (in Sec. 2.1.2) that the conductance has the *same* probability distribution in the two geometries. The equivalence holds for *all* moments of the conductance,

[1] It was assumed in Ref. [1] that the constriction has a spatial symmetry such that coupling between even and odd modes is forbidden in the absence of disorder. This assumption seems to be irrelevant in the presence of disorder.

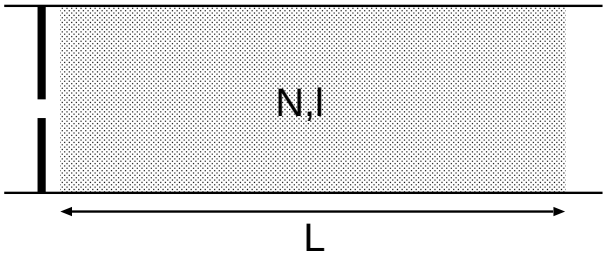

Figure 2-3. Constricted geometry with all disorder at one side of the point contact. For isotropic transfer matrices this geometry is statistically equivalent to that of Fig. 2-1.

so that it allows us to obtain (in Sec. 2.1.3) the effect of the point contact on weak localization and universal conductance fluctuations directly from known results for disordered wires [7] — without the restriction $l \gg L$ of Ref. [1]. It also holds for other transport properties than the conductance (in fact it holds for the *complete* distribution of the transmission eigenvalues). As an example of current interest, we will compute the suppression of shot noise in the point contact geometry.

In Sec. 2.1.4 we consider the case $N_0 = 1$ of a quantum point contact with a single transmitted channel. The mapping is then onto a single-mode wire (or one-dimensional chain) of length L and mean free path $\frac{1}{2}(\beta N + 2 - \beta)l$. The 1D chain has been studied extensively in the past as the simplest possible system exhibiting localization [8, 9]. The precise correspondence with the problem of a single-channel ballistic constriction in a multi-channel disordered wire seems to be both novel and unexpected. From this correspondence we predict that the resistance R of the point contact has an exponential distribution,

$$\mathcal{P}(R) = \beta \frac{e^2}{h} \frac{Nl}{L} \exp\left[-\beta \frac{e^2}{h} \frac{Nl}{L} (R - h/2e^2) \right], \quad R \geq h/2e^2, \tag{2.1.2}$$

provided the disordered wire is metallic ($Nl/L \gg 1$). The width of the distribution decreases by a factor of two upon breaking time-reversal symmetry in the absence of spin-orbit scattering ($\beta = 1 \rightarrow \beta = 2$).

To test the theoretical predictions we present (in Sec. 2.1.5) results of numerical simulations, both for $N_0 \gg 1$ and for $N_0 = 1$. The numerical data for the density of transmission eigenvalues provides independent support for the mapping. In particular, we find good agreement with Eq. (2.1.2), including the decrease in width upon application of a magnetic field.

2.1.2 Mapping of constricted unto unconstricted geometry

The first step is to show that the geometry of Fig. 2-1, with lengths L_1 and L_2 of disordered wire to the left and right of the point contact, is equivalent to the geometry of Fig. 2-3, with a length $L = L_1 + L_2$ of disordered wire to one side

only. The transfer matrix for Fig. 2-1 is $M = M_2 M_0 M_1$, the transfer matrix of Fig. 2-3 is $M' = M_0 M_1 M_2$. The corresponding probability distributions $p(M)$ and $p'(M')$ are

$$p = p_2 * p_0 * p_1, \tag{2.1.3}$$
$$p' = p_0 * p_1 * p_2, \tag{2.1.4}$$

where the symbol $*$ denotes a convolution:

$$p_i * p_j(M) = \int dM_j \, p_i(M M_j^{-1}) p_j(M_j). \tag{2.1.5}$$

(The invariant measure dM on the group of transfer matrices is introduced in Refs. [6] and [7].) Isotropic distributions have the property that their convolution does not depend on the order: $p_i * p_j = p_j * p_i$ if both p_i and p_j are isotropic (see the Appendix for a proof). It follows that $p = p'$, and hence that the geometries of Figs. 2-1 and 2-3 are equivalent. Note that the isotropy assumption is crucial here, otherwise the convolution would not commute.

The second step is to show the equivalence of the constricted geometry of Fig. 2-3 with the unconstricted geometry of Fig. 2-2. We recall [4] that the $2N$ eigenvalues of the transfer matrix product $MM^\dagger$ come in inverse pairs $\exp(\pm 2x_n)$, $n = 1, 2, \ldots N$. The ratio $L/x_n \in [0, \infty)$ has the significance of a channel-dependent localization length. We define

$$T_n = 1/\cosh^2 x_n, \tag{2.1.6}$$
$$\lambda_n = \sinh^2 x_n = (1 - T_n)/T_n. \tag{2.1.7}$$

The numbers $T_n \in [0, 1]$ are the transmission eigenvalues (i.e. the eigenvalues of the matrix product $tt^\dagger$, with t the $N \times N$ transmission matrix). A ballistic point contact, with conductance $N_0(2e^2/h)$, has to a good approximation $T_n = 1$ ($\lambda_n = 0$) for $1 \le n \le N_0$, and $T_n = 0$ ($\lambda_n \to \infty$) for $N_0 + 1 \le n \le N$. (This is a statement about transmission *eigenvalues*, not about the transmission probabilities of individual modes, which are all of order N_0/N.) The joint probability distribution $P_N(\lambda_1, \lambda_2, \ldots \lambda_N, L)$ of the λ-variables depends on the length L of the disordered wire according to the DMPK equation [5, 6],

$$\tfrac{1}{2} l(\beta N + 2 - \beta) \frac{\partial P_N}{\partial L} = \sum_{n=1}^{N} \frac{\partial}{\partial \lambda_n} \lambda_n (1 + \lambda_n) J_N \frac{\partial}{\partial \lambda_n} \frac{P_N}{J_N}, \tag{2.1.8}$$

$$J_N = \prod_{i=1}^{N} \prod_{j=i+1}^{N} |\lambda_i - \lambda_j|^\beta. \tag{2.1.9}$$

In this formulation the ballistic point contact appears as an initial condition

$$\lim_{L \to 0} P_N = \lim_{\Lambda \to \infty} \prod_{n=1}^{N_0} \delta(\lambda_n) \prod_{n=N_0+1}^{N} \delta(\lambda_n - \Lambda). \tag{2.1.10}$$

The closed channels $N_0 + 1 \leq n \leq N$ are irrelevant for conduction and can be integrated out. The reduced distribution function $\tilde{P}_N(\lambda_1, \lambda_2, \ldots \lambda_{N_0}, L)$ is defined by

$$\tilde{P}_N = \int_0^\infty d\lambda_{N_0+1} \int_0^\infty d\lambda_{N_0+2} \cdots \int_0^\infty d\lambda_N \, P_N, \tag{2.1.11}$$

and satisfies the evolution equation

$$\begin{aligned} \tfrac{1}{2} l(\beta N + 2 - \beta) \frac{\partial \tilde{P}_N}{\partial L} &= \sum_{n=1}^{N_0} \frac{\partial}{\partial \lambda_n} \lambda_n (1 + \lambda_n) J_{N_0} \frac{\partial}{\partial \lambda_n} \frac{\tilde{P}_N}{J_{N_0}}, \\ \lim_{L \to 0} \tilde{P}_N &= \prod_{n=1}^{N_0} \delta(\lambda_n). \end{aligned} \tag{2.1.12}$$

We now compare with the unconstricted geometry of Fig. 2-2, which consists of a wire with N_0 transverse modes, length L, and mean free path l/ν. The probability distribution $P_{N_0}(\lambda_1, \lambda_2, \ldots \lambda_{N_0}, L)$ for this geometry is determined by

$$\begin{aligned} \tfrac{1}{2} (l/\nu)(\beta N_0 + 2 - \beta) \frac{\partial P_{N_0}}{\partial L} &= \sum_{n=1}^{N_0} \frac{\partial}{\partial \lambda_n} \lambda_n (1 + \lambda_n) J_{N_0} \frac{\partial}{\partial \lambda_n} \frac{P_{N_0}}{J_{N_0}}, \\ \lim_{L \to 0} P_{N_0} &= \prod_{n=1}^{N_0} \delta(\lambda_n). \end{aligned} \tag{2.1.13}$$

Comparison of Eqs. (2.1.12) and (2.1.13) shows that $\tilde{P}_N = P_{N_0}$ if ν is given by Eq. (2.1.1), as advertized in the Introduction.

We will apply the mapping between constricted and unconstricted geometries to study the distribution of transport properties A of the form $A = \sum_n a(\lambda_n)$, with $\lim_{\lambda \to \infty} a(\lambda) = 0$ (so that only the channels $n \leq N_0$ contribute). We denote by $\mathcal{P}(A, s)$ and $\mathcal{P}_0(A, s)$ the distribution of A in, respectively, the constricted and unconstricted geometries, with $s = L/\text{mean free path}$. Since the mean free path in the constricted geometry is a factor ν smaller than in the unconstricted geometry, we conclude that

$$\mathcal{P}(A, s) = \mathcal{P}_0(A, \nu s). \tag{2.1.14}$$

This is the key result which allows us to solve the problem of a ballistic constriction in a disordered wire, for arbitrary ratio s of wire length to mean free path.

2.1.3 Many-channel point contact

In this Section we study a point contact which has a conductance much greater than e^2/h, so that $N_0 \gg 1$. We mainly consider the metallic regime $Nl/L \gg 1$, in which the conductance of the disordered region separately is also much

greater than e^2/h. Two transport properties are studied in detail: Firstly the conductance G, given by the Landauer formula

$$G = G_0 \sum_n T_n, \tag{2.1.15}$$

where $G_0 = 2e^2/h$ is the conductance quantum. Secondly the shot-noise power S, given by [10]

$$S = S_0 \sum_n T_n(1 - T_n), \tag{2.1.16}$$

with $S_0 = 2e|V|G_0$ for an applied voltage V. We also study the transmission-eigenvalue density, from which other transport properties can be computed. In each case we apply the mapping (2.1.14) between the constricted and unconstricted geometries. The fraction ν which rescales the mean free path in this mapping has, according to Eq. (2.1.1), the series expansion

$$\nu = \frac{1}{N}\left[N_0 - (1 - 2/\beta)(1 - N_0/N) + \mathcal{O}(N_0^{-1})\right]. \tag{2.1.17}$$

To lowest order, $\nu = N_0/N$. The next term, proportional to $1 - 2/\beta$, contributes to the weak localization effect.

A. Weak localization and conductance fluctuations

The mean $\bar{G}$ and variance $\mathrm{Var}\, G$ of the conductance distribution $\mathcal{P}_0(G, \nu s)$ in the unconstricted geometry were computed by Mello and Stone [Eq. (C23) in Ref. [7]]

$$\bar{G}/G_0 = \frac{N_0}{1 + \nu s} + \frac{1}{3}(1 - 2/\beta)\left(\frac{\nu s}{1 + \nu s}\right)^3 + \mathcal{O}(\nu s/N_0), \tag{2.1.18}$$

$$\mathrm{Var}\, G/G_0 = \frac{2}{15}\beta^{-1}\left(1 - \frac{1 + 6\nu s}{(1 + \nu s)^6}\right) + \mathcal{O}(\nu s/N_0). \tag{2.1.19}$$

Substitution of the expansion (2.1.17) yields for the constricted geometry the average conductance $\bar{G} = G_{\mathrm{series}} + \delta G$, with G_{series} given by $G_{\mathrm{series}} = G_0(N_0^{-1} + s/N)^{-1}$ and δG given by (denoting $\gamma \equiv N_0 s/N$):

$$\delta G/G_0 = (1 - 2/\beta)\left[\frac{1}{3}\left(\frac{\gamma}{1 + \gamma}\right)^3 + \left(1 - \frac{N_0}{N}\right)\frac{\gamma}{(1 + \gamma)^2}\right] + \mathcal{O}(s/N). \tag{2.1.20}$$

The term of order $s/N = L/Nl$ can be neglected in the metallic regime. The term G_{series} is the series addition of the Sharvin conductance $G_{\mathrm{Sharvin}} = G_0 N_0$ of the ballistic point contact and the Drude conductance [2] $G_{\mathrm{Drude}} = G_0 Nl/L$ of

[2] The Drude formula for the conductance is $G_{\mathrm{Drude}} = \alpha_d G_0 N l_{\mathrm{tr}}/L$, with l_{tr} the transport mean free path and α_d a number which depends on the dimensionality d of the density of states: $\alpha_2 = \pi/2$ (Fermi circle) and $\alpha_3 = 4/3$ (Fermi sphere). A 1D chain has $\alpha_1 = 2$. These numerical coefficients are absorbed into the mean free path $l \equiv \alpha_d l_{\mathrm{tr}}$ which appears in the DMPK equation.

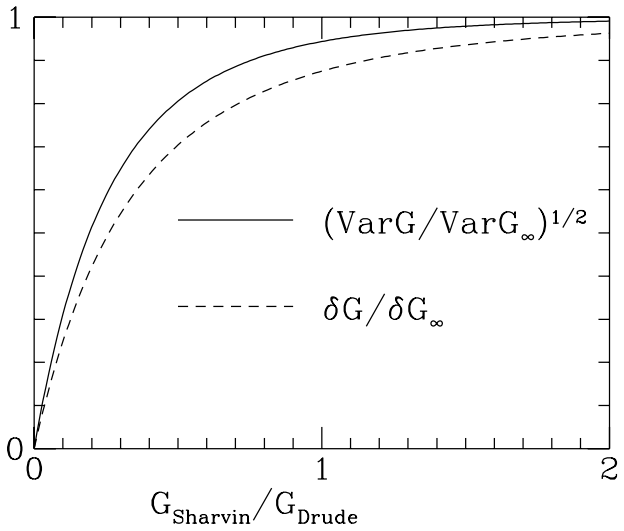

Figure 2-4. Suppression by the point contact of the weak localization correction δG and the root-mean-square conductance fluctuations $(\mathrm{Var}\, G)^{1/2}$. The dashed and solid curves are from Eqs. (2.1.21) and (2.1.22), respectively. For $\gamma = G_{\mathrm{Sharvin}}/G_{\mathrm{Drude}} = N_0 s/N \gg 1$ the curves approach the values δG_∞ and $(\mathrm{Var}\, G_\infty)^{1/2}$ of an unconstricted disordered wire (normalized to unity in the plot).

the disordered region. The term δG is the weak localization correction to the classical series conductance. This term depends on the ratio γ of the Sharvin and Drude conductances as well as on the ratio N_0/N of the width of the point contact and the wide regions. In the limit $N_0/N \to 0$ at constant γ, Eq. (2.1.20) simplifies to

$$\delta G/G_0 = \frac{1}{3}(1 - 2/\beta)[1 - (1+\gamma)^{-3}]. \tag{2.1.21}$$

The variance $\mathrm{Var}\, G$ of the sample-to-sample fluctuations of the conductance around the average depends only on γ (to order s/N). From Eqs. (2.1.17) and (2.1.19) we find

$$\mathrm{Var}\, G/G_0 = \frac{2}{15}\beta^{-1}\left(1 - \frac{1+6\gamma}{(1+\gamma)^6}\right). \tag{2.1.22}$$

In Fig. 2-4 we have plotted δG and $(\mathrm{Var}\, G)^{1/2}$ as a function of $\gamma = G_{\mathrm{Sharvin}}/G_{\mathrm{Drude}}$. (The limit $N_0/N \to 0$ is assumed for δG.) For large γ the curves tend to $\delta G_\infty = \frac{1}{3}(1 - 2/\beta)G_0$ and $\mathrm{Var}\, G_\infty = \frac{2}{15}\beta^{-1}G_0^2$, which are the familiar values [7] for weak localization and universal conductance fluctuations in a wire geometry without a point contact. These values are universal to the extent that they are independent of wire length and mean free path. The presence of a point contact breaks this universality, but only if the Sharvin conductance is smaller than the Drude conductance. For $\gamma > 1$ the universality is quickly restored, according to

$$\frac{\delta G}{\delta G_\infty} = 1 - \gamma^{-3} + \mathcal{O}(\gamma^{-4}), \tag{2.1.23}$$

$$\frac{\mathrm{Var}\, G}{\mathrm{Var}\, G_\infty} = 1 - 6\gamma^{-5} + \mathcal{O}(\gamma^{-6}). \tag{2.1.24}$$

For $\gamma < 1$ both δG and $\mathrm{Var}\, G$ are suppressed by the presence of the point contact, according to

$$\delta G/G_0 = (1 - 2/\beta)\gamma + \mathcal{O}(\gamma^2), \tag{2.1.25}$$

$$\mathrm{Var}\, G/G_0 = 2\beta^{-1}\gamma^2 + \mathcal{O}(\gamma^3). \tag{2.1.26}$$

Maslov, Barnes, and Kirczenow [1] have studied the quasi-ballistic regime $l \gg L$. They consider a geometry as in Fig. 2-1, with $L_1 = L_2$, and relate the variance $\mathrm{Var}\, G$ of the whole system to the variance $\mathrm{Var}\, G_1$ of one of the two disordered segments of length $\frac{1}{2}L$. Their result (in the present notation) is

$$\mathrm{Var}\, G = \gamma^2 (l/L_1)^2\, \mathrm{Var}\, G_1, \tag{2.1.27}$$

in precise agreement with our small-γ result (2.1.26) [since $\mathrm{Var}\, G_1 = 2\beta^{-1}(L_1/l)^2$ for $l \gg L_1$].

So far we have considered the metallic regime $N/s \gg 1$. We now briefly discuss the insulating regime $N/s \ll 1$. In the unconstricted geometry the conductance then has a log-normal distribution [4, 11],

$$\mathcal{P}_0(G, \nu s) = C \exp\left(-\frac{(2\beta^{-1}\nu s/N_0 + \ln G/G_0)^2}{8\beta^{-1}\nu s/N_0} \right), \quad \text{if } \nu s/N_0 \gg 1, \tag{2.1.28}$$

with C a normalization constant. The mapping (2.1.14) implies that the conductance in the constricted geometry has also a log-normal distribution, with mean $\langle \ln G/G_0 \rangle = -2\beta^{-1} s/N$ and variance $\mathrm{Var}(\ln G/G_0) = 4\beta^{-1} s/N$. This distribution is independent of the conductance of the point contact, as long as $N_0 \gg 1$.

B. Suppression of shot noise

The average shot-noise power in the unconstricted geometry is [Eq. (A10) in Ref. [12]]

$$\bar{S}/S_0 = \frac{1}{3} N_0 (1 + \nu s)^{-1} [1 - (1 + \nu s)^{-3}] + \mathcal{O}(1). \tag{2.1.29}$$

The term $\mathcal{O}(1)$ is the weak localization correction on the shot noise, which is not considered here. The mapping (2.1.14) implies for the constricted geometry

$$\bar{S}/S_0 = \frac{1}{3} N_0 (1 + \gamma)^{-1} [1 - (1 + \gamma)^{-3}], \tag{2.1.30}$$

with $\gamma \equiv N_0 s/N$. Since $S_0 N_0 (1 + \gamma)^{-1} = 2e|V| G_{\mathrm{series}} = 2e|I|$ (with I the current through the point contact), we can write Eq. (2.1.30) in terms of the Poisson noise $S_{\mathrm{Poisson}} = 2e|I|$,

$$\bar{S} = \frac{1}{3} S_{\mathrm{Poisson}} [1 - (1 + \gamma)^{-3}]. \tag{2.1.31}$$

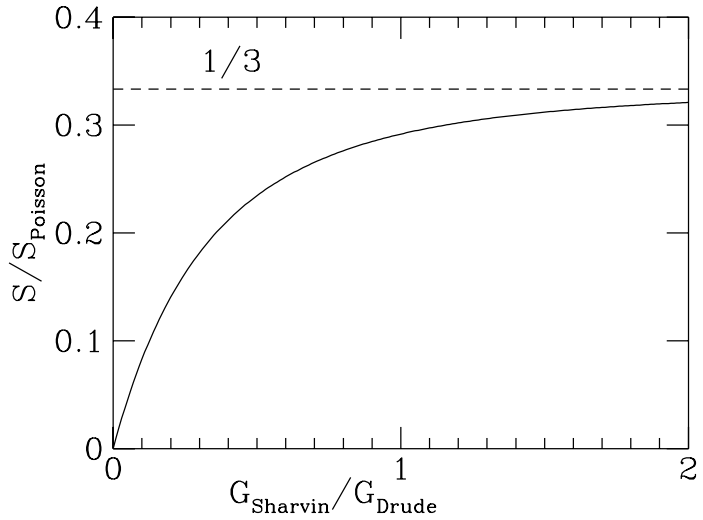

Figure 2-5. Suppression of the shot-noise power S below the Poisson noise $S_{\rm Poisson}$. The solid curve is computed from Eq. (2.1.31). The one-third suppression of a diffusive conductor is indicated by the dashed line.

The suppression of the shot-noise power below the value $S_{\rm Poisson}$ of a Poisson process is plotted in Fig. 2-5, as a function of the ratio γ of Sharvin and Drude conductances. For $\gamma \ll 1$ the shot noise is zero, as expected for a ballistic constriction [10,13–15]. For $\gamma \gg 1$ the shot noise is one third the Poisson noise, as expected for a diffusive conductor [12,16,17]. The formula (2.1.31) describes the crossover between these two regimes.

C. Density of transmission eigenvalues

We consider the eigenvalue densities

$$\rho(x,s) = \left\langle \sum_{n=1}^{N_0} \delta(x-x_n) \right\rangle, \tag{2.1.32}$$

$$\rho(T,s) = \left\langle \sum_{n=1}^{N_0} \delta(T-T_n) \right\rangle, \tag{2.1.33}$$

which are related by $\rho(T,s) = \rho(x,s)|dT/dx|^{-1}$ (with $T = 1/\cosh^2 x$). The (irrelevant) closed channels $n > N_0$ have been excluded from the densities. In the unconstricted geometry we have, according to Ref. [18],

$$\rho(x,\nu s) = \frac{2}{\pi} N_0 \,\mathrm{Im}\, U(x - \mathrm{i}0^+, \nu s) + \mathcal{O}(1), \tag{2.1.34}$$

where the complex function $U(z,s)$ is determined by

$$U = \mathrm{cotanh}\,(z - sU), \quad 0 > \mathrm{Im}\,(z - sU) > -\tfrac{1}{2}\pi. \tag{2.1.35}$$

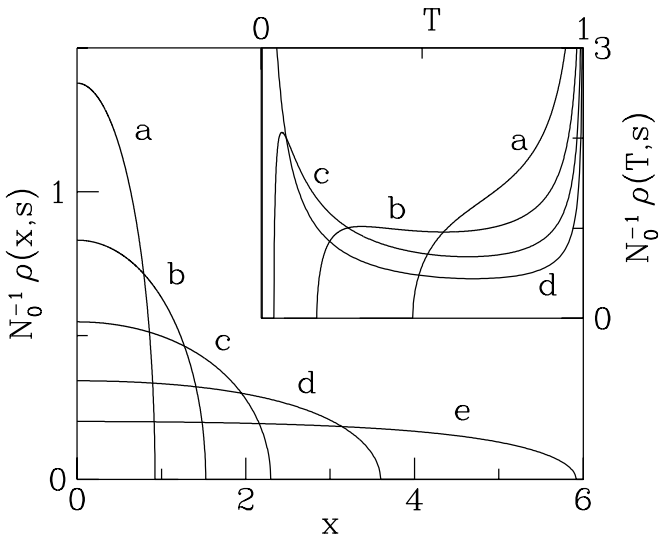

Figure 2-6. Density $\rho(x,s)$ as a function of x, computed from Eqs. (2.1.35) and (2.1.36) for several values of $\gamma \equiv N_0 s/N$. Curves a, b, c, d, and e correspond, respectively, to $\gamma = 0.2$, 0.5, 1, 2, and 4. The inset shows the corresponding density $\rho(T,s) = \rho(x,s)|dT/dx|^{-1}$ of transmission eigenvalues $T = 1/\cosh^2 x$. Note the crossover from unimodal to bimodal distribution near $\gamma = 1$.

The mapping (2.1.14) implies for the constricted geometry

$$\rho(x,s) = \frac{2}{\pi} N_0 \,\mathrm{Im}\, U(x - \mathrm{i}0^+, N_0 s/N) + \mathcal{O}(1). \tag{2.1.36}$$

The solution $\rho(x,s)$ of Eqs. (2.1.35) and (2.1.36) is plotted in Fig. 2-6, for several values of $\gamma \equiv N_0 s/N$. The inset shows the corresponding density of transmission eigenvalues $\rho(T,s)$. For $\gamma \lesssim 1$, $\rho(T,s)$ has a single peak at unit transmission. For $\gamma \gtrsim 1$ a second peak develops near zero transmission, so that the distribution becomes *bimodal*. A crossover from unimodal to bimodal distribution on increasing the disorder has also been found in the case of a tunnel barrier [18, 19]. The difference with a point contact is that for a tunnel barrier the single peak is near zero, rather than near unit, transmission.

2.1.4 Single-channel point contact

In this Section we study a point contact with a quantized conductance of $2e^2/h$, so that $N_0 = 1$. The DMPK equation (2.1.13) for the distribution $P_1(\lambda_1, L) \equiv P(\lambda, L)$ of the single transmitted channel is

$$(l/\nu)\frac{\partial}{\partial L} P(\lambda, L) = \frac{\partial}{\partial \lambda} \lambda(1+\lambda) \frac{\partial}{\partial \lambda} P(\lambda, L), \tag{2.1.37}$$

$$\lim_{L \to 0} P(\lambda, L) = \delta(\lambda), \tag{2.1.38}$$

since $J_1 \equiv 1$. Eq. (2.1.1) for the fraction ν which rescales the mean free path becomes

$$\nu = \frac{2}{\beta N + 2 - \beta}. \tag{2.1.39}$$

The partial differential equation (2.1.37,2.1.38) has been studied as early as 1959 in the context of propagation of radio-waves through a waveguide with a random refractive index [20,21]. In the eighties it was rederived and investigated in great detail [22–26], in connection with the problem of localization in a 1D chain [8,9]. The solution can be written in terms of Legendre functions, or more conveniently in the integral representation

$$P(\lambda, L) = \frac{\mathrm{e}^{-\nu L/4l}}{\sqrt{2\pi(\nu L/l)^3}} \int_{\operatorname{arccosh}(1+2\lambda)}^{\infty} du \frac{u \exp(-u^2 l/4\nu L)}{(\cosh u - 1 - 2\lambda)^{1/2}}. \tag{2.1.40}$$

According to the Landauer formula (2.1.15), the conductance G of the whole system is related to the variable $\lambda \equiv (1-T)/T$ by $G = G_0(1+\lambda)^{-1}$ (with $G_0 = 2e^2/h$). It follows that the resistance $\delta R = 1/G - h/2e^2$ after subtraction of the contact resistance is just given by $\delta R = \lambda/G_0$. In view of the mapping (2.1.14), the resistance distribution $\mathcal{P}(\delta R, s)$ is given by

$$\mathcal{P}(\delta R, s) = \frac{G_0 \mathrm{e}^{-\nu s/4}}{\sqrt{2\pi(\nu s)^3}} \int_{\operatorname{arccosh}(1+2G_0\delta R)}^{\infty} du \frac{u \exp(-u^2/4\nu s)}{(\cosh u - 1 - 2G_0\delta R)^{1/2}}. \tag{2.1.41}$$

The mean and variance of δR can be computed either by integrating the distribution (2.1.41), or directly from the differential equation (2.1.37,2.1.38) [22]. The result is

$$\overline{\delta R} = \frac{1}{2G_0}\left(\mathrm{e}^{2\nu s} - 1\right), \tag{2.1.42}$$

$$\operatorname{Var} \delta R = \frac{1}{6G_0^2}\left(\mathrm{e}^{6\nu s} - \tfrac{3}{2}\mathrm{e}^{4\nu s} + \tfrac{1}{2}\right). \tag{2.1.43}$$

These results hold in both the metallic and the insulating regimes. We now consider in some more detail the metallic regime $N/s \gg 1$. This implies $\nu s \ll 1$. Eqs. (2.1.42) and (2.1.43) reduce to

$$\overline{\delta R} = \frac{2s}{G_0}(\beta N + 2 - \beta)^{-1} + \mathcal{O}(s/N)^2 = (\operatorname{Var} \delta R)^{1/2}. \tag{2.1.44}$$

The complete distribution of the resistance δR (which follows from Eq. (2.1.41) in the limit $\nu s \ll 1$) is the exponential distribution

$$\mathcal{P}(\delta R, s) = \frac{G_0}{\nu s} \exp\left(-\frac{G_0}{\nu s}\delta R\right), \ \delta R \geq 0. \tag{2.1.45}$$

For $N \gg 1$ the width $\nu s \simeq 2s/\beta N$ of the distribution (2.1.45) has the $1/\beta$ dependence announced in the Introduction [Eq. (2.1.2)]. In Fig. 2-7 we have plotted the

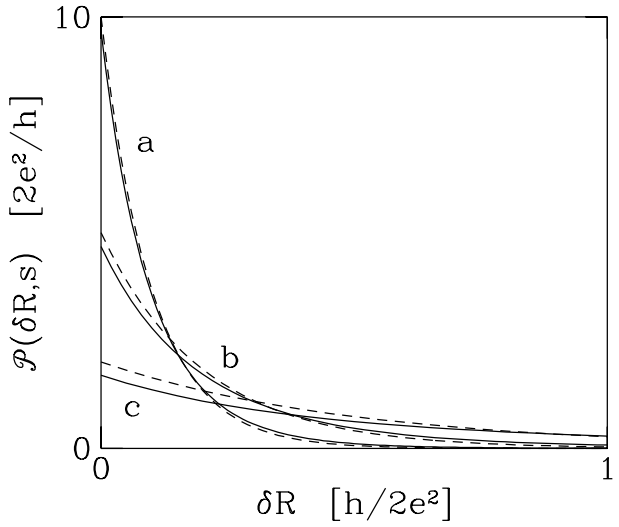

Figure 2-7. Probability distribution of the resistance $\delta R = R - h/2e^2$ of a single-channel point contact, for several values of $\nu s = 2(L/l)(\beta N + 2 - \beta)^{-1}$. Curves a, b, and c, correspond, respectively, to $\nu s = 0.1$, 0.2, and 0.5. The solid curves are computed from Eq. (2.1.41), the dashed curves are the exponential distribution (2.1.45) which is approached in the metallic regime $\nu s \ll 1$.

exact distribution (2.1.41) [solid curves] for several values of s and compared with the metallic limit (2.1.45) [dashed curves]. For $\nu s \lesssim 0.1$ [curves labeled a] the two results are almost indistinguishable.

To make connection with some of the recent literature, we remark that the exponential resistance distribution (2.1.45) implies for the conductance the distribution

$$\mathcal{P}(G,s) = \frac{G_0}{\nu s} G^{-2} \exp\left(\frac{1 - G_0/G}{\nu s}\right),\ 0 \le G \le G_0, \tag{2.1.46}$$

which is strongly peaked at $G = G_0$. This is completely different from the conductance distribution of a quantum dot which is weakly coupled by two point contacts to electron reservoirs [27,28].

2.1.5 Numerical simulations

To test the analytical predictions we have carried out numerical simulations of the Anderson model in the geometry of Fig. 2-3, using the recursive Green's function technique [29]. The disordered region (dotted) was modeled by a tight-binding Hamiltonian on a square lattice (lattice constant a), with a random impurity potential at each site (uniformly distributed between $\pm\frac{1}{2}U_{\rm d}$). The constriction was introduced by assigning a large potential energy to sites at one end of the lattice (black in Fig. 2-1), so as to create a nearly impenetrable barrier with an

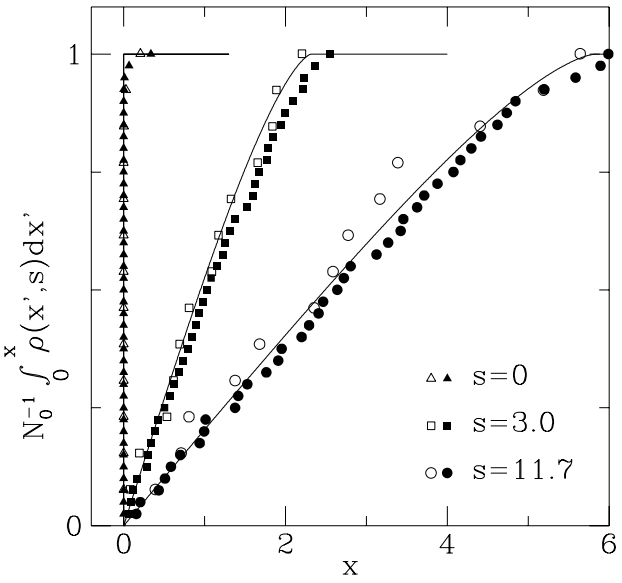

Figure 2-8. Comparison between theory and simulation of the integrated eigenvalue density for $N_0/N = 1/3$ and for three different disorder strengths ($s = 0, 3, 11.7$). Solid curves are from Eqs. (2.1.35) and (2.1.36), data points are the N_0 smallest x_n's from the simulation plotted in ascending order versus n/N_0 [filled data points are for a square geometry, open points for a rectangular disordered region ($L/W = 3$)].

opening in the center. The constriction itself contained no disorder (the disordered region started at two sites from the barrier). The Fermi energy was chosen at $E_F = 1.5\,u_0$ from the band bottom (with $u_0 \equiv \hbar^2/2ma^2$). The ratio s of sample length to mean free path which appears in the theory was computed numerically from $\mathrm{Tr}\, t_d t_d^\dagger = N(1+s)^{-1}$, with t_d the transmission matrix of the disordered region without the constriction.[3]

The simulations for the many-channel and single-channel point contact are discussed in two separate sub-sections.

A. Many-channel point contact

Two geometries were considered for the wide disordered region: a square geometry ($L = W = 285\,a$, corresponding to $N = 119$), and a rectangular geometry ($L = 285\,a$, $W = 93\,a$, corresponding to $N = 39$). In each case the width of the constriction was $\frac{1}{3}W$ (corresponding to $N_0 = 40$ and $N_0 = 13$ in the square and rectangular geometries, respectively). The length of the constriction was one site. The strength U_d of the impurity potential was varied between 0 and $1.5\,u_0$, corresponding to s between 0 and 11.7.

In Fig. 2-8 we compare the integrated eigenvalue density $N_0^{-1}\int_0^x dx'\,\rho(x',s)$,

[3]The identification $\mathrm{Tr}\, t_d t_d^\dagger = N(1+s)^{-1}$ has the status of an interpolation formula between the Sharvin and Drude conductances, which differs by only a few percent from the exact result: M. J. M. de Jong, Phys. Rev. B **49**, 16070 (1994).

which is the quantity following directly from the simulation. The points are raw data from a single sample. (Sample-to-sample fluctuations are small, because the x_n's are self-averaging quantities [4].) The data is in good agreement with the analytical result of Sec. 2.1.3C, *without any adjustable parameters*. No significant geometry dependence was found (compare open and closed symbols in Fig. 2-8).

B. Single-channel point contact

We considered a square geometry ($L = W = 47\,a$, corresponding to $N = 20$), and a rectangular geometry ($L = 47\,a$, $W = 23\,a$, corresponding to $N = 10$). The point contact was three sites wide and two sites long, corresponding to $N_0 = 1$. (The conductance in the absence of disorder was within 5% of $2e^2/h$.) The distribution $P(\delta R, s)$ of the resistance $\delta R \equiv R - h/2e^2$ was computed by collecting data for some 10^4 realizations of the impurity potential. To compare the cases $\beta = 1$ and $\beta = 2$, we repeated the simulations in the presence of a magnetic field of 50 flux quanta h/e through the disordered region. (The magnetic field was graded to zero in the ideal leads.) Two disorder strengths were considered: $U_\mathrm{d} = 1.5\,u_0$ (corresponding to $s = 1.8$) and $U_\mathrm{d} = 3.0\,u_0$ (corresponding to $s = 8.3$). The results are collected in Fig. 2-9 and are in good agreement with the theoretical prediction (2.1.41), again without any adjustable parameters. The theory agrees comparably well with the simulations for the square and rectangular geometries, which shows that the condition $L \gg W$ for the validity of the DMPK equation can be relaxed to a considerable extent.

We find it altogether quite remarkable that the amusingly simple mapping (2.1.14) between the constricted and unconstricted geometries is capable of reliably predicting the *complete* distribution of the point-contact resistance, including the effect of broken time-reversal symmetry. We know of no other conventional theoretical technique which could do the same.

2.2 Conductance fluctuations in a disordered double-barrier junction

Resonant tunneling through two planar barriers in series is a textbook problem in quantum mechanics. Because of the separation of longitudinal and transverse motion, the problem is essentially one-dimensional and can be solved in an elementary way. Realistic double-barrier junctions contain in general some amount of disorder in the region between the barriers. At low temperatures and small applied voltages, the inelastic electron-phonon and electron-electron scattering processes are suppressed, but the elastic scattering by impurities remains. Scattering events couple the transverse and longitudinal motion of the tunneling electron, which substantially complicates the problem but also leads to novel physical effects.

The effects of disorder have been studied in the past [30–33] with an em-

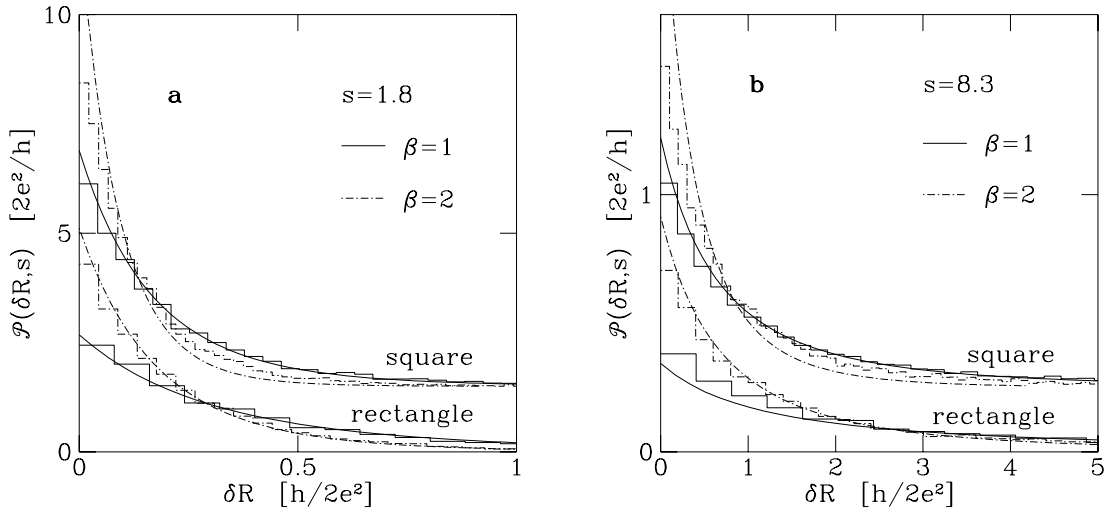

Figure 2-9. Comparison between theory and simulation of the distribution of the excess resistance δR of a single-channel point contact, for $s = 1.8$ (a) and $s = 8.3$ (b). The histograms are the numerical data (for square and rectangular disordered regions), the smooth curves are computed from Eq. (2.1.41) — without any adjustable parameters. Solid curves are for zero magnetic field ($\beta = 1$), dash-dotted curves for a magnetic flux of $50\,h/e$ through the disordered region ($\beta = 2$). For clarity, the curves for the square geometry are offset vertically by 1.5 and 0.25 in figures (a) and (b), respectively.

phasis on isolated transmission resonances (energy spacing between the resonances much greater than their width). Those studies are relevant for tunneling through a semiconductor quantum well, where the resonances are widely separated because the barrier separation L is comparable to the Fermi wavelength λ_F. Here we consider the opposite regime $L \gg \lambda_F$ of strongly overlapping resonances, relevant to metal structures (where λ_F is very short, comparable to the inter-atomic separation), or to tunneling in the plane of a two-dimensional electron gas (where L can be quite long, because of the large phase-coherence length). Two types of disorder can play a role, interface roughness at the barriers and impurities between the barriers. Interface roughness leads to mesoscopic (sample-to-sample) fluctuations in the conductance even in the absence of any phase coherence, because the tunnel probability Γ of a single barrier depends strongly on its thickness. Conductance fluctuations for a single rough tunnel barrier have been studied by Raikh and Ruzin [34]. Here we consider the case of impurity scattering in the absence of interface roughness. Phase coherence is then essential.

A methodological difference with earlier work on resonant tunneling is our use of random-matrix theory to describe the mode-mixing in the inter-barrier region. We assume that the disorder is weak enough that its effect on the average conductance is negligibly small. This requires a mean free path $l \gg \Gamma L$. Still,

the disorder should be sufficiently strong to fully mix the transverse modes in the inter-barrier region. This requires both $l \ll L/\Gamma$ and $W \ll L/\Gamma$ (where W is the transverse dimension of the junction). We may then describe the disorder-induced mode-mixing by a random $N \times N$ unitary matrix (N being the total number of propagating transverse modes at the Fermi energy). This single assumption permits a complete analytical solution of the statistical properties of the conductance, using basic results for the so-called circular ensemble of random matrices [35]. The circular ensemble is fully characterized by the symmetry index β, which equals 1 in the presence of time-reversal symmetry (circular orthogonal ensemble) and 2 if time-reversal symmetry is broken by a magnetic field (circular unitary ensemble). (A third possibility, $\beta = 4$, applies to zero magnetic field in the presence of strong spin-orbit scattering.)

As described in Section 2.2.1, we find that the conductance G of the double-barrier junction exhibits sample-to-sample fluctuations around the classical series conductance

$$G_{\rm series} = (2e^2/h)N(1/\Gamma_1 + 1/\Gamma_2)^{-1}. \tag{2.2.1}$$

(We denote by Γ_1 and Γ_2 the transmission probabilities per mode through barrier 1 and 2, and assume that these are mode-independent and $\ll 1$.) We find that the root-mean-square fluctuations rms G of the conductance depend only on the ratio $\nu = \Gamma_1/\Gamma_2$ of the two transmission probabilities, according to

$$\text{rms}\, G = \frac{4e^2}{h}\beta^{-1/2}\frac{\nu}{(1+\nu)^2}. \tag{2.2.2}$$

Corrections to Eq. (2.2.2) are smaller by a factor $e^2/hG_{\rm series}$, which is $\ll 1$ if $N\Gamma_i \gg 1$. For a symmetric junction ($\nu = 1$) the fluctuations are of order e^2/h, independent of N or Γ_i (as long as $N\Gamma_i \gg 1$). This universality is reminiscent of the universal conductance fluctuations in diffusive metals [36, 37]. Just as in those systems, we expect the sample-to-sample fluctuations to be observable in a single sample, as reproducible fluctuations of the conductance as a function of Fermi energy or magnetic field.

Eq. (2.2.2) assumes weak disorder, $l \gg \Gamma_i L$ (but still $l \ll L/\Gamma_i$). We generalize our results in Sec. 2.2.2 to stronger disorder, when the effects of the impurities on the average conductance have to be taken into account. We do this by means of the Dorokhov-Mello-Pereyra-Kumar (DMPK) equation [5,6]. We find that impurity scattering leads to the appearance of a weak-localization effect on the average conductance (observable as a negative magnetoresistance). The conductance fluctuations become independent of Γ_1 and Γ_2 if $L \gg l(\Gamma_1^{-1} + \Gamma_2^{-1})$. A similar conclusion was reached previously by Iida, Weidenmüller, and Zuk [38], who studied the conductance fluctuations of a chain of disordered grains as a function of the coupling strength to two electron reservoirs. These authors found that the universal conductance fluctuations are recovered for a chain length L much greater than some length L_0 which is parametrically greater than the mean free path. A

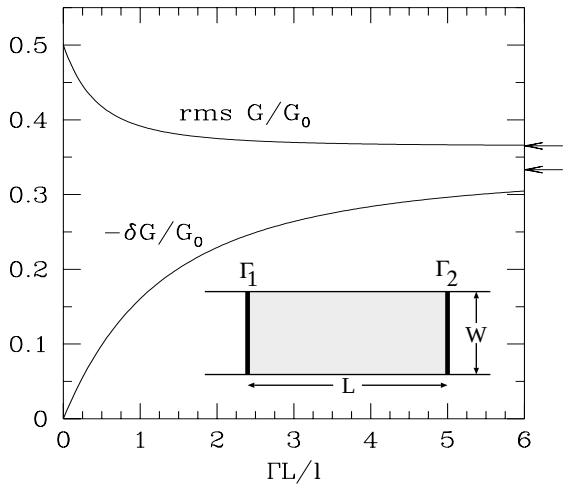

Figure 2-10. Weak-localization correction δG to the average conductance (in units of $G_0 = 2e^2/h$) and root-mean-square fluctuations $\mathrm{rms}\, G \equiv (\mathrm{Var}\, G)^{1/2}$, computed from Eqs. (2.2.21) and (2.2.22) for $\beta = 1$. The arrows give the limit $\Gamma L/l \gg 1$. The inset shows the geometry of the double-barrier junction (the disordered region is dotted). The curves plotted in the figure are for a symmetric junction, $\Gamma_1 = \Gamma_2 \equiv \Gamma \ll 1$.

more detailed comparison with Ref. [38] is not possible, because we consider a homogeneously disordered conductor rather than a chain of disordered grains.

To test our random-matrix description of mode-mixing by weak disorder, we present in Sec. 2.2.3 results from a numerical simulation of a disordered double-barrier junction defined on a two-dimensional lattice. The agreement with the theory is quite reasonable.

2.2.1 Double-barrier junction with strong mode-mixing

The double-barrier junction considered is shown schematically in the inset of Fig. 2-10. Since we assume $\lambda_F \ll L$, the scattering matrix S of the whole system can be constructed from the scattering matrices S_i of the individual barriers. Similar to the case of a wire geometry (1.1.5), the $2N \times 2N$ unitary matrix S_i can be written as a polar decomposition [4, 39]

$$\begin{aligned} S_i &\equiv \begin{pmatrix} r_i & t_i' \\ t_i & r_i' \end{pmatrix} \\ &= \begin{pmatrix} U_i & 0 \\ 0 & V_i \end{pmatrix} \begin{pmatrix} -\mathrm{i}(1-\Gamma_i)^{1/2} & \Gamma_i^{1/2} \\ \Gamma_i^{1/2} & -\mathrm{i}(1-\Gamma_i)^{1/2} \end{pmatrix} \begin{pmatrix} U_i' & 0 \\ 0 & V_i' \end{pmatrix}, \end{aligned} \tag{2.2.3}$$

where the U's and V's are $N \times N$ unitary matrices. In zero magnetic field, $U_i' = U_i^{\mathrm{T}}$ and $V_i' = V_i^{\mathrm{T}}$, so that S_i is symmetric — as it should be in the presence of time-

reversal symmetry. The transmission matrix t of the whole system is given by

$$t = t_2(1 - r_1' r_2)^{-1} t_1. \tag{2.2.4}$$

Substitution of the polar decomposition (2.2.3) yields the matrix product $tt^\dagger$ in the form

$$\begin{aligned} tt^\dagger &= V_2 \left[a + \tfrac{1}{2} b(\Omega + \Omega^\dagger) \right]^{-1} V_2^\dagger, && (2.2.5)\\ \Omega &= U_2' V_1 V_1' U_2, && (2.2.6)\\ a &= [1 + (1 - \Gamma_1)(1 - \Gamma_2)]/\Gamma_1\Gamma_2, && (2.2.7)\\ b &= 2\sqrt{(1 - \Gamma_1)(1 - \Gamma_2)}/\Gamma_1\Gamma_2. && (2.2.8) \end{aligned}$$

The eigenvalues T_n of $tt^\dagger$ are related to the eigenvalues $\exp(i\phi_n)$ of Ω by

$$T_n = (a + b\cos\phi_n)^{-1}. \tag{2.2.9}$$

The T_n's determine the conductance G of the double-barrier junction, according to the Landauer formula 2.1.15.

We consider an *isotropic* ensemble of double-barrier junctions, analogous to the isotropic ensemble of disordered wires [4]. We assume that $l \ll L/\Gamma_i$ and $W \ll L/\Gamma_i$, so that the tunneling is accompanied by strong mode-mixing: An electron entering the junction in mode n is randomly distributed among all modes m before leaving the junction. We assume in this section that mode-mixing is the dominant effect of the disorder, and that the reduction of the average conductance by the impurity scattering can be neglected. This requires $l \gg \Gamma_i L$. (The case of stronger disorder is treated in the next section.) In the polar decomposition (2.2.3) the mode-mixing is accounted for by the unitary matrices U and V. The number of different unitary matrices is 2β, where $\beta = 1$ in zero magnetic field and $\beta = 2$ if time-reversal symmetry is broken by a magnetic field. The isotropic ensemble is the ensemble where the 2β unitary matrices are *independently* and *uniformly* distributed over the unitary group. In other words, the U's and V's are drawn independently from the circular unitary ensemble (CUE) of random-matrix theory [35].

To determine the statistics of the conductance (2.1.15) we need the probability distribution $P(\{\phi_n\})$ of the eigenvalues of Ω. For $\beta = 2$, $\Omega = U_2' V_1 V_1' U_2$ is the product of four independent matrices from the CUE, and hence Ω is also distributed according to the CUE. For $\beta = 1$, $\Omega = U_2^{\mathrm{T}} V_1 V_1^{\mathrm{T}} U_2$ is of the form WW^{T} with W a member of the CUE. The ensemble of Ω is then the circular orthogonal ensemble (COE). The distribution of the eigenvalues in the CUE and COE is given by [35]

$$P(\{\phi_n\}) = C \prod_{n<m} \left| \exp(i\phi_n) - \exp(i\phi_m) \right|^\beta, \tag{2.2.10}$$

where C is a normalization constant.

We compute the average $\langle A\rangle$ and variance $\mathrm{Var}\,A = \langle A^2\rangle - \langle A\rangle^2$ of linear statistics $A = \sum_{n=1}^{N} a(\phi_n)$ on the eigenphases ϕ_n. Since in the circular ensemble the ϕ_n's are uniformly distributed in $(0, 2\pi)$, the average is exactly equal to

$$\langle A\rangle = \frac{N}{2\pi}\int_0^{2\pi} \mathrm{d}\phi\, a(\phi). \tag{2.2.11}$$

An exact expression for the variance can also be given [35], but is cumbersome to evaluate. For $N \gg 1$ we can use a variation on the Dyson-Mehta formula [40] (derived in App. A) [41],

$$\mathrm{Var}\,A = \frac{1}{\pi^2\beta}\sum_{n=1}^{\infty} n|a_n|^2 + \mathcal{O}(N^{-1}), \tag{2.2.12}$$

$$a_n = \int_0^{2\pi} \mathrm{d}\phi\, \mathrm{e}^{\mathrm{i}n\phi} a(\phi). \tag{2.2.13}$$

For the conductance [given by Eqs. (2.2.9) and (2.1.15)], we substitute $a(\phi) = (a + b\cos\phi)^{-1}$, with Fourier coefficients
$a_n = 2\pi(a^2 - b^2)^{-1/2} b^{-n}\left[(a^2 - b^2)^{1/2} - a\right]^n$. The results are

$$\langle G/G_0\rangle = N(1/\Gamma_1 + 1/\Gamma_2 - 1)^{-1}, \tag{2.2.14}$$

$$\mathrm{Var}\,G/G_0 = \frac{4}{\beta}\frac{(1-\Gamma_1)(1-\Gamma_2)\Gamma_1^2\Gamma_2^2}{(\Gamma_1+\Gamma_2-\Gamma_1\Gamma_2)^4}. \tag{2.2.15}$$

Equation (2.2.14) for the average conductance is what one would expect from classical addition of the resistances $(N\Gamma_i G_0)^{-1}$ of the individual barriers. (The -1 in Eq. (2.2.14) corrects for a double counting of the contact resistance and becomes irrelevant for $\Gamma_i \ll 1$.) Each member of the ensemble contains a different set of overlapping transmission resonances, and the ensemble average removes any trace of resonant tunneling in $\langle G\rangle$. In a previous paper [42], we have shown that the average conductance differs drastically from the series conductance if the double-barrier junction is connected to a superconductor, but here we consider only normal-metal conductors.

Eq. (2.2.15) for the conductance fluctuations tells us that $\mathrm{Var}\,G$ becomes completely independent of N in the limit $N \to \infty$. [More precisely, corrections to Eq. (2.2.15) are of order $\langle G/G_0\rangle^{-1}$, which is $\ll 1$ if $N\Gamma_i \gg 1$.] Since $\Gamma_i \ll 1$, we may simplify Eq. (2.2.15) to

$$\mathrm{Var}\,G/G_0 = \frac{4}{\beta}\frac{\Gamma_1^2\Gamma_2^2}{(\Gamma_1+\Gamma_2)^4}, \tag{2.2.16}$$

which depends only on the ratio Γ_1/Γ_2 and not on the individual Γ_i's. The variance reaches a Γ-independent maximum for two equal barriers,

$$\mathrm{Var}\,G/G_0 = \tfrac{1}{4}\beta^{-1}, \quad \text{if } \Gamma_1 = \Gamma_2. \tag{2.2.17}$$

The variance is almost twice the result $\frac{2}{15}\beta^{-1}$ for an isotropic ensemble of disordered wires [43,44], and precisely twice the result $\frac{1}{8}\beta^{-1}$ for an isotropic ensemble of ballistic quantum dots [28, 38].

2.2.2 Effects of strong disorder

In this section we relax the assumption $l \gg \Gamma_i L$ of Sec. II, to include the case that the impurity scattering is sufficiently strong to affect the average conductance. We assume $W \ll L$, so that we are justified in using an isotropic distribution for the scattering matrix S_L of the inter-barrier region [4]. The scattering matrix S of the entire system is now composed from the three scattering matrices S_1, S_L, and S_2 in series. The composition is most easily carried out in terms of the transfer matrices M_1, M_L, and M_2 associated with S_1, S_L, and S_2, respectively. The transfer matrix M of the entire system is the matrix product $M = M_2 M_L M_1$, so the total distribution $P(M)$ is a convolution of the individual distributions $P_1(M_1), P_L(M_L)$, and $P_2(M_2)$: $P = P_2 * P_L * P_1$. The convolution $*$ is defined in Eq. (2.1.5). The isotropy assumption implies that each distribution $P_i(M_i)$ is only a function of the eigenvalues of $M_i M_i^\dagger$.

We now use the fact that the convolution of isotropic distributions of transfer matrices commutes. (A proof is given in Appendix A.) This permits us to consider an equivalent system, with transfer matrix $M = M_L M_2 M_1$, where all disorder is at one side of the double-barrier junction — instead of in between the barriers. The L-dependence of the distribution of transmission eigenvalues for this system is governed by the DMPK equation (1.1.6).The initial condition of Eq. (1.1.6) now corresponds to taking $M_L = 1$, which implies for P the isotropic ensemble given by Eq. (2.2.10).

To compute the L-dependence of the mean and variance of the conductance, we use the method of moments of Mello and Stone [43, 44], who have derived a hierarchy of differential equations for the moments of $\mathcal{T}_q \equiv \sum_{n=1}^{N} T_n^q$. The hierarchy closes order by order in an expansion in powers of $1/N$. Mello and Stone considered a ballistic initial condition, corresponding to $\langle \mathcal{T}_q^p \rangle \to N^p$ for $s \equiv L/l \to 0$. We have the different initial condition of a double-barrier junction. The differential equations and initial conditions for the moments are given in App. B. For the mean conductance and its variance we obtain

$$\begin{aligned} \langle G/G_0 \rangle &= \frac{N}{s+\rho} + \frac{1}{3}(1-2/\beta) \\ &\quad - \frac{1-2/\beta}{(s+\rho)^3}\left(s^2 - s(a-\rho-\rho^2) + \tfrac{1}{3}\rho^3\right), \qquad (2.2.18) \\ \mathrm{Var}\, G/G_0 &= \frac{2}{15\beta} + \frac{2}{\beta(s+\rho)^6}\Big(s^2(\tfrac{1}{2}a^2 + \tfrac{1}{2}\rho^2 - 2a\rho^2 + \rho^4) \\ &\quad + s(-2a^2\rho + 2a\rho^3 - \tfrac{2}{5}\rho^5) + \tfrac{1}{2}a^2\rho^2 - \tfrac{1}{2}\rho^4 - \tfrac{1}{15}\rho^6\Big), \qquad (2.2.19) \end{aligned}$$

where a has been defined in Eq. (2.2.5) and ρ is defined by

$$\rho = 1/\Gamma_1 + 1/\Gamma_2 - 1. \qquad (2.2.20)$$

Corrections to Eqs. (2.2.18) and (2.2.19) are of order $(s+\rho)/N$. For two equal barriers ($\Gamma_1 = \Gamma_2 \equiv \Gamma$) in the limit $\Gamma \to 0$ at fixed Γs, Eqs. (2.2.18) and (2.2.19)

simplify to

$$\begin{aligned} \delta G/G_0 &\equiv \langle G/G_0\rangle - N(s+\rho)^{-1} \\ &= \frac{1}{3}(1-2/\beta) - \frac{1-2/\beta}{(2+\Gamma s)^3}\left(\frac{8}{3}+2\Gamma s\right), \qquad (2.2.21) \\ \mathrm{Var}\, G/G_0 &= \frac{2}{15\beta} + \frac{4}{\beta(2+\Gamma s)^6}\left(\Gamma^2 s^2 + \frac{8}{5}\Gamma s + \frac{28}{15}\right). \qquad (2.2.22) \end{aligned}$$

Eqs. (2.2.21) and (2.2.22) are plotted in Fig. 1 (for $\beta = 1$). In the limit of large disorder ($\Gamma s \gg 1$), we recover the familiar results [43,44] for a disordered wire: $\delta G/G_0 = \frac{1}{3}(1-2/\beta)$, $\mathrm{Var}\, G/G_0 = \frac{2}{15}\beta^{-1}$ (indicated by arrows in Fig. 1). In the opposite limit $\Gamma s \ll 1$, we find $\delta G = 0$, $\mathrm{Var}\, G/G_0 = \frac{1}{4}\beta^{-1}$ — as in Sec. 2.2.1 [cf. Eqs. (2.2.14) and (2.2.17)].

2.2.3 Numerical simulations

To test our results we have performed numerical simulations, using the recursive Green's function method of Ref. [29], which is described in Sec. 2.1.5:. The sample geometry consisted of a rectangle with length $L = 142d$, and width $W = 71d$ (corresponding to $N = 30$ propagating modes). We chose $U_\mathrm{d} = 0.6\,u_0$, corresponding to $L/l = 0.9$. The transfer matrix M_L was computed numerically, and then multiplied with the transfer matrices M_1 and M_2 of the two barriers (which we constructed analytically, given the mode-independent tunnel probabilities Γ_1 and Γ_2). We took $\Gamma_2 = 0.15$ and varied Γ_1 between 0.05 and 0.5. These parameter values were chosen in order to be close to the regime $\Gamma_i L \ll l \ll L/\Gamma_i$, $W \ll L/\Gamma_i$ in which disorder is expected to cause strong mode-mixing, without having a large effect on the average conductance (the regime studied in Sec. 2.2.1).

In Fig. 2-11 we show the comparison between theory and simulation. The solid curve is $\mathrm{Var}\, G/G_0$ computed from 2250 realizations of the disorder potential. The dotted curve is the theoretical prediction from Eq. (2.2.19) for the parameter values of the simulation (and for $\beta = 1$, since there was no magnetic field). There are no adjustable parameters. The agreement is quite reasonable. It is likely that the remaining discrepancy is due to the fact that the theoretical condition $N\Gamma_i \gg 1$ was not well met in the simulation (where $N\Gamma_2 = 4.5$). The value $N = 30$ of the simulation is already at the limit of our computational capabilities and we are not able to provide a more stringent numerical test of the theory.

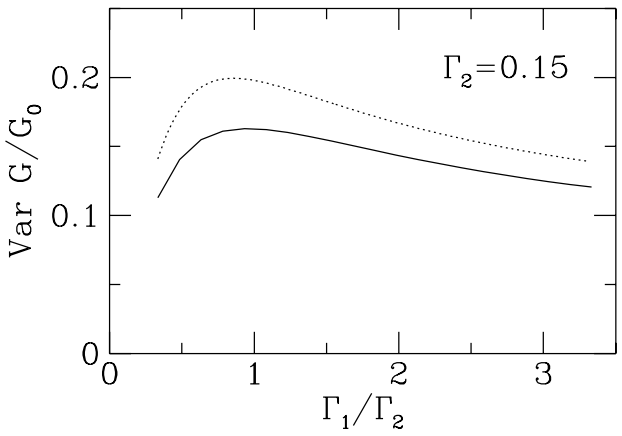

Figure 2-11. Solid curve: variance of the conductance from a numerical simulation of an ensemble of disordered double-barrier junctions ($L/W = 2$, $N = 30$, $s = 0.9$), as a function of the ratio Γ_1/Γ_2, with $\Gamma_2 = 0.15$ held constant. There is no magnetic field ($\beta = 1$). The dashed curve is the prediction from Eq. (2.2.19) . There are no adjustable parameters.

Appendix A: Isotropically distributed transfer matrices commute

We wish to show that the probability distribution $p(M)$ of a product $M = M_1 M_2 M_3 \cdots$ of transfer matrices is independent of the order of the matrix product, under the assumption that the matrices M_i are independently distributed with isotropic distributions p_i. Since $p = p_1 * p_2 * p_3 \cdots$, it is sufficient to show that the convolution

$$p_i * p_j(M) = \int dM_j \, p_i(MM_j^{-1}) p_j(M_j) \tag{A.1}$$

of any two isotropic distributions commutes.

By definition, the distribution $p(M)$ is isotropic if it is only a function of the eigenvalues of the product $MM^\dagger$. This implies that $p(M) = p(M^{\mathrm{T}})$. (The superscripts † and T denote, respectively, the hermitian conjugate and the transpose of a matrix.) As shown by Mello et al. [6, 7], the convolution of two isotropic distributions is again isotropic. Hence

$$\begin{aligned} p_i * p_j(M) &= p_i * p_j(M^{\mathrm{T}}) \\ &= \int dM_j \, p_i(M^{\mathrm{T}} M_j^{-1}) p_j(M_j) \\ &= \int dM_j \, p_i(M_j^{\mathrm{T}\,-1} M) p_j(M_j^{\mathrm{T}}) \end{aligned}$$

$$\begin{aligned} &= \int dM_i\, p_i(M_i) p_j(MM_i^{-1}) \\ &= p_j * p_i(M), \end{aligned} \tag{A.2}$$

which proves the commutativity of the convolution of isotropic distributions.

Appendix B: Dyson-Mehta formula for the circular ensemble

The variance $\mathrm{Var}\, A$ of a linear statistic $A = \sum_{n=1}^{N} a(\phi_n)$ on the eigenphases is given by a double integral,

$$\mathrm{Var}\, A = -\int_0^{2\pi} \mathrm{d}\phi \int_0^{2\pi} \mathrm{d}\phi'\, a(\phi) a(\phi') K(\phi, \phi'), \tag{B.1}$$

over the two-point correlation function

$$K(\phi, \phi') = \langle \rho(\phi) \rangle \langle \rho(\phi') \rangle - \langle \rho(\phi) \rho(\phi') \rangle. \tag{B.2}$$

The brackets $\langle \cdots \rangle$ denote an average over the circular ensemble, and

$$\rho(\phi) = \sum_{n=1}^{N} \delta(\phi - \phi_n) \tag{B.3}$$

is the microscopic density of eigenphases. In this appendix we compute $K(\phi, \phi')$ in the large N-limit, using the method of functional derivatives of Ref. [45]. This leads to Eq. (2.2.12) for $\mathrm{Var}\, A$, which is the analogue for the circular ensemble of the Dyson-Mehta formula for the Gaussian ensemble [40]. The analogy is straightforward, but we have not found it in the literature [41].

We consider a generalized circular ensemble, with probability distribution

$$P_V(\{\phi_n\}) = C \exp\left[-\beta \left(\sum_{i<j} U(\phi_i - \phi_j) + \sum_{i=1}^{N} V(\phi_i) \right) \right], \tag{B.4}$$

$$C^{-1} = \int_0^{2\pi} \mathrm{d}\phi_1 \int_0^{2\pi} \mathrm{d}\phi_2 \cdots \int_0^{2\pi} \mathrm{d}\phi_N\, P_V(\{\phi_n\}), \tag{B.5}$$

$$U(\phi) = -\ln |2 \sin \tfrac{1}{2}\phi|. \tag{B.6}$$

The "potential" $V(\phi)$ is arbitrary. If $V \equiv 0$, Eq. (B.4) is the same as the distribution (2.2.10) of the circular ensemble. The brackets $\langle \cdots \rangle_V$ denote an average with the V-dependent distribution (B.4). Following Ref. [45], we express the two-point correlation function as a functional derivative of the density with respect to the potential,

$$K(\phi, \phi') = \frac{1}{\beta} \frac{\delta \langle \rho(\phi) \rangle_V}{\delta V(\phi')}. \tag{B.7}$$

The functional derivative can be computed in the large-N limit from the relationship [46]

$$-\int_0^{2\pi} \mathrm{d}\phi'\, U(\phi-\phi')\langle\rho(\phi')\rangle_V = V(\phi) + \text{const.} \tag{B.8}$$

Corrections to Eq. (B.8) are smaller by a factor $1/N$. The additive constant is obtained from the normalization $\int \mathrm{d}\phi\, \langle\rho(\phi)\rangle_V = N$.

Fourier transformation of Eq. (B.8) yields

$$-\frac{\pi}{|n|}\langle\rho_n\rangle_V = V_n, \quad n \neq 0. \tag{B.9}$$

We have defined the Fourier coefficients

$$f_n = \int_0^{2\pi} \mathrm{d}\phi\, \mathrm{e}^{\mathrm{i}n\phi} f(\phi), \tag{B.10}$$

and we have used that $U_n = \pi/|n|$ for $n \neq 0$. From Eqs. (B.7) and (B.8) we see that $K(\phi,\phi') = K(\phi-\phi')$ depends on the difference $\phi-\phi'$ only, and is independent of V. The Fourier coefficients of $K(\phi)$ are

$$K_n = -|n|/\pi\beta, \tag{B.11}$$

for $n \neq 0$. Since $K_0 = 0$ by definition, Eq. (B.11) holds in fact for all n. Inversion of the Fourier transform yields the correlation function

$$K(\phi) = -\frac{1}{\pi^2\beta}\frac{\mathrm{d}^2}{\mathrm{d}\phi^2}\ln\left|\sin\tfrac{1}{2}\phi\right|, \tag{B.12}$$

which has an integrable singularity at $\phi = 0$.
For $\phi \neq 0$, $K(\phi) = [4\pi^2\beta\sin^2(\phi/2)]^{-1}$. Substitution of Eq. (B.12) into Eq. (B.1) gives the required analogue of the Dyson-Mehta formula for the large N-limit of the variance of a linear statistic,

$$\begin{aligned}\operatorname{Var} A &= -\frac{1}{\pi^2\beta}\int_0^{2\pi}\mathrm{d}\phi\int_0^{2\pi}\mathrm{d}\phi'\left(\frac{\mathrm{d}a(\phi)}{\mathrm{d}\phi}\right)\left(\frac{\mathrm{d}a(\phi')}{\mathrm{d}\phi'}\right)\ln\left|\sin\frac{\phi-\phi'}{2}\right| \\ &= \frac{1}{\pi^2\beta}\sum_{n=1}^{\infty} n|a_n|^2. \end{aligned}\tag{B.13}$$

Appendix C: Moment expansion of the DMPK equation

Mello and Stone [44] have derived from the DMPK equation (1.1.6) a hierarchy of differential equations for the moments of $\mathcal{T}_q = \sum_{n=1}^{N} T_n^q$. The hierarchy closes order by order in the series expansion

$$\langle\mathcal{T}^p\rangle = N^p f_{p,0}(s) + N^{p-1} f_{p,1}(s) + N^{p-2} f_{p,2}(s) + \ldots, \tag{C.1}$$

$$\langle\mathcal{T}^p\mathcal{T}_2\rangle = N^{p+1} g_{p+1,0}(s) + N^p g_{p+1,1}(s) + N^{p-1} g_{p+1,2}(s) + \ldots, \tag{C.2}$$

$$\langle\mathcal{T}^p\mathcal{T}_3\rangle = N^{p+1} h_{p+1,0}(s) + N^p h_{p+1,1}(s) + N^{p-1} h_{p+1,2}(s) + \ldots, \tag{C.3}$$

$$\langle\mathcal{T}^p\mathcal{T}_2^2\rangle = N^{p+2} l_{p+2,0}(s) + N^{p+1} l_{p+2,1}(s) + N^p l_{p+2,2}(s) + \ldots, \tag{C.4}$$

where we have defined $\mathcal{T} \equiv \mathcal{T}_1$. The functions given above suffice to calculate expectation values up to second moments of the conductance. To that end, one needs to determine $\langle \mathcal{T}^p \rangle$ down to $\mathcal{O}(N^{p-2})$, $\langle \mathcal{T}^p \mathcal{T}_2 \rangle$ down to $\mathcal{O}(N^p)$, and $\langle \mathcal{T}^p \mathcal{T}_3 \rangle$ and $\langle \mathcal{T}^p \mathcal{T}_2^2 \rangle$ only to the highest occurring order. The resulting set of differential equations we have to solve is [44]

$$f'_{p,0}(s) + p f_{p+1,0}(s) = 0, \tag{C.5}$$
$$g'_{p,0}(s) + (p+3) g_{p+1,0}(s) = 2 f_{p+1,0}(s), \tag{C.6}$$
$$f'_{p,1}(s) + p f_{p+1,1}(s) = (1 - 2/\beta) \left[f'_{p,0}(s) + p g_{p,0}(s) \right], \tag{C.7}$$
$$l'_{p,0}(s) + (p+6) l_{p+1,0}(s) = 4 g_{p+1,0}(s), \tag{C.8}$$
$$h'_{p,0}(s) + (p+5) h_{p+1,0}(s) = 6 g_{p+1,0}(s) - 3 l_{p+1,0}(s), \tag{C.9}$$
$$\begin{aligned} g'_{p,1}(s) + (p+3) g_{p+1,1}(s) = {} & 2 f_{p+1,1}(s) - (1 - 2/\beta) \left[-g'_{p,0}(s) + 2 g_{p,0}(s) \right. \\ & \left. -4 h_{p,0}(s) - (p-1) l_{p,0}(s) \right], \end{aligned} \tag{C.10}$$
$$\begin{aligned} f'_{p,2}(s) + p f_{p+1,2}(s) = {} & (1 - 2/\beta) \left[f'_{p,1}(s) + p g_{p,1}(s) \right] \\ & + 2\beta^{-1} p (p-1) \left[g_{p-1,0}(s) - h_{p-1,0}(s) \right]. \end{aligned} \tag{C.11}$$

We need to determine the initial conditions $f(0), g(0), h(0)$, and $l(0)$ from the distribution function (2.2.10) for the eigenphases in the circular ensemble. In the large-N limit, the linear statistic $\mathcal{T}_q$ on the eigenphases has a Gaussian distribution wit h a width of order N^0. Therefore, if we write $\mathcal{T}_q = \langle \mathcal{T}_q \rangle + \delta \mathcal{T}_q$, we know that $\langle \mathcal{T}_q \rangle = \mathcal{O}(N)$, $\langle \delta \mathcal{T}_q \rangle = 0$, $\langle (\delta \mathcal{T}_q)^{2n+1} \rangle = \mathcal{O}(N^{-1})$ and $\langle (\delta \mathcal{T}_q)^{2n} \rangle = \mathcal{O}(N^0)$. This implies that, for $s \to 0$,

$$\langle \mathcal{T}^p \rangle = \langle \mathcal{T} \rangle^p + \tfrac{1}{2} p (p-1) \langle \mathcal{T} \rangle^{p-2} \langle (\delta \mathcal{T})^2 \rangle + \mathcal{O}(N^{p-4}), \tag{C.12}$$
$$\langle \mathcal{T}^p \mathcal{T}_2 \rangle = \langle \mathcal{T} \rangle^p \langle \mathcal{T}_2 \rangle + \mathcal{O}(N^{p-1}), \tag{C.13}$$
$$\langle \mathcal{T}^p \mathcal{T}_3 \rangle = \langle \mathcal{T} \rangle^p \langle \mathcal{T}_3 \rangle + \mathcal{O}(N^{p-1}), \tag{C.14}$$
$$\langle \mathcal{T}^p \mathcal{T}_2^2 \rangle = \langle \mathcal{T} \rangle^p \langle \mathcal{T}_2 \rangle^2 + \mathcal{O}(N^p). \tag{C.15}$$

The average $\langle (\delta \mathcal{T})^2 \rangle$ is just $\mathrm{Var}\, G/G_0$, which is given by Eq. (2.2.15),

$$\langle (\delta \mathcal{T})^2 \rangle = \beta^{-1} b^2 \rho^{-4} + \mathcal{O}(N^{-1}). \tag{C.16}$$

The other averages in Eq. (C.12-C.15) follow from

$$\langle \mathcal{T}_q \rangle = \frac{N}{2\pi} \int_0^{2\pi} \mathrm{d}\phi \, (a + b \cos\phi)^{-q}. \tag{C.17}$$

The resulting initial conditions read

$$f_{p,0}(0) = \rho^{-p}, \quad f_{p,1}(0) = 0, \quad f_{p,2}(0) = \tfrac{1}{2} \beta^{-1} p (p-1) \rho^{-(p+2)} b^2, \tag{C.18}$$
$$g_{p,0}(0) = a \rho^{-(p+2)}, \quad g_{p,1}(0) = 0, \tag{C.19}$$
$$h_{p,0}(0) = \rho^{-(p+2)} (\tfrac{3}{2} a^2 \rho^{-2} - \tfrac{1}{2}), \quad l_{p,0}(0) = a^2 \rho^{-(p+4)}. \tag{C.20}$$

The set of differential equations (C.5) can be solved by substitution of the following Ansatz for the p-dependence (adapted from Ref. [12]):

$$x_{p,l}(s) = (s+\rho)^{-(p+2l+n)}[p^2\varphi(s) + p\chi(s) + \psi(s)], \tag{C.21}$$

where $n = 0$ if x is f, $n = 3$ if x is g, and $n = 6$ if x is h or x is l.The mean and variance of the conductance, to order N^{-1}, then follow from

$$\begin{aligned} \langle G/G_0 \rangle &= N f_{1,0}(s) + f_{1,1}(s), & \text{(C.22)} \\ \operatorname{Var} G/G_0 &= N^2[f_{2,0}(s) - f_{1,0}(s)^2] + N[f_{2,1}(s) - 2f_{1,0}(s)f_{1,1}(s)] + \\ &\quad f_{2,2}(s) - 2f_{1,0}(s)f_{1,2}(s) - f_{1,1}(s)^2. & \text{(C.23)} \end{aligned}$$

The results are Eqs. (2.2.18) and (2.2.19).

References

[1] D. L. Maslov, C. Barnes, and G. Kirczenow, Phys. Rev. Lett. **70**, 1984 (1993); Phys. Rev. B **48**, 2543 (1993).

[2] S. Das Sarma and S. He, Int. J. Mod. Phys. **7**, 3375 (1993).

[3] A. Szafer and A. D. Stone, Phys. Rev. Lett. **62**, 300 (1989).

[4] A. D. Stone, P. A. Mello, K. A. Muttalib, and J.-L. Pichard, in *Mesoscopic Phenomena in Solids*, edited by B. L. Al'tshuler, P. A. Lee, and R. A. Webb (North-Holland, Amsterdam, 1991).

[5] O. N. Dorokhov, Pis'ma Zh. Eksp. Teor. Fiz. **36**, 259 (1982) [JETP Lett. **36**, 318 (1982)].

[6] P. A. Mello, P. Pereyra, and N. Kumar, Ann. Phys. **181**, 290 (1988).

[7] P. A. Mello and A. D. Stone, Phys. Rev. B **44**, 3559 (1991).

[8] R. Landauer, Phil. Mag. **21**, 863 (1970).

[9] P. W. Anderson, D. J. Thouless, E. Abrahams, and D. S. Fisher, Phys. Rev. B **22**, 3519 (1980).

[10] M. Büttiker, Phys. Rev. Lett. **65**, 2901 (1990).

[11] J.-L. Pichard, in *Quantum Coherence in Mesoscopic Systems*, edited by B. Kramer, NATO ASI Series B254 (Plenum, New York, 1991).

[12] M. J. M. de Jong and C. W. J. Beenakker, Phys. Rev. B **46**, 13400 (1992).

[13] I. O. Kulik and A. N. Omel'yanchuk, Fiz. Nisk. Temp. **10**, 305 (1984) [Sov. J. Low Temp. Phys. **10**, 158 (1984)].

[14] V. A. Khlus, Zh. Eksp. Teor. Fiz. **93**, 2179 (1987) [Sov. Phys. JETP **66**, 1243 (1987)].

[15] G. B. Lesovik, Pis'ma Zh. Eksp. Teor. Fiz. **49**, 513 (1989) [JETP Lett. **49**, 592 (1989)].

[16] C. W. J. Beenakker and M. Büttiker, Phys. Rev. B **46**, 1889 (1992).

[17] K. E. Nagaev, Phys. Lett. A **169**, 103 (1992).

[18] C. W. J. Beenakker, B. Rejaei, and J. A. Melsen, Phys. Rev. Lett. **72**, 2470 (1994).

[19] Yu. V. Nazarov, Phys. Rev. Lett. **73**, 134 (1994).

[20] M. E. Gertsenshtein and V. B. Vasil'ev, Teor. Veroyatn. Primen. **4**, 424 (1959) [Theor. Probab. Appl. **4**, 391 (1959)].

[21] G. C. Papanicolaou, SIAM J. Appl. Math. **21**, 13 (1971).

[22] V. I. Mel'nikov, Fiz. Tverd. Tela **23**, 782 (1981) [Sov. Phys. Solid State **23**, 444 (1981)].

[23] A. A. Abrikosov, Sol. State Comm. **37**, 997 (1981).

[24] P. D. Kirkman and J. B. Pendry, J. Phys. C **17**, 5707 (1984).

[25] N. Kumar, Phys. Rev. B **31**, 5513 (1985).

[26] P. A. Mello, J. Math. Phys. **27**, 2876 (1986).

[27] V. N. Prigodin, K. B. Efetov, and S. Iida, Phys. Rev. Lett. **71**, 1230 (1993).

[28] R. A. Jalabert, J.-L. Pichard, and C. W. J. Beenakker, Europhys. Lett. **27**, 255 (1994); H. U. Baranger and P. A. Mello, Phys. Rev. Lett. **73**, 142 (1994).

[29] H. U. Baranger, D. P. DiVincenzo, R. A. Jalabert, and A. D. Stone, Phys. Rev. B **44**, 10637 (1991). The computer code for the recursive Green's function calculation was kindly made available to us by Dr. Jalabert.

[30] H. A. Fertig and S. Das Sarma, Phys. Rev. B **40**, 7410 (1989); H. A. Fertig, S. He, and S. Das Sarma, Phys. Rev. B **41**, 3596 (1990).

[31] J. Leo and A. H. MacDonald, Phys. Rev. Lett. **64**, 817 (1990).

[32] R. Berkovits and S. Feng, Phys. Rev. B **45**, 97 (1992).

[33] I. V. Lerner and M. E. Raikh, Phys. Rev. B **45**, 14036 (1992).

[34] M. E. Raikh and I. M. Ruzin, in: *Mesoscopic Phenomena in Solids*, edited by B. L. Al'tshuler, P. A. Lee, and R. A. Webb (North-Holland, Amsterdam, 1991).

[35] M. L. Mehta, *Random Matrices* (Academic, New York, 1991).

[36] B. L. Al'tshuler, Pis'ma Zh. Eksp. Teor. Fiz. **41**, 530 (1985) [JETP Lett. **41**, 648 (1985)].

[37] P. A. Lee and A. D. Stone, Phys. Rev. Lett. **55**, 1622 (1985).

[38] S. Iida, H. A. Weidenmüller, and J. A. Zuk, Phys. Rev. Lett. **64**, 583 (1990); Ann. Phys. **200**, 219 (1990).

[39] Th. Martin and R. Landauer, Phys. Rev. B **45**, 1742 (1992).

[40] F. J. Dyson and M. L. Mehta, J. Math. Phys. **4**, 701 (1963).

[41] A different derivation of Eq. (2.2.12) has been given recently by P. J. Forrester, Nucl. Phys. B **435**, 421 (1995).

[42] J. A. Melsen and C. W. J. Beenakker, Physica B **203**, 219 (1994).

[43] P. A. Mello, Phys. Rev. Lett. **60**, 1089 (1988).

[44] P. A. Mello and A. D. Stone, Phys. Rev. B **44**, 3559 (1991).

[45] C. W. J. Beenakker, Phys. Rev. Lett. **70**, 1155 (1993); Phys. Rev. B **47**, 15763 (1993).

[46] F. J. Dyson, J. Math. Phys. **13**, 90 (1972).

3 Reflectionless tunneling through a double-barrier NS junction

3.1 Introduction

Reflectionless tunneling is a novel quantum interference effect which occurs when dissipative normal current is converted into dissipationless supercurrent at the interface between a normal metal (N) and a superconductor (S) [1]. Experimentally, the effect is observed as a peak in the differential conductance around zero voltage or around zero magnetic field [2]. Its name refers to the fact that, for full phase coherence, the Andreev-reflected quasiparticle can tunnel through the potential barrier at the NS interface without suffering reflections. (The potential barrier can be the insulator (I) in an NIS junction, or the Schottky barrier in a semiconductor–superconductor junction.) Application of a voltage or magnetic field destroys the phase coherence between electrons and holes, and thus reduces the conductance of the junction. We now have a good theoretical understanding of the effect, based on a combination of numerical [3,4], and analytical work [5–10]. The basic requirement for reflectionless tunneling is that the normal region has a resistance which is larger than the resistance of the interface. In that case the disorder is able to open a fraction of the tunneling channels, i.e. it induces the appearance of transmission eigenvalues close to one [10]. As a result of these open channels, the resistance has a linear dependence on the transparency of the interface, instead of the quadratic dependence expected for Andreev reflection [11] (which is a two-particle process).

The purpose of this work is to present a study of reflectionless tunneling in its simplest form, when the resistance of the normal metal is due to a second tunnel barrier, in series with the barrier at the NS interface. This allows an exact calculation, which shows many of the features of the more complicated case when the resistance of the normal region is due to disorder. Furthermore, the double-barrier geometry provides an experimentally realizable model system, for example in tunneling from an STM into a superconductor via a metal particle [12].

The outline of this chapter is as follows. In Section 3.2 we consider the problem of a NI_1NI_2S junction without disorder. We compute the resistance of the junction as a function of the transmission probabilities per mode Γ_1 and Γ_2 of the two barriers. The resistance at fixed Γ_2 shows a *minimum* as a function of Γ_1 when $\Gamma_1 \approx \sqrt{2}\Gamma_2 \equiv \Gamma$. The resistance in the minimum depends *linearly* on $1/\Gamma$, in contrast to the quadratic dependence in the case of a single barrier. In Section 3.3 we apply a recent scaling theory [9], to find the influence on the resistance

minimum of disorder in the region between the barriers (length L, mean free path l). The resistance minimum persists as long as $l \gtrsim \Gamma L$. In the diffusive regime ($l \ll L$) our results agree with a previous Green's function calculation by Volkov, Zaitsev, and Klapwijk [7]. The analytical results are supported by numerical simulations, using the recursive Green's function technique [13]. We conclude in Section 3.4.

3.2 NINIS junction without disorder

We consider a NI_1NI_2S junction, where N = normal metal, S = superconductor, and I_i = insulator or tunnel barrier (see inset of Fig. 2-10). The transmission probability per mode of I_i is denoted by Γ_i. For simplicity we neglect the mode-dependence of Γ_i. In this section, we assume ballistic motion between the barriers. (The effect of disorder in the normal region is considered in Sec. 3.3.) A straightforward calculation yields the transmission probabilities T_n of the two barriers in series,

$$T_n = (a + b\cos\phi_n)^{-1}, \tag{3.2.1}$$

where

$$a = 1 + \frac{2-\Gamma_1-\Gamma_2}{\Gamma_1\Gamma_2}, \tag{3.2.2}$$

$$b = \frac{2\,(1-\Gamma_1)^{1/2}(1-\Gamma_2)^{1/2}}{\Gamma_1\Gamma_2}, \tag{3.2.3}$$

and ϕ_n is the phase accumulated between the barriers by mode $n = 1, 2, \cdots N$ (with N the number of propagating modes at the Fermi level). If we substitute $\Gamma_i = 1/\cosh^2\alpha_i$ ($\alpha_i \geq 0$), the coefficients a and b can be rewritten as

$$a = \tfrac{1}{2} + \tfrac{1}{2}\cosh 2\alpha_1 \cosh 2\alpha_2, \tag{3.2.4}$$

$$b = \tfrac{1}{2}\sinh 2\alpha_1 \sinh 2\alpha_2. \tag{3.2.5}$$

Since the transmission matrix t is diagonal, the transmission probabilities T_n are identical to the eigenvalues of $tt^\dagger$. We use the general relationship between the conductance $G_{\rm NS} \equiv G_{\rm NINIS}$ of the NINIS junction and the transmission eigenvalues of the normal region [14],

$$G_{\rm NS} = \frac{4e^2}{h}\sum_{n=1}^{N}\frac{T_n^2}{(2-T_n)^2}, \tag{3.2.6}$$

which is the analogue of the Landauer formula

$$G_{\rm N} = \frac{2e^2}{h}\sum_{n=1}^{N} T_n, \tag{3.2.7}$$

for the conductance $G_N \equiv G_{NININ}$ in the normal state. We assume that $L \gg \lambda_F$ (λ_F is the Fermi wavelength) and $N\Gamma_i \gg 1$, so that the conductance is not dominated by a single resonance. In this case, the phases ϕ_n are distributed uniformly in the interval $(0, 2\pi)$ and we may replace the summations in Eqs. (3.2.6), (3.2.7) by integrals over ϕ: $\sum_{n=1}^{N} f(\phi_n) \to (N/2\pi) \int_0^{2\pi} d\phi\, f(\phi)$. The result is

$$G_{NS} = \frac{4e^2N}{h} \frac{\cosh 2\alpha_1 \cosh 2\alpha_2}{\left(\cosh^2 2\alpha_1 + \cosh^2 2\alpha_2 - 1\right)^{3/2}}, \tag{3.2.8}$$

$$G_N = \frac{4e^2N}{h} (\cosh 2\alpha_1 + \cosh 2\alpha_2)^{-1}. \tag{3.2.9}$$

These expressions are symmetric in the indices 1 and 2: it does not matter which of the two barriers is closest to the superconductor.

In the same way we can compute the entire distribution of the transmission eigenvalues, $\rho(T) \equiv \sum_n \delta(T - T_n) \to (N/2\pi) \int_0^{2\pi} d\phi\, \delta(T - T(\phi))$. Substituting $T(\phi) = (a + b\cos\phi)^{-1}$ from Eq. (3.2.1), we find

$$\rho(T) = \frac{N}{\pi T} \left(b^2T^2 - (aT-1)^2\right)^{-1/2}. \tag{3.2.10}$$

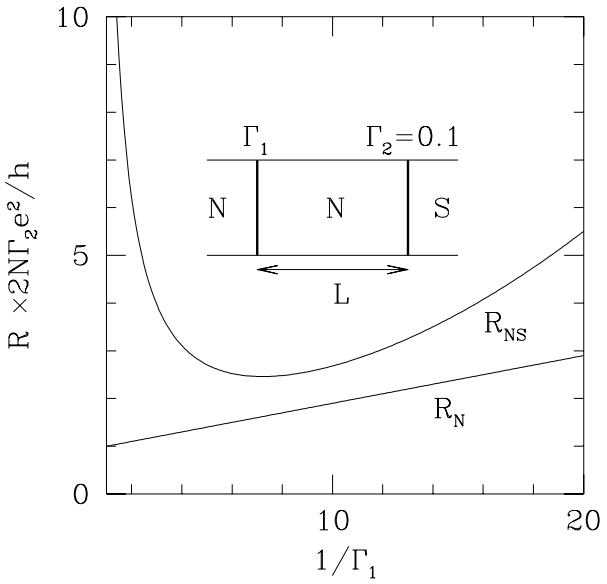

Figure 3-1. Dependence of the resistances R_N and R_{NS} of ballistic NININ and NINIS structures, respectively, on barrier transparancy Γ_1, while transparancy $\Gamma_2 = 0.1$ is kept fixed [computed from Eqs. (3.2.8) and (3.2.9)]. The inset shows the NINIS structure considered.

In Fig. 3-1 we plot the resistance $R_N = 1/G_N$ and $R_{NS} = 1/G_{NS}$, following from Eqs. (3.2.8) and (3.2.9). Notice that R_N follows Ohm's law,

$$R_N = \frac{h}{2Ne^2}(1/\Gamma_1 + 1/\Gamma_2 - 1), \tag{3.2.11}$$

as expected from classical considerations. In contrast, the resistance $R_{\rm NS}$ has a *minimum* if one of the Γ's is varied while keeping the other fixed. This resistance minimum cannot be explained by classical series addition of barrier resistances. If $\Gamma_2 \ll 1$ is fixed and Γ_1 is varied, as in Fig. 3-1, the minimum occurs when $\Gamma_1 = \sqrt{2}\Gamma_2$. The minimal resistance $R_{\rm NS}^{\rm min}$ is of the same order of magnitude as the resistance $R_{\rm N}$ in the normal state at the same value of Γ_1 and Γ_2. (For $\Gamma_2 \ll 1$, $R_{\rm NS}^{\rm min} = 1.52\, R_{\rm N}$) In particular, we find that $R_{\rm NS}^{\rm min}$ depends linearly on $1/\Gamma_i$, whereas for a single barrier $R_{\rm NS} \propto 1/\Gamma^2$.

The linear dependence on the barrier transparency shows the qualitative similarity of a ballistic NINIS junction to a disordered NIS junction. To illustrate the similarity, we compare in Fig. 3-2 the densities of transmission eigenvalues throught the normal region. The left panel is for an NIS junction (computed using the results of Ref. [9]), the right panel is for an NINIS junction (computed from Eq. (3.2.10)). In the NIS junction, disorder leads to a bimodal distribution $\rho(T)$, with a peak near zero transmission and another peak near unit transmisssion (dashed curve). A similar bimodal distribution appears in the ballistic NINIS junction, for approximately equal transmission probabilities of the two barriers. There are also differences between the two cases: The NIS junction has a unimodal $\rho(T)$ if $L/l < 1/\Gamma$, while the NINIS junction has a bimodal $\rho(T)$ for any ratio of Γ_1 and Γ_2. In both cases, the opening of tunneling channels, *i.e.*, the appearance of a peak in $\rho(T)$ near $T = 1$, is the origin for the $1/\Gamma$ dependence of the resistance.

3.3 Effects of disorder

Let us now investigate what happens to the resistance minimum if the region of length L between the tunnel barriers contains impurities, with elastic mean free path l. We denote $s \equiv L/l$. When introducing disorder, it is necessary to consider ensemble-averaged quantities. To calculate the ensemble-averaged conductance $\langle G_{\rm NS}\rangle$, we need to know the density ρ of the transmission eigenvalues T_n as a function of s. It is convenient to work with the parameterization

$$T_n = 1/\cosh^2 x_n, \quad x_n \geq 0. \tag{3.3.1}$$

The density of the x_n's is defined by $\rho(x,s) \equiv \langle \sum_n \delta(x - x_n)\rangle$. From Eq. (3.2.1) we know that, for $s = 0$ (no disorder),

$$\begin{aligned} \rho(x,0) &= N \int_0^{2\pi} \frac{{\rm d}\phi}{2\pi}\, \delta(x - {\rm arccosh}\sqrt{a + b\cos\phi}) \\ &= \frac{N}{\pi} \sinh 2x \left(b^2 - (a - \cosh^2 x)^2\right)^{-\frac{1}{2}}, \end{aligned} \tag{3.3.2}$$

for ${\rm arccosh}\sqrt{a-b} \equiv x_{\rm min} \leq x \leq x_{\rm max} \equiv {\rm arccosh}\sqrt{a+b}$.

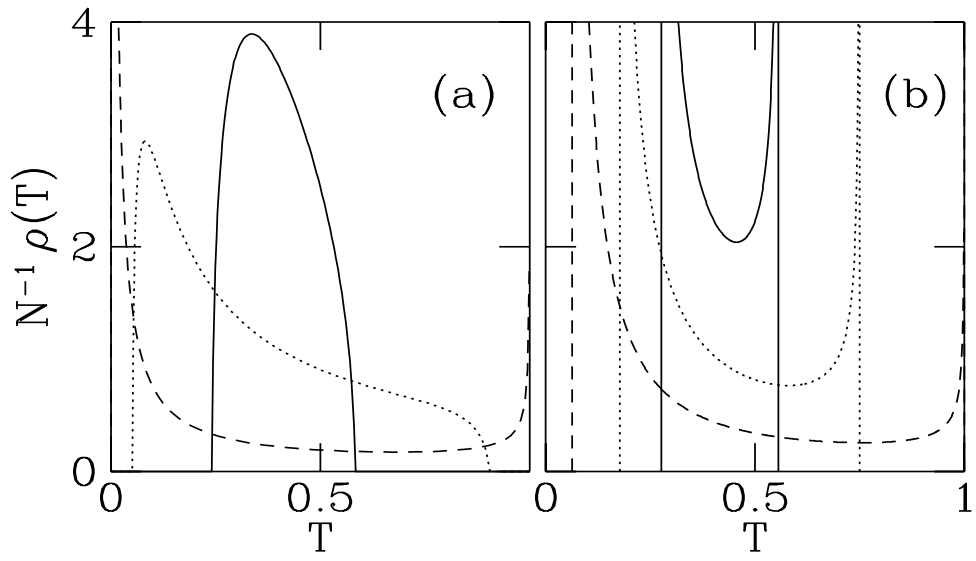

Figure 3-2. Density of normal-state transmission eigenvalues for an NS junction with a potential barrier at the interface (transmission probability $\Gamma = 0.4$). The left panel (a) shows the disorder-induced opening of tunneling channels in an NIS junction (solid curve: $s = 0.04$; dotted: $s = 0.4$; dashed: $s = 5$; where $s \equiv L/l$). The right panel (b) shows the opening of channels by a second tunnel barrier (transparancy Γ') in an NINIS junction (solid curve: $\Gamma' = 0.95$; dotted: $\Gamma' = 0.8$; dashed: $\Gamma' = 0.4$). The curves in (a) are computed from Ref. [9], the curves in (b) from Eq. (3.2.10). Notice the similarity of the dashed curves.

For $s > 0$ we obtain the density $\rho(x,s)$ from the integro-differential equation [15]

$$\frac{\partial}{\partial s}\rho(x,s) = -\frac{1}{2N}\frac{\partial}{\partial x}\rho(x,s)\frac{\partial}{\partial x}\int_0^\infty \mathrm{d}x'\rho(x',s)\ln|\sinh^2 x - \sinh^2 x'|, \quad (3.3.3)$$

which is the large N-limit of the scaling equation that one obtains after multiplying the DMPK equation (1.1.6) on both sides with $\sum_{n=1}^N \delta(x-x_n)$ and integrating over $x_1, x_2, \ldots, x_N$. This equation describes the evolution of $\rho(x,s)$ when an infinitesimal slice of disordered material is added. With initial condition (3.3.2) it therefore describes a geometry where all disorder is on one side of the two tunnel barriers, rather than in between. In fact, only the total length L of the disordered region matters, and not the location relative to the barriers. The argument is similar to that in Ref. [18]. The total transfer matrix M of the normal region is a product of the transfer matrices of its constituents (barriers and disordered segments): $M = M_1 M_2 M_3 \cdots$. The probability distribution of M is given by the convolution $p(M) = p_1 * p_2 * p_3 * \cdots$ of the distributions p_i of transfer matrices M_i [this convolution is defined in Eq. (2.1.5)]. It is shown in Appendix A of Chapter 2 that the convolution of the p_i commutes, if for all parts i of the system, $p_i(M_i)$ is a function of the eigenvalues of $M_i M_i^\dagger$ only. The

distributions p_i are then called isotropic. A disordered segment (length L, width W) has an isotropic distribution if $L \gg W$. A planar tunnel barrier does not mix the modes, so a priori it does not have an isotropic distribution. However, if the mode-dependence of the transmission probabilities is neglected (as we do here), it does not make a difference if we replace its distribution by an isotropic one. The commutativity of the convolution of isotropic distributions implies that the location of the tunnel barriers with respect to the disordered region does not affect $\rho(x,s)$. The systems in Figs. 3-3a, b, and c then have identical statistical properties.

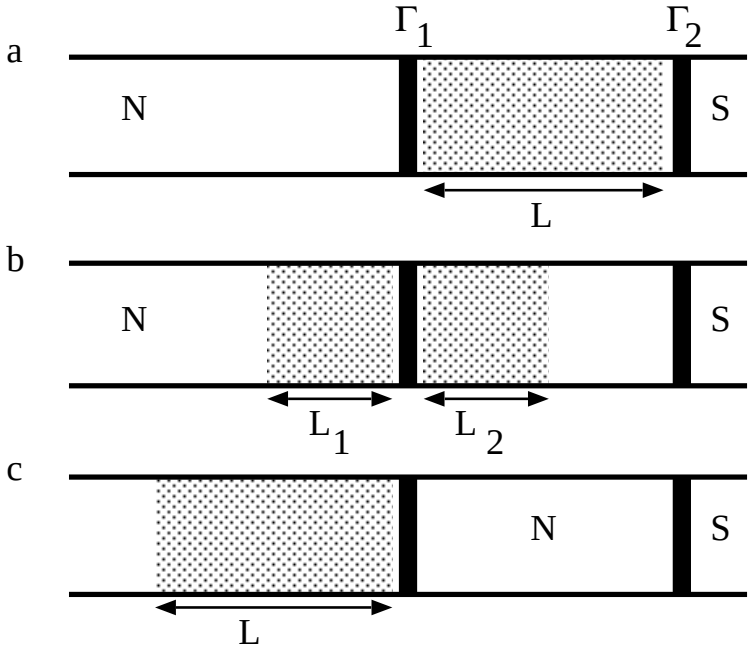

Figure 3-3. The systems a,b, and c are statistically equivalent, if the transfer matrices of each of the two barriers (solid vertical lines) and the disordered regions (shaded areas, $L_1 + L_2 = L$ in case b) have isotropic distributions; in that case, the position of the disorder with respect to the barriers does not affect the eigenvalue density $\rho(x,s)$.

Once $\rho(x,s)$ is known, the conductances $\langle G_{\rm NS}\rangle$ and $\langle G_{\rm N}\rangle$ can be determined from

$$\langle G_{\rm NS}\rangle = \frac{4e^2}{h}\int_0^\infty {\rm d}x\,\frac{\rho(x,s)}{\cosh^2 2x}, \tag{3.3.4}$$

$$\langle G_{\rm N}\rangle = \frac{2e^2}{h}\int_0^\infty {\rm d}x\,\frac{\rho(x,s)}{\cosh^2 x}, \tag{3.3.5}$$

where we have substituted Eq. (3.3.1) into Eqs. (3.2.6), (3.2.7). In Ref. [18] a general solution to the evolution equation was obtained for arbitrary initial condition. It was shown that Eq. (3.3.3) can be mapped onto Euler's equation of

hydrodynamics

$$\frac{\partial}{\partial s}U(\zeta,s)+U(\zeta,s)\frac{\partial}{\partial\zeta}U(\zeta,s)=0, \tag{3.3.6}$$

by means of the substitution

$$U(\zeta,s)=\frac{\sinh 2\zeta}{2N}\int_0^\infty \mathrm{d}x'\,\frac{\rho(x',s)}{\sinh^2\zeta-\sinh^2 x'}. \tag{3.3.7}$$

Here, $U\equiv U_x+\mathrm{i}U_y$ and $\zeta\equiv x+\mathrm{i}y$. Eq. (3.3.6) describes the velocity field $U(\zeta,s)$ of a 2D ideal fluid at constant pressure in the x-y plane. Its solution is[1]

$$U(\zeta,s)=U_0(\zeta-sU(\zeta,s)), \tag{3.3.8}$$

in terms of the initial value $U_0(\zeta)\equiv U(\zeta,0)$. The probability distribution $\rho(x,s)$ follows from the velocity field by inversion of Eq. (3.3.7),

$$\rho(x,s)=\frac{2N}{\pi}U_y(x-\mathrm{i}\epsilon,s), \tag{3.3.9}$$

where ϵ is a positive infinitesimal.

In our case, the initial velocity field [from Eqs. (3.3.2) and (3.3.7)] is

$$U_0(\zeta)=-\tfrac{1}{2}\sinh 2\zeta\left[(\cosh^2\zeta-a)^2-b^2\right]^{-\frac{1}{2}}. \tag{3.3.10}$$

The resulting density (3.3.9) is plotted in Fig. 3-4 for $\Gamma_1=\Gamma_2\equiv\Gamma$ and several disorder strengths. The region near $x=0$ is of importance for the conductance (since x near zero corresponds to near-unit transmission). The number $N_{\mathrm{open}}\equiv\rho(0,s)$ is an estimate for the number of transmission eigenvalues close to 1 (so-called "open channels" [19]). In the absence of disorder, N_{open} is non-zero only if $\Gamma_1\approx\Gamma_2$ (then $a-b=1\Rightarrow x_{\min}=0$). From Eq. (3.3.2) we find $N_{\mathrm{open}}=N\Gamma/\pi$ for $s=0$ and $\Gamma_1=\Gamma_2\equiv\Gamma\ll 1$. Adding disorder reduces the number of open channels. If $\Gamma_1\neq\Gamma_2$ there are no open channels for $s=0$ ($x_{\min}>0$). Disorder then has the effect of increasing N_{open}, such that $N_{\mathrm{open}}\approx N/s$ if $(\Gamma_1+\Gamma_2)s\gg 1$. The disorder-induced opening of channels was studied in Refs. [9, 10] for the case of a single tunnel barrier.

To test our analytical results for the eigenvalue density $\rho(x,s)$, we have carried out numerical simulations, similar to those reported in Ref. [9]. The sample was modeled by a tight-binding Hamiltonian on a square lattice with lattice constant a. The tunnel barriers were accounted for by assigning a non-random potential energy $U_{\mathrm{B}}=2.3\,E_{\mathrm{F}}$ to a single row of sites at both ends of the lattice, which corresponds to a mode averaged barrier transparency $\Gamma_1=\Gamma_2=0.18$. The Fermi energy was chosen at $1.5\,u_0$, with $u_0=\hbar^2/2ma^2$. Disorder was introduced by randomly assigning a value between $\pm\frac{1}{2}U_{\mathrm{D}}$ to the on-site potential of

[1] The implicit equation (3.3.8) has multiple solutions in the entire complex plane; we need the solution for which both ζ and $\zeta-sU(\zeta,s)$ lie in the strip between the lines $y=0$ and $y=-\pi/2$.

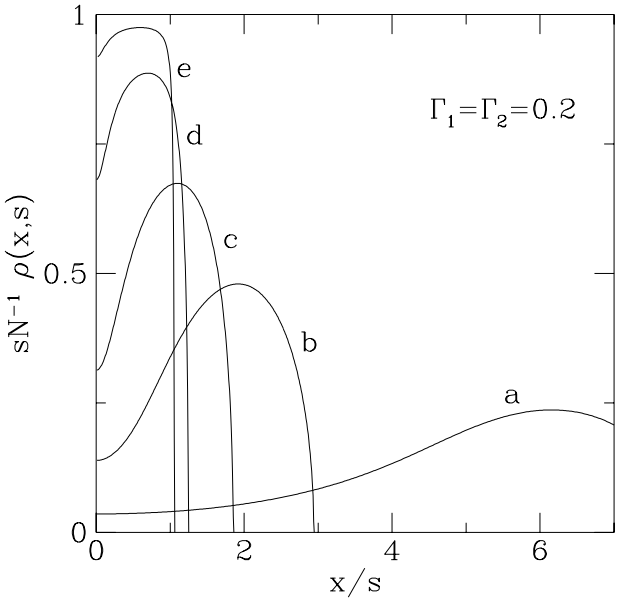

Figure 3-4. Eigenvalue density $\rho(x,s)$ as a function of x (in units of $s \equiv L/l$) for $\Gamma_1 = \Gamma_2 = 0.2$. Curves a,b,c,d, and e are for $s = 0.5, 2, 5, 20, 100$, respectively. In the special case of equal tunnel barriers, open channels exist already in the absence of disorder.

the lattice points between the barriers. The disorder strength U_D was varied between 0 and $1.5\,u_0$, corresponding to s between 0 and 11.7. We considered geometries with both a square disordered region (285×285 sites, $N = 119$) and a rectangular one (285×75 sites, $N = 31$), to test the geometry dependence of our results. In Fig. 3-5, we compare the integrated eigenvalue density $\nu(x,s) \equiv N^{-1} \int_0^x \mathrm{d}x' \rho(x',s)$ with the numerical results.

The quantity $\nu(x,s)$ follows directly from our simulations, by plotting the x_n's in ascending order versus $n/N \equiv \nu$. We want to sample $\nu(x,s)$ at many points along the x-axis, so we need N large. Since the x_n's are self-averaging (fluctuations are of the order of $1/N$), it is not necessary to average over many samples. The data shown in Fig. 3-5 are from a single realization of the impurity potential. There is good agreement with the analytical results. No geometry dependence is observed, which indicates that the restriction $L \gg W$ of Eq. (3.3.3) can be relaxed to a considerable extent.

Using Eqs. (3.3.4) and (3.3.7), the average conductance $\langle G_{NS} \rangle$ can be directly expressed in terms of the velocity field,

$$\langle G_{NS} \rangle = \frac{2Ne^2}{h} \lim_{\zeta \to -i\pi/4} \frac{\partial}{\partial \zeta} U(\zeta, s). \tag{3.3.11}$$

For $\zeta \to -i\pi/4$, $U \to iU_y$, $U_y > 0$. The implicit solution (3.3.8) then takes the form

$$\phi \sqrt{(2a + \sin\phi - 1)^2 - 4b^2} = 2s \cos\phi, \tag{3.3.12}$$

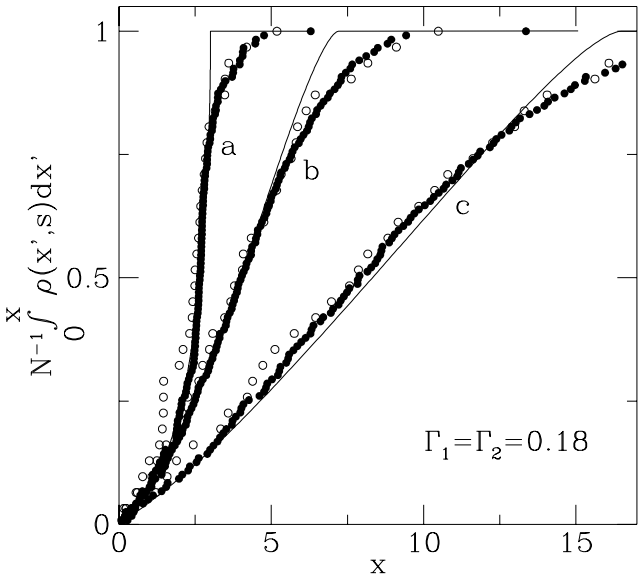

Figure 3-5. Comparison between theory and simulation of the integrated eigenvalue density for $\Gamma_1 = \Gamma_2 = 0.18$. The labels a, b, c indicate, respectively, $s = 0, 3, 11.7$. Solid curves are from Eq. (3.3.8); data points are the x_n's from the simulation plotted in ascending order versus n/N. Filled data points are for a square geometry, open points are for an aspect ratio $L/W = 3.8$.

where $\phi \equiv 2sU_y \in [0, \pi/2]$. We now use that

$$\frac{\partial}{\partial\zeta}U(\zeta,s)|_{\zeta=-\frac{i\pi}{4}} = -[\frac{\partial}{\partial s}U(-\frac{i\pi}{4},s)]/U(-\frac{i\pi}{4},s) \tag{3.3.13}$$

[see Eq. (3.3.6)]. Combining Eqs. (3.3.11) and (3.3.12) we find

$$\langle G_{\rm NS}\rangle = \frac{2Ne^2}{h}(s+1/Q)^{-1}, \tag{3.3.14}$$

where the effective tunnel rate Q is given in terms of the angle ϕ in Eq. (3.3.12) by

$$Q = \frac{\phi}{s\cos\phi}\left(\sin\phi + \frac{\phi^2}{4s^2}\left[\sin\phi + (1-2/\Gamma_1)(1-2/\Gamma_2)\right]\right). \tag{3.3.15}$$

Eqs. (3.3.12)–(3.3.15) completely determine the conductance of a double-barrier NS-junction containing disorder.

In Fig. 3-6, we plot $\langle R_{\rm NS}\rangle$ for several values of the disorder, keeping $\Gamma_2 = 0.1$ fixed and varying the transparency of barrier 1. For weak disorder ($\Gamma_2 s \ll 1$), the resistance minimum is retained, but its location moves to larger values of Γ_1. On increasing the disorder, the minimum becomes shallower and eventually disappears. In the regime of strong disorder ($\Gamma_2 s \gg 1$), the resistance behaves nearly Ohmic.

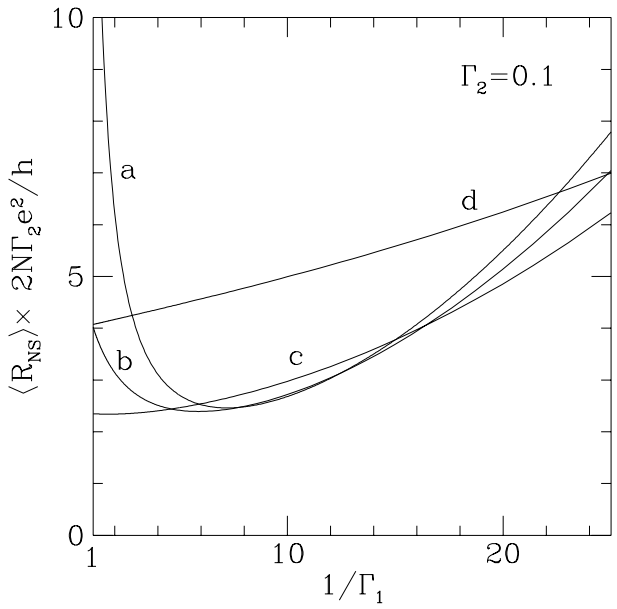

Figure 3-6. Dependence of the ensemble-averaged resistance $\langle R_{\rm NS}\rangle$ for a disordered NINIS junction on barrier transparancy Γ_1, while $\Gamma_2 = 0.1$ is kept fixed [computed from Eqs. (3.3.14) and (3.3.15)]. Curves a, b, c, d are for $s = 0, 2, 7, 30$, respectively. The resistance minimum persists for small disorder.

We stress that these results hold for arbitrary $s \equiv L/l$, all the way from the ballistic into the diffusive regime. Volkov, Zaitsev, and Klapwijk [7] have computed $\langle G_{\rm NS}\rangle$ in the diffusive limit $s \gg 1$. In that limit our Eqs. (3.3.12) and (3.3.15) take the form:

$$\frac{s\cos\phi}{\phi} = \frac{1}{\Gamma_1}\sqrt{1-\left(\frac{\phi}{\Gamma_2 s}\right)^2} + \frac{1}{\Gamma_2}\sqrt{1-\left(\frac{\phi}{\Gamma_1 s}\right)^2}, \tag{3.3.16}$$

$$\frac{1}{Q} = \sum_{i=1}^{2}\frac{1}{\Gamma_i}\left[1-\left(\frac{\phi}{\Gamma_i s}\right)^2\right]^{-1/2}, \tag{3.3.17}$$

in precise agreement with Ref. [7]. Nazarov's circuit theory [10], which is equivalent to the Green's function theory of Ref. [7], also leads to this result for $\langle G_{\rm NS}\rangle$ in the diffusive regime.

Two limiting cases of Eqs. (3.3.16) and (3.3.17) are of particular interest. For strong barriers, $\Gamma_1, \Gamma_2 \ll 1$, and strong disorder, $s \gg 1$, one has the two asymptotic formulas

$$\langle G_{\rm NS}\rangle = \frac{2Ne^2}{h}\frac{\Gamma_1^2\Gamma_2^2}{\left(\Gamma_1^2+\Gamma_2^2\right)^{3/2}}, \quad \text{if} \quad \Gamma_1, \Gamma_2 \ll 1/s, \tag{3.3.18}$$

$$\langle G_{\rm NS}\rangle = \frac{2Ne^2}{h}(s + 1/\Gamma_1 + 1/\Gamma_2)^{-1}, \quad \text{if} \quad \Gamma_1, \Gamma_2 \gg 1/s. \tag{3.3.19}$$

Eq. (3.3.18) coincides with Eq. (3.2.8) in the limit $\alpha_1, \alpha_2 \gg 1$ (recall that $\Gamma_i \equiv 1/\cosh^2 \alpha_i$). This shows that the effect of disorder on the resistance minimum can be neglected as long as the resistance of the junction is dominated by the barriers. In this case $\langle G_{\rm NS} \rangle$ depends linearly on Γ_1 and Γ_2 only if $\Gamma_1 \approx \Gamma_2$. Eq. (3.3.19) shows that if the disorder dominates, $\langle G_{\rm NS} \rangle$ has a linear Γ-dependence regardless of the relative magnitude of Γ_1 and Γ_2.

3.4 Conclusions

In summary, we have derived an expression for the conductance of a ballistic NINIS junction in the limit $N\Gamma \gg 1$ that the tunnel resistance is much smaller than h/e^2. In this regime the double-barrier junction contains a large number of overlapping resonances, so that in the normal state the resistance depends monotonically on $1/\Gamma$. In contrast, the NINIS junction shows a resistance minimum when one of the barrier transparencies is varied while the other is kept fixed. The minimal resistance (at $\Gamma_1 \simeq \Gamma_2 \equiv \Gamma$) is proportional to $1/\Gamma$, instead of the $1/\Gamma^2$ dependence expected for two-particle tunneling into a superconductor. This is similar to the reflectionless tunneling which occurs in an NIS junction. Using the results of the ballistic junction, we have described the transition to a disordered NINIS junction by means of an evolution equation for the transmission eigenvalue density [9]. We found that the resistance minimum is unaffected by disorder, as long as $l \gg L/\Gamma$, *i.e.*, as long as the barrier resistance dominates the junction resistance. As the disorder becomes more dominant, a transition to a monotonic Γ-dependence takes place. In the limit of diffusive motion between the barriers, our results agree with Ref. [7].

Throughout this chapter we have assumed zero temperature, zero magnetic field, and infinitesimal applied voltage. Each of these quantities is capable of destroying the phase coherence between the electrons and the Andreev-reflected holes, which is responsible for the resistance minimum. As far as the temperature T and voltage V are concerned, we require $k_{\rm B}T, eV \ll \hbar/\tau_{\rm dwell}$ for the appearance of a resistance minimum, where $\tau_{\rm dwell}$ is the dwell time of an electron in the region between the two barriers. For a ballistic NINIS junction we have $\tau_{\rm dwell} \sim L/\nu_{\rm F}\Gamma$, while for a disordered junction $\tau_{\rm dwell} \sim L^2/\nu_{\rm F}\Gamma l$ is larger by a factor L/l. It follows that the condition on temperature and voltage becomes more restrictive if the disorder increases, even if the resistance remains dominated by the barriers. As far as the magnetic field B is concerned, we require $B \ll h/eS$ (with S the area of the junction perpendicular to B), if the motion between the barriers is diffusive. For ballistic motion the trajectories enclose no flux, so no magetic field dependence is expected.

A possible experiment to verify our results might be scanning tunneling microscopy of a metal particle on top of a superconducting substrate [12]. The metal-superconductor interface has a fixed tunnel probability Γ_2. The probabil-

ity Γ_1 for an electron to tunnel from STM to particle can be controlled by varying the distance. (Volkov has recently analyzed this geometry in the regime that the motion from STM to particle is diffusive rather than by tunneling [20].) Another possibility is to create an NINIS junction using a two-dimensional electron gas in contact with a superconductor. The tunnel barriers could then be implemented by means of two gate electrodes. In this way both transparancies might be tuned independently.

References

[1] For a review of quantum interference effects in NS junctions, see: C. W. J. Beenakker, in: *Mesoscopic Quantum Physics*, edited by E. Akkermans, G. Montambaux, and J.-L. Pichard (North-Holland, Amsterdam, 1995).

[2] A. Kastalsky, A. W. Kleinsasser, L. H. Greene, R. Bhat, F. P. Milliken, and J. P. Harbison, Phys. Rev. Lett. **67** (1991) 3026.

[3] I. K. Marmorkos, C. W. J. Beenakker, and R. A. Jalabert, Phys. Rev. B **48** (1993) 2811.

[4] Y. Takane and H. Ebisawa, J. Phys. Soc. Jpn. **62** (1993) 1844.

[5] B. J. van Wees, P. de Vries, P. Magnée, and T. M. Klapwijk, Phys. Rev. Lett. **69** (1992) 510.

[6] Y. Takane and H. Ebisawa, J. Phys. Soc. Jpn. **61** (1992) 3466.

[7] A. F. Volkov, A. V. Zaitsev, and T. M. Klapwijk, Physica C **210** (1993) 21.

[8] F. W. J. Hekking and Yu. V. Nazarov, Phys. Rev. Lett. **71** (1993) 1625; Phys. Rev. B **49** (1994) 6847.

[9] C. W. J. Beenakker, B. Rejaei, and J. A. Melsen, Phys. Rev. Lett. **72** (1994) 2470.

[10] Yu. V. Nazarov, Phys. Rev. Lett. **73**, 134 (1994).

[11] A. L. Shelankov, Pis'ma Zh. Eksp. Teor. Fiz. **32** (1 980) 122 [JETP Lett. **32** (1980) 111].

[12] D. R. Heslinga, S. E. Shafranjuk, H. van Kempen, and T. M. Klap wijk, Phys. Rev. B **49** (1994) 10484.

[13] H. U. Baranger, D. P. DiVincenzo, R. A. Jalabert, and A. D. Ston e, Phys. Rev. B **44** (1991) 10637.

[14] C. W. J. Beenakker, Phys. Rev. B **46** (1992) 12841.

[15] P. A. Mello and J.-L. Pichard, Phys. Rev. B **40** (1 989) 5276.

[16] O. N. Dorokhov, Pis'ma Zh. Eksp. Teor. Fiz. **36** (198 2) 259 [JETP Lett. **36** (1982) 318].

[17] P. A. Mello, P. Pereyra, and N. Kumar, Ann. Phys. (N.Y.) **18 1** (1988) 290.

[18] C. W. J. Beenakker and J. A. Melsen, Phys. Rev. B **50**, 2450 (1994).

[19] Y. Imry, Europhys. Lett. **1** (1986) 249.

[20] A. F. Volkov, Physics Lett. A **187** (1994) 404.

4 Giant backscattering peak in angle-resolved Andreev reflection

4.1 Enhanced backscattering

Coherent backscattering is a fundamental effect of time-reversal symmetry on the reflection of electrons by a disordered metal [1, 2]. The angular reflection distribution has a narrow peak at the angle of incidence, due to the constructive interference of time-reversed sequences of multiple scattering events. At zero temperature, the peak is twice as high as the background. Coherent backscattering manifests itself in a transport experiment as a small negative correction of order $G_0 = 2e^2/h$ to the average conductance G of the metal (*weak localization* [3]). Here we report the theoretical prediction, supported by numerical simulations, of a giant enhancement of the backscattering peak if the normal metal (N) is in contact with a superconductor (S). At the NS interface an electron incident from N is reflected either as an electron (normal reflection) or as a hole (Andreev reflection). Both scattering processes contribute to the backscattering peak. Normal reflection contributes a factor of two. In contrast, we find that Andreev reflection contributes a factor G/G_0, which is $\gg 1$.

If the backscattering peak in an NS junction is so large, why has it not been noticed before in a transport experiment? The reason is a cancellation in the integrated angular reflection distribution which effectively eliminates the contribution from enhanced backscattering to the conductance of the NS junction. However, this cancellation does not occur if one uses a ballistic point contact to inject the current into the junction. We discuss two configurations, both of which show an excess conductance due to enhanced backscattering which is a factor G/G_0 greater than the weak-localization correction.

We consider a disordered normal-metal conductor (length L, width W, mean free path l, with N propagating transverse modes at the Fermi energy E_F) which is connected at one end to a superconductor (see inset of Fig. 1). An electron (energy E_F) incident from the opposite end in mode m is reflected into some other mode n, either as an electron or as a hole, with probability amplitudes r^{ee}_{nm} and r^{he}_{nm}, respectively. The $N \times N$ matrices r^{ee} and r^{he} are given by [4]

$$r^{ee} = s_{11} - s_{12}s^*_{22}(1 + s_{22}s^*_{22})^{-1}s_{21}, \tag{4.1.1}$$

$$r^{he} = -is^*_{12}(1 + s_{22}s^*_{22})^{-1}s_{21}. \tag{4.1.2}$$

The s_{ij}'s are submatrices of the scattering matrix S of the disordered normal region,

$$S = \begin{pmatrix} s_{11} & s_{12} \\ s_{21} & s_{22} \end{pmatrix} = \begin{pmatrix} u & 0 \\ 0 & v \end{pmatrix} \begin{pmatrix} -\sqrt{\mathbf{R}} & \sqrt{\mathbf{T}} \\ \sqrt{\mathbf{T}} & \sqrt{\mathbf{R}} \end{pmatrix} \begin{pmatrix} u' & 0 \\ 0 & v' \end{pmatrix},$$

where u, v, u', v' are $N \times N$ unitary matrices, $\mathbf{R} = 1 - \mathbf{T}$, and $\mathbf{T}$ is a diagonal matrix with the transmission eigenvalues $T_1, T_2, \ldots T_N$ on the diagonal.

We first consider zero magnetic field ($B = 0$). Time-reversal symmetry then requires that S is a symmetric matrix, hence $u' = u^{\mathrm{T}}$, $v' = v^{\mathrm{T}}$. Eq. (4.1.1) simplifies to

$$r^{\mathrm{ee}} = -2u\frac{\sqrt{1-\mathbf{T}}}{2-\mathbf{T}}u^{\mathrm{T}}, \quad r^{\mathrm{he}} = -\mathrm{i}u^*\frac{\mathbf{T}}{2-\mathbf{T}}u^{\mathrm{T}}. \tag{4.1.3}$$

We seek the average reflection probabilities $\langle |r_{nm}|^2 \rangle$, where $\langle \cdots \rangle$ denotes an average over impurity configurations. Following Mello, Akkermans, and Shapiro [5], we assume that u is uniformly distributed over the unitary group. This "isotropy assumption" is an approximation which ignores the finite time scale of transverse diffusion. The reflection probabilities contain a product of four u's, which can be averaged by means of the formula [6]

$$\begin{aligned}\langle u_{ni}u_{mj}u^*_{nk}u^*_{ml}\rangle &= (N^2-1)^{-1}(\delta_{ik}\delta_{jl}+\delta_{nm}\delta_{il}\delta_{jk}) - \\ &\quad (N^3-N)^{-1}(\delta_{il}\delta_{jk}+\delta_{nm}\delta_{ik}\delta_{jl}).\end{aligned} \tag{4.1.4}$$

The result is (with the definition $\tau_k \equiv T_k(2-T_k)^{-1}$)

$$\langle |r^{\mathrm{ee}}_{nm}|^2 \rangle = \frac{\delta_{nm}+1}{N^2+N}\left(N - \langle \textstyle\sum_k \tau_k^2 \rangle\right), \tag{4.1.5}$$

$$\langle |r^{\mathrm{he}}_{nm}|^2 \rangle = \frac{\delta_{nm}+1}{N^2+N}\langle \textstyle\sum_k \tau_k^2 \rangle + \frac{N\delta_{nm}-1}{N^3-N}\langle \textstyle\sum_{k\neq k'} \tau_k\tau_{k'} \rangle. \tag{4.1.6}$$

In the metallic regime $N \gg L/l \gg 1$. In this large-N limit we may factorize $\langle \sum_{k\neq k'} \tau_k\tau_{k'} \rangle$ into $\langle \sum_k \tau_k \rangle^2$, which can be evaluated using [7]

$$\langle \textstyle\sum_k f(T_k) \rangle = (Nl/L)\int_0^\infty dx\, f(1/\cosh^2 x). \tag{4.1.7}$$

The result for normal reflection is

$$\langle |r^{\mathrm{ee}}_{nm}|^2 \rangle = (1+\delta_{nm})N^{-1}(1-\tfrac{1}{2}l/L). \tag{4.1.8}$$

Off-diagonal ($n \neq m$) and diagonal ($n = m$) reflection differ by precisely a factor of two, just as in the normal state [5]. In contrast, for Andreev reflection we find

$$\langle |r^{\mathrm{he}}_{nm}|^2 \rangle = \tfrac{1}{2}l/NL \ \ (n \neq m), \ \ \langle |r^{\mathrm{he}}_{nn}|^2 \rangle = (\pi l/4L)^2. \tag{4.1.9}$$

Off-diagonal and diagonal reflection now differ by an order of magnitude $Nl/L \simeq G/G_0 \gg 1$.

Eqs. (4.1.8) and (4.1.9) hold for $B = 0$. If time-reversal symmetry is broken (by a magnetic field $B \gtrsim B_{\mathrm{c}} \equiv h/eLW$), then the matrices u, u', v, v' are all independent [7]. Carrying out the average in the large-N limit, we find

$$\langle |r^{\mathrm{ee}}_{nm}|^2 \rangle = N^{-1}(1-\tfrac{1}{2}l/L), \ \ \langle |r^{\mathrm{he}}_{nm}|^2 \rangle = \tfrac{1}{2}l/NL. \tag{4.1.10}$$

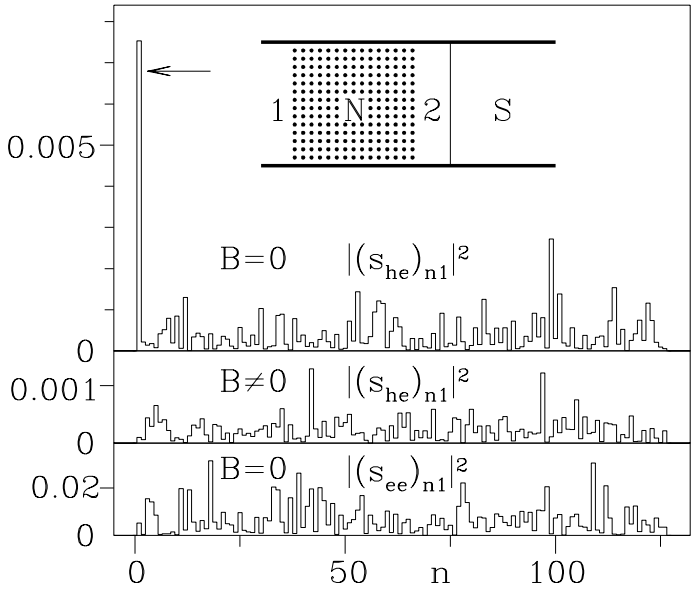

Figure 4-1. Numerical simulation of a 300×300 tight-binding model for a disordered normal metal ($L = 9.5\,l$), in series with a superconductor (inset). The histograms give the modal distribution for reflection of an electron at normal incidence (mode number 1). The top two panels give the distribution of reflected holes (for $B = 0$ and $B = 10\,h/eL^2$), the bottom panel of reflected electrons (for $B = 0$). The arrow indicates the ensemble-averaged height of the backscattering peak for Andreev reflection, predicted from Eq. (4.1.9).

Diagonal and off-diagonal reflection now occur with the same probability.

We have checked this theoretical prediction of a giant backscattering peak by a numerical simulation along the lines of Ref. [8]. The disordered normal region was modeled by a tight-binding Hamiltonian on a two-dimensional square lattice (dimensions 300×300, $N = 126$), with a random impurity potential at each site ($L/l = 9.5$). The scattering matrix S was computed numerically and then substituted into Eq. (4.1.1) to yield $r^{\rm ee}$ and $r^{\rm he}$. Results are shown in Fig. 4-1. This is raw data from a single sample. For normal reflection (bottom panel) the backscattering peak is not visible due to statistical fluctuations in the reflection probabilities (speckle noise). The backscattering peak for Andreev reflection is much larger than the fluctuations and is clearly visible (top panel). A magnetic flux of $10\,h/e$ through the disordered region completely destroys the peak (middle panel). The arrow in the top panel indicates the ensemble-averaged peak height from Eq. (4.1.9), consistent with the simulation within the statistical fluctuations. The peak is just one mode wide, as predicted by Eq. (4.1.9). If $W > L$ the isotropy assumption breaks down [5] and we expect the peak to broaden over W/L modes. Fig. 4-1 tells us that for $L = W$ the isotropy assumption is still reasonably accurate in this problem.

4.2 Large magnetoresistance in a point contact

Coherent backscattering in the normal state is intimately related to the weak-localization correction to the average conductance. We have found that the backscattering peak for Andreev reflection is increased by a factor G/G_0. However, the weak-localization correction in an NS junction remains of order G_0 [4,9]. The reason is that the conductance

$$G = 2G_0 \sum_{n,m} |r^{\rm he}_{nm}|^2 \tag{4.2.1}$$

contains the sum over all Andreev reflection probabilities [10], so that the backscattering peak is averaged out. Indeed, Eqs. (4.1.9) and (4.1.10) give the same G, up to corrections smaller by factors $1/N$ and l/L. In order to observe the enhanced backscattering in a transport experiment one has to increase the sensitivity to Andreev reflection at the angle of incidence. This can be done by injecting the electrons through a ballistic [1] point contact (width $\ll l$, number of transmitted modes N_0). For $B = 0$, one can compute the average conductance from [4]

$$\langle G \rangle = 2G_0 \textstyle\int_0^1 dT\, \rho(T) T^2 (2-T)^{-2}. \tag{4.2.2}$$

The density of transmission eigenvalues $\rho(T)$ is known [11, 12], in the regime $N_0 \gg 1$, $N \gg L/l$. One finds

$$\langle G \rangle = G_0 [\tfrac{1}{2}(1+\sin\vartheta)/N_0 + L/Nl\,]^{-1}, \tag{4.2.3}$$

$$\tfrac{1}{2}\vartheta(1+\sin\vartheta) = (N_0 L/Nl)\cos\vartheta, \quad \vartheta \in (0,\pi/2). \tag{4.2.4}$$

In the absence of time-reversal symmetry ($B \gtrsim B_{\rm c}$) we find from the large-N limit of Eqs. (4.1.1) and (4.2.1) that

$$\langle G \rangle = G_0 (1/N_0 + L/Nl)^{-1}. \tag{4.2.5}$$

This is just the classical addition in series of the Sharvin conductance $N_0 G_0$ of the point contact and the Drude conductance $(Nl/L)G_0$ of the disordered region.

In Fig. 4-2 we have plotted the difference $\Delta G = \langle G(B=0)\rangle - \langle G(B \gtrsim B_{\rm c})\rangle$ of Eqs. (4.2.3) and (4.2.5). If $N_0/N \ll l/L \ll 1$ the conductance drops from $2N_0G_0$ to N_0G_0 upon breaking time-reversal symmetry. A doubling of the contact conductance at $B = 0$ is well-known [13] in *ballistic* NS junctions ($l \gg L$). There it has a simple classical origin: An electron injected towards the NS interface is reflected back as a hole, doubling the current through the point contact. Here we find that the conductance doubling can survive multiple scattering by a disordered region ($l \ll L$), as a result of enhanced backscattering at the angle of incidence.

[1] It is essential that the point contact is ballistic. The conductance doubling at $B = 0$ was *not* found in a recent study of a diffusive point contact (width $\gg l$), by A. F. Volkov, Phys. Lett. A **187**, 404 (1994).

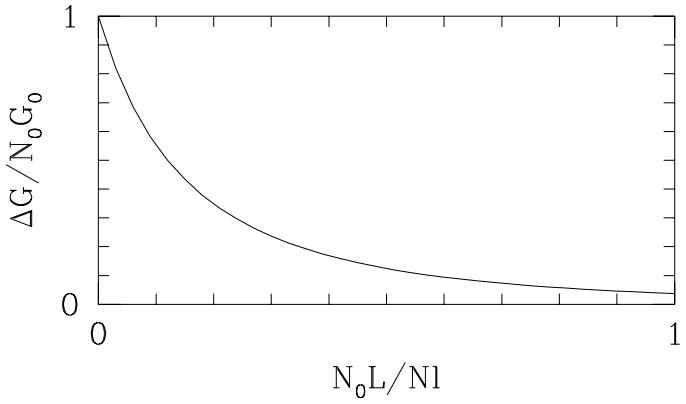

Figure 4-2. Excess conductance $\Delta G = \langle G(B=0)\rangle - \langle G(B \gtrsim B_c)\rangle$ of a ballistic point contact in series with a disordered NS junction (inset), computed from Eqs. (4.2.3) and (4.2.5). At $B = 0$ the contact conductance is twice the Sharvin conductance $N_0 G_0$, provided $N_0 L/Nl \ll 1$.

4.3 Excess conductance in a Josephson junction

As a second example we discuss how enhanced backscattering manifests itself when electrons are injected into a Josephson junction. The system considered is shown schematically in Fig. 4-3. A disordered metal grain is contacted by four ballistic point contacts (with N_i modes transmitted through contact $i = 1, 2, 3, 4$). The scattering matrix S has submatrices s_{ij}, the matrix element $s_{ij,nm}$ being the scattering amplitude from mode m in contact j to mode n in contact i. The grain forms a Josephson junction in a superconducting ring. Coupling to the two superconducting banks is via point contacts 3 and 4 (phase difference ϕ, same electrostatic potential). Contacts 1 and 2 are connected to normal metals (potential difference V). A current I is passed between contacts 1 and 2 and one measures the conductance $G = I/V$ as a function of ϕ. Spivak and Khmel'nitskiĭ computed $\langle G(\phi)\rangle$ at temperatures higher than the Thouless energy [14]. They found a periodic modulation of the weak-localization correction, with amplitude of order G_0. Zaitsev and Kadigrobov et al. have discovered that at lower temperatures the amplitude increases to become much greater than G_0 [15, 16]. Here we identify enhanced backscattering as the origin of this increase.

The reflection matrices $r^{\rm ee}$ and $r^{\rm he}$ (with elements $r_{ij,nm}$) contain the combined effect of scattering in the normal grain (described by the matrix S) and Andreev reflection at the two contacts with the superconductor. By summing a series of multiple Andreev reflections we obtain expressions analogous to Eq. (4.1.1),

$$r^{\rm ee} = a - b\,\Omega c^*\Omega^*(1 + c\,\Omega c^*\Omega^*)^{-1}d, \tag{4.3.1}$$

$$r^{\rm he} = -{\rm i}b^*\Omega^*(1 + c\,\Omega c^*\Omega^*)^{-1}d, \tag{4.3.2}$$

where we have abbreviated

$$a = \begin{pmatrix} s_{11} & s_{12} \\ s_{21} & s_{22} \end{pmatrix},\quad b = \begin{pmatrix} s_{13} & s_{14} \\ s_{23} & s_{24} \end{pmatrix},\quad c = \begin{pmatrix} s_{33} & s_{34} \\ s_{43} & s_{44} \end{pmatrix},$$

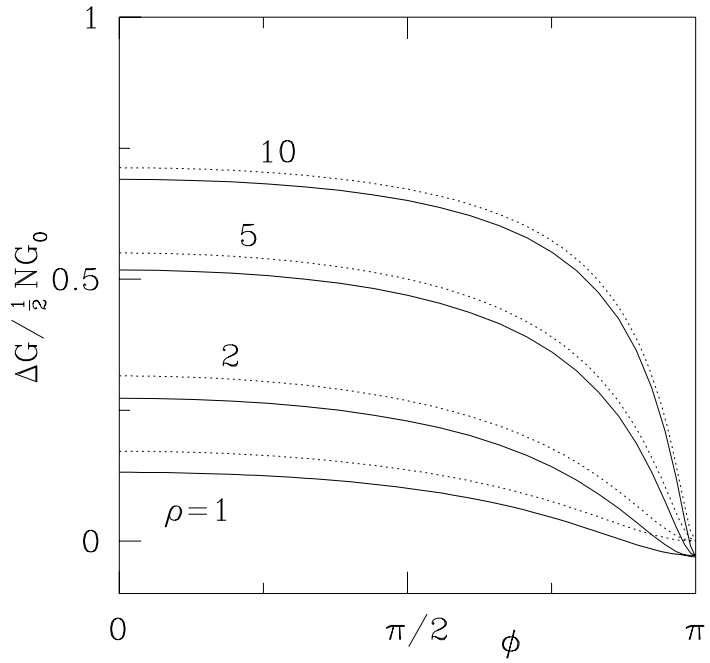

Figure 4-3. Solid curves: excess conductance $\Delta G = \langle G(\phi)\rangle_{\rm COE} - \langle G\rangle_{\rm CUE}$ of a four-terminal Josephson junction (inset), computed from Eqs. (4.3.1) and (4.3.3) for $N_1 = N_2 \equiv N$, $N_3 = N_4 \equiv \rho N$, with $N = 10$. The dotted curves are the large-N limit calculated according to [12]. The excess conductance at $\phi = 0$ is a factor $G/G_0 = \mathcal{O}(N)$ larger than the negative weak-localization correction at $\phi = \pi$.

$$d = \begin{pmatrix} s_{31} & s_{32} \\ s_{41} & s_{42} \end{pmatrix}, \quad \Omega = \begin{pmatrix} e^{i\phi/2} & 0 \\ 0 & e^{-i\phi/2} \end{pmatrix}.$$

The four-terminal generalization of Eq. (4.2.1) is [17]

$$G/G_0 = R^{\rm ee}_{21} + R^{\rm he}_{21} + \frac{2(R^{\rm he}_{11}R^{\rm he}_{22} - R^{\rm he}_{12}R^{\rm he}_{21})}{R^{\rm he}_{11} + R^{\rm he}_{22} + R^{\rm he}_{12} + R^{\rm he}_{21}}, \tag{4.3.3}$$

$$R^{\rm ee}_{ij} = \textstyle\sum_{n,m} |r^{\rm ee}_{ij,nm}|^2, \quad R^{\rm he}_{ij} = \sum_{n,m} |r^{\rm he}_{ij,nm}|^2. \tag{4.3.4}$$

Following Ref. [18], we evaluate $\langle G\rangle$ by averaging S over the circular ensemble. At $B = 0$ this means that $S = UU^{\rm T}$ with U uniformly distributed in the group $\mathcal{U}(M)$ of $M \times M$ unitary matrices ($M = \sum_{i=1}^4 N_i$). This is the circular orthogonal ensemble (COE). If time-reversal symmetry is broken, then S itself is uniformly distributed in $\mathcal{U}(M)$. This is the circular unitary ensemble (CUE). In the CUE we can do the average analytically for any N_i and ϕ. The result is

$$\langle G\rangle_{\rm CUE} = G_0 N_1 N_2/(N_1 + N_2), \tag{4.3.5}$$

independent of ϕ. In the COE we can do the average analytically for $N_i \gg 1$

and $\phi = 0$, and numerically [2] for any N_i and ϕ. We find that the difference $\Delta G(\phi) = \langle G(\phi)\rangle_{\rm COE} - \langle G\rangle_{\rm CUE}$ is positive for $\phi = 0$,

$$\frac{\Delta G(0)}{\langle G\rangle_{\rm CUE}} = \rho + \tfrac{1}{2}(1+\rho)^2 - (1+\rho)\sqrt{\rho + \tfrac{1}{4}(1+\rho)^2}, \tag{4.3.6}$$

with $\rho \equiv (N_3+N_4)/(N_1+N_2)$. The excess conductance (4.3.6) is a factor G/G_0 greater than the negative weak-localization correction, which is observable in Fig. 3 at $\phi = \pi$. For $N_i \gtrsim 10$ the finite-N curves (solid) are close to the large-N limit [3] (dotted) which we have obtained using the Green's function formulation of Refs. [12,15].

The excess conductance is a direct consequence of enhanced backscattering. This is easiest to see for the symmetric case $N_1 = N_2 \equiv N$, when $\langle R_{12}^{\rm he}\rangle = \langle R_{21}^{\rm he}\rangle$, $\langle R_{11}^{\rm he}\rangle = \langle R_{22}^{\rm he}\rangle$. Current conservation requires $R_{11}^{\rm he} + R_{21}^{\rm he} + R_{11}^{\rm ee} + R_{21}^{\rm ee} = N$. For $N \gg 1$ we may replace $\langle f(R_{ij})\rangle$ by $f(\langle R_{ij}\rangle)$. The average of Eq. (4.3.3) then becomes

$$\langle G/G_0\rangle = \tfrac{1}{2}N - \tfrac{1}{2}\langle R_{11}^{\rm ee} - R_{21}^{\rm ee}\rangle + \tfrac{1}{2}\langle R_{11}^{\rm he} - R_{21}^{\rm he}\rangle. \tag{4.3.7}$$

The first term $\frac{1}{2}N$ is the classical series conductance. The second term is the weak-localization correction due to enhanced backscattering for normal reflection. Since $\langle R_{11}^{\rm ee} - R_{21}^{\rm ee}\rangle = \mathcal{O}(1)$ this negative correction to $\frac{1}{2}N$ can be neglected if $N \gg 1$. The third term gives the excess conductance due to enhanced backscattering for Andreev reflection. Since $\langle R_{11}^{\rm he} - R_{21}^{\rm he}\rangle = \mathcal{O}(N)$ this positive contribution is a factor $G/G_0 = \mathcal{O}(N)$ greater than the negative weak-localization correction.

In conclusion, we have predicted (and verified by numerical simulation) an order G/G_0 enhancement of coherent backscattering by a disordered metal connected to a superconductor. The enhancement can be observed as an excess conductance which is a factor G/G_0 greater than the weak-localization correction, provided ballistic point contacts are used to inject the current into the junction. The junction should be sufficiently small that phase coherence is maintained throughout. Several recent experiments [19] are close to this size regime, and might well be equipped with ballistic point contacts.

[2] To average Eq. (4.3.3) numerically we generated up to 10^4 random matrices in $\mathcal{U}(M)$. This can be done efficiently by parameterizing the matrix elements by Euler angles [K. Życzkowski and M. Kuś, Phys. Rev. E **53**, 319 (1996)].

[3] By applying Nazarov's large-N formulas [12] to the geometry of Fig. 3, we find $\Delta G(\phi) = \frac{1}{2}NG_0\tan^2\frac{1}{2}\vartheta$, with $\vartheta \in (0,\pi/2)$ determined by $\sin\vartheta + \sin^2\vartheta\cos\frac{1}{2}\phi = \rho(\cos\vartheta + \cos^2\vartheta)\cos\frac{1}{2}\phi$.

References

[1] *Mesoscopic Phenomena in Solids*, edited by B. L. Al'tshuler, P. A. Lee, and R. A. Webb (North-Holland, Amsterdam, 1991).

[2] R. Berkovits and S. Feng, Phys. Rep. **238**, 135 (1994).

[3] G. Bergmann, Phys. Rep. **107**, 1 (1984).

[4] C. W. J. Beenakker, Phys. Rev. B **46**, 12841 (1992); reviewed in *Mesoscopic Quantum Physics*, edited by E. Akkermans, G. Montambaux, and J.-L. Pichard (North-Holland, Amsterdam, 1995).

[5] P. A. Mello, E. Akkermans, and B. Shapiro, Phys. Rev. Lett. **61**, 459 (1988).

[6] P. A. Mello, J. Phys. A **23**, 4061 (1990).

[7] A. D. Stone, P. A. Mello, K. A. Muttalib, and J.-L. Pichard, in Ref. [1].

[8] I. K. Marmorkos, C. W. J. Beenakker, and R. A. Jalabert, Phys. Rev. B **48**, 2811 (1993).

[9] Y. Takane and H. Otani, J. Phys. Soc. Japan **63**, 3361 (1994).

[10] Y. Takane and H. Ebisawa, J. Phys. Soc. Japan **61**, 1685 (1992).

[11] C. W. J. Beenakker and J. A. Melsen, Phys. Rev. B **50**, 2450 (1994).

[12] Yu. V. Nazarov, Phys. Rev. Lett. **73**, 134 (1994); **73**, 1420 (1994); in *Quantum Dynamics of Submicron Structures*, edited by H. A. Cerdeira, B. Kramer, and G. Schön, NATO ASI Series E291 (Kluwer, Dordrecht, 1995).

[13] P. C. van Son, H. van Kempen, and P. Wyder, Phys. Rev. Lett. **59**, 2226 (1987).

[14] B. Z. Spivak and D. E. Khmel'nitskiĭ, Pis'ma Zh. Eksp. Teor. Fiz. **35**, 334 (1982) [JETP Lett. **35**, 412 (1982)].

[15] A. V. Zaitsev, Phys. Lett. A **194**, 315 (1994).

[16] A. Kadigrobov, A. Zagoskin, R. I. Shekhter, and M. Jonson, Phys. Rev. B **52**, 8662 (1995).

[17] C. J. Lambert, J. Phys. Condens. Matter **3**, 6579 (1991).

[18] H. U. Baranger and P. A. Mello, Phys. Rev. Lett. **73**, 142 (1994); R. A. Jalabert, J.-L. Pichard, and C. W. J. Beenakker, Europhys. Lett. **27**, 255 (1994).

[19] P. G. N. de Vegvar, T. A. Fulton, W. H. Mallison, and R. E. Miller, Phys. Rev. Lett. **73**, 1416 (1994); V. T. Petrashov, V. N. Antonov, P. Delsing, and T. Claeson, Phys. Rev. Lett. bf 74, 5268 (1995).

5 Induced superconductivity distinguishes chaotic from integrable billiards

The quantization of a system with a chaotic classical dynamics is the fundamental problem of the field of "quantum chaos" [1, 2]. It is known that the statistics of the energy levels of a two-dimensional confined region (a "billiard") is different if the dynamics is chaotic or integrable [3–5]: A chaotic billiard has Wigner-Dyson statistics, while an integrable billiard has Poisson statistics. The two types of statistics are entirely different as far as the level correlations are concerned [6]. However, the mean level spacing is essentially the same: Particles of mass m in a billiard of area A have density of states $mA/2\pi\hbar^2$, regardless of whether their dynamics is chaotic or not.

In the solid state, chaotic billiards have been realized in semiconductor microstructures known as "quantum dots" [7]. These are confined regions in a two-dimensional electron gas, of sufficiently small size that the electron motion remains ballistic and phase-coherent on long time scales. (Long compared to the mean dwell time $t_{\rm dwell}$ of an electron in the confined region, which itself is much longer than the ergodic time $t_{\rm erg}$ in which an electron explores the available phase space.) A tunneling experiment measures the density of states in the quantum dot, if its capacitance is large enough that the Coulomb blockade can be ignored. As mentioned above, this measurement does not distinguish chaotic from integrable dynamics.

In this chapter we show that the density of states becomes a probe for quantum chaos if the electron gas is brought into contact with a superconductor. We first consider a chaotic billiard. Using random-matrix theory, we compute in Sec. 5.1 the density of states $\rho(E)$ near the Fermi level ($E = 0$), and find that the coupling to a superconductor via a tunnel barrier induces an energy gap $E_{\rm gap}$ of the order of the Thouless energy $E_{\rm T} \simeq \hbar/t_{\rm dwell}$. More precisely,

$$E_{\rm gap} = cN\Gamma\delta/2\pi, \tag{5.0.1}$$

where N is the number of transverse modes in the barrier, Γ is the tunnel probability per mode, 2δ is the mean level spacing of the isolated billiard, and c is a number which is weakly dependent on Γ (c decreases from 1 to 0.6 as Γ increases from 0 to 1). Eq. (5.0.1) requires $1 \ll N\Gamma \ll \Delta_0/\delta$, where Δ_0 is the energy gap in the bulk of the superconductor. In this limit $\rho(E)$ vanishes identically for $E \leq E_{\rm gap}$. In contrast, for an integrable billiard we do not find an energy gap in which $\rho = 0$, but instead find in Sec. 5.2 that the density of states vanishes linearly with energy near the Fermi level. We present a general argument that in an integrable billiard ρ has a power-law dependence on E for small E. In section 5.3 we describe the transition to the case of broken time-reversal symmetry.

5.1 Chaotic billiards

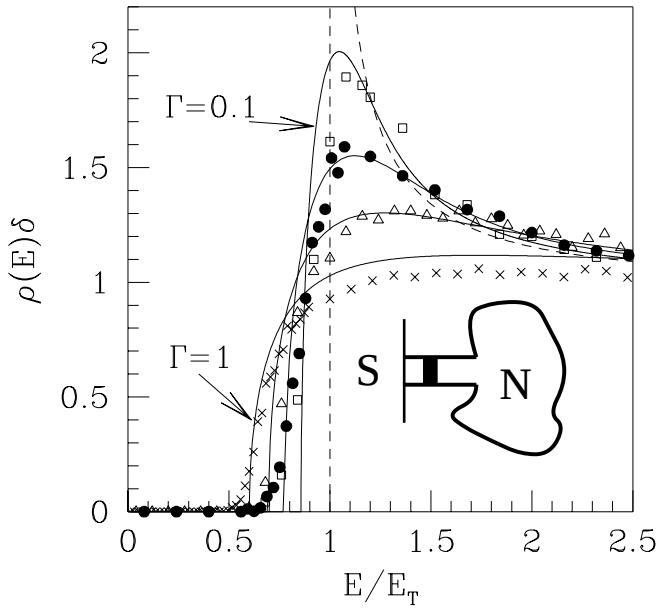

Figure 5-1. Density of states of a chaotic billiard coupled to a superconductor (inset), for various coupling strengths. The energy is in units of the Thouless energy $E_{\rm T} = N\Gamma\delta/2\pi$. The solid curves are computed from Eqs. (5.1.8) and (5.1.10), for Γ = 1, 0.5, 0.25, 0.1. The dashed curve is the asymptotic result (5.1.15) for $\Gamma \ll 1$. The data points are a numerical solution of Eq. (5.1.2), averaged over 10^5 matrices H_0 in the Gaussian orthogonal ensemble (M = 400, N = 80). The deviation from the analytical curves is mainly due to the finite dimensionality M of H_0 in the numerics.

The system considered is shown schematically in the inset of Fig. 5-1. A confined region in a normal metal (N) is connected to a superconductor (S) by a narrow lead containing a tunnel barrier. The lead supports N propagating modes at the Fermi energy. Each mode may have a different tunnel probability Γ_n, but later on we will take all Γ_n's equal to Γ for simplicity. The confined region is characterized by a scattering matrix S_0. The modes in the leads which form the basis of S_0 are chosen such that their wave functions are real at the NS interface. Evanescent modes in the leads are disregarded. The proximity effects considered here require time-reversal symmetry, so we assume zero magnetic field. (The transition to the case of broken time-reversal symmetry is studied in Sec. 5.3. The case of completely broken time-reversal symmetry has been studied previously [8–10].) The quasi-particle excitation spectrum of the system is discrete for energies below Δ_0. We are interested in the low-lying part of the spectrum, consisting of (positive) excitation energies $E_n \ll \Delta_0$. The energy de-

pendence of S_0 is set by the Thouless energy E_T, which is inversely proportional to the dwell time of an electron in the billiard. We assume that the Thouless energy $E_T \equiv N\Gamma\delta/2\pi$ is also much smaller than Δ_0.[1] Andreev reflection at the superconductors scatters electrons (at energy $E > 0$) into holes (at energy $-E$), with a phase increment $-\arccos(E/\Delta_0)$. (Normal reflection at the superconductors can be neglected if $\Delta_0 \ll E_F$.) We assume that E and E_T are both $\ll \Delta_0$, so that we may replace $\arccos(E/\Delta_0)$ by $\pi/2$, while retaining the E-dependence of S_0. The excitation spectrum is obtained from the determinantal equation [11]

$$\mathrm{Det}[1 + S_0(E)S_0^*(-E)] = 0. \tag{5.1.1}$$

The $N \times N$ unitary matrix $S_0(E)$ is the scattering matrix of the quantum dot plus tunnel barrier at an energy E above the Fermi level. Eq. (5.1.1) is a convenient starting point for the case that the quantum dot is an integrable billiard. For the chaotic case, we will use an alternative — but equivalent — determinant equation involving an effective Hamiltonian [10],

$$\mathrm{Det}(E - H_{\mathrm{eff}}) = 0,\ H_{\mathrm{eff}} = \begin{pmatrix} H & -\pi WW^{\mathrm{T}} \\ -\pi WW^{\mathrm{T}} & -H^* \end{pmatrix}. \tag{5.1.2}$$

The equivalence is proved by the relation between the scattering matrix S_0 and the Hamiltonian matrix H of the isolated billiard [12],

$$S_0(E) = 1 - 2\pi i W^\dagger (E - H + i\pi WW^\dagger)^{-1} W. \tag{5.1.3}$$

The $M \times M$ Hermitian matrix H is the Hamiltonian of the isolated quantum dot. (The finite dimension M is taken to infinity later on.) Because of time-reversal symmetry, $H = H^*$. The $M \times N$ coupling matrix W has elements

$$\begin{aligned} W_{mn} &= \delta_{mn} \left(\frac{2M\delta}{\pi^2}\right)^{1/2} \left(2\Gamma_n^{-1} - 1 + 2\Gamma_n^{-1}\sqrt{1-\Gamma_n}\right)^{1/2}, \\ & \qquad m = 1, 2, \ldots M, \quad n = 1, 2, \ldots N. \end{aligned} \tag{5.1.4}$$

The energy δ is one half the mean level spacing of H, which equals the mean level spacing of H_{eff} if $W = 0$.

We now proceed to compute the density of states. We first consider the case of a chaotic billiard. The Hamiltonian H then has the distribution of the Gaussian orthogonal ensemble [6],

$$P(H) \propto \exp\left(-\tfrac{1}{4}M\lambda^{-2}\,\mathrm{Tr}\,H^2\right),\ \lambda = 2M\delta/\pi. \tag{5.1.5}$$

We seek the density of states

$$\rho(E) = -\pi^{-1}\mathrm{Im}\,\mathrm{Tr}\,\langle (E + i0^+ - H_{\mathrm{eff}})^{-1}\rangle, \tag{5.1.6}$$

[1] The opposite regime $E_T \gg \Delta_0$ has a trivial discrete spectrum, consisting of N states with energies E_n just below Δ_0.

where $\langle\cdots\rangle$ denotes an average over $H_{\rm eff}$ for fixed W and H distributed according to Eq. (5.1.5). The method we use to evaluate this average is a perturbation expansion in $1/M$, adapted from Refs. [13, 14]. Because of the block structure of $H_{\rm eff}$ [see Eq. (5.1.2)], the Green function $G(z) = \langle (z - H_{\rm eff})^{-1}\rangle$ consists of four $M \times M$ blocks G_{11}, G_{12}, G_{21}, G_{22}. By taking the trace of each block separately, one arrives at a 2×2 matrix Green function

$$G = \frac{\lambda}{M} \begin{pmatrix} \mathrm{Tr}\, G_{11} & \mathrm{Tr}\, G_{12} \\ \mathrm{Tr}\, G_{21} & \mathrm{Tr}\, G_{22} \end{pmatrix}. \tag{5.1.7}$$

(We have multiplied by $\lambda/M = 2\delta/\pi$ for later convenience.) One more trace yields the density of states,

$$\rho(E) = -\tfrac{1}{2}\delta^{-1}\mathrm{Im}\mathrm{Tr}\, G(E + i0^+). \tag{5.1.8}$$

To leading order in $1/M$, the matrix G satisfies

$$G = \frac{\lambda}{M} \sum_{n=1}^{M} \begin{pmatrix} z - \lambda G_{11} & \pi w_n^2 + \lambda G_{12} \\ \pi w_n^2 + \lambda G_{21} & z - \lambda G_{22} \end{pmatrix}^{-1}, \tag{5.1.9}$$

where we have abbreviated $w_n^2 = (WW^{\rm T})_{nn}$. Eq. (5.1.9) is a matrix-generalization of Pastur's equation [15]. A unique solution is obtained by demanding that G goes to λ/z times the unit matrix as $|z| \to \infty$.

We now restrict ourselves to identical tunnel probabilities, $\Gamma_n \equiv \Gamma$. For $M \gg N \gg 1/\Gamma$ Eq. (5.1.9) simplifies to

$$NG_{11}\delta = \pi z G_{12}(-G_{12} + 1 - 2/\Gamma),\ G_{22} = G_{11},\ G_{21} = G_{12},\ G_{12}^2 = 1 + G_{11}^2. \tag{5.1.10}$$

This set of equations can be solved analytically.[2] The result is that $\rho(E) = 0$ for $E \le E_{\rm gap}$, where $E_{\rm gap}$ is determined by

$$\begin{aligned} &\frac{k^6 - k^4}{(1-k)^6}x^6 - \frac{3k^4 - 20k^2 + 16}{(1-k)^4}x^4 + \frac{3k^2 + 8}{(1-k)^2}x^2 = 1, \\ &x = E_{\rm gap}/E_{\rm T},\ k = 1 - 2/\Gamma. \end{aligned} \tag{5.1.11}$$

The solution of this gap equation is the result (5.0.1) announced in the introduction. The complete analytical solution of Eq. (5.1.10) is not very insightfull and is therefore omitted here. In Fig. 5-1 we plot the resulting density of states. In

[2] It is worth noting that Eqs. (5.1.10-5.1.15) also apply to the case that the chaotic billiard is coupled via two identical leads to two superconductors, having a phase difference ϕ. The density of states of such a quantum-dot Josephson junction is obtained by the replacement $\Gamma \to \Gamma_{\rm eff} = 2\cos(\frac{1}{2}\phi)[\cos(\frac{1}{2}\phi) - 1 + 2/\Gamma]^{-1}$. For a phase shift of π the excitation gap closes (since $\phi \to \pi$ corresponds to $\Gamma_{\rm eff} \to 0$), in agreement with Ref. [9].

the limit $\Gamma = 1$ of ideal coupling it is given by

$$\rho(E) = \frac{E_T\sqrt{3}}{6E\delta}[Q_+(E/E_T) - Q_-(E/E_T)], \tag{5.1.12}$$

$$Q_\pm(x) = \left[8 - 36x^2 \pm 3x\sqrt{3x^4 + 132x^2 - 48}\right]^{1/3}, \tag{5.1.13}$$

$$E > E_{gap} = 2E_T\,\gamma^{5/2} \approx 0.6\,E_T, \tag{5.1.14}$$

where $\gamma = \frac{1}{2}(\sqrt{5} - 1)$ is the golden number. In the opposite limit $\Gamma \ll 1$ of weak coupling we find

$$\rho(E) \;=\; E\delta^{-1}(E^2 - E_T^2)^{-1/2},\; E > E_{gap} = E_T. \tag{5.1.15}$$

To check the validity of the perturbation theory, we have computed $\rho(E)$ numerically from Eq. (5.1.2) by generating a large number of random matrices H in the Gaussian orthogonal ensemble. The numerical results (data points in Fig. 5-1) are consistent with Eq. (5.1.10), given the finite dimensionality of H in the numerics.

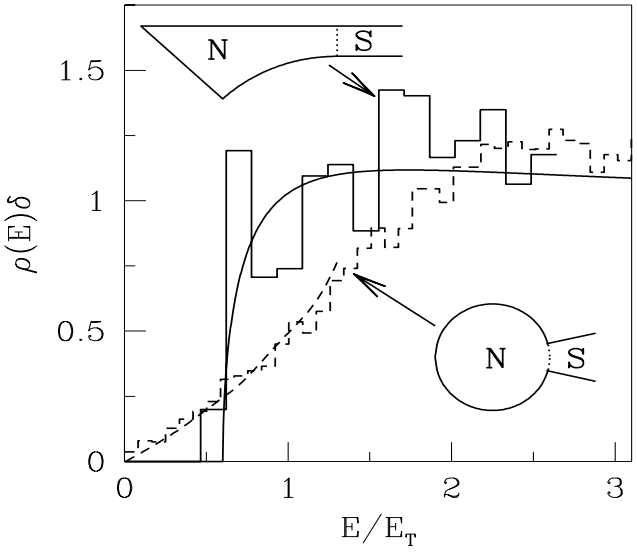

Figure 5-2. Histograms: density of states of a billiard coupled to a superconductor, computed from Eq. (5.1.1) and averaged over a range of Fermi energies. A chaotic Sinai billiard (top inset, solid histogram) is contrasted with an integrable circular billiard (bottom inset, dashed histogram). The number of propagating transverse modes at the normal-metal—superconductor interface (dotted line in the insets) equals $N = 20$ in the chaotic billiard and $N = 30$ in the circular billiard. The solid curve is the prediction from random-matrix theory, the dashed curve is the prediction from the Bohr-Sommerfeld approximation.

So far we have used random-matrix theory to describe the chaotic system. As a more rigorous test, we can compute the exact quantum mechanical density

of states of a specific billiard, coupled to a superconductor. Following Doron, Smilansky, and Frenkel [16] we study a segment of a Sinai billiard, drawn to scale in the top inset of Fig. 5-2. The scattering matrix $S_0(E)$ is determined by matching wave functions at the dotted line separating the billiard (area A) from the lead (width W). The NS interface is also chosen at the dotted line. The density of states $\rho(E)$ follows from Eq. (5.1.1). We average $\rho(E)$ over a small variation of E_F, such that the number of modes $N = \text{Int}[m v_F W/\pi\hbar]$ in the lead does not change. The result for $N = 20$ is shown in Fig. 5-2 (solid histogram), and is seen to agree quite well with the prediction from random-matrix theory (solid curve). There is no adjustable parameter in this comparison, the mean level spacing δ following directly from $\delta = \pi\hbar^2/mA$.

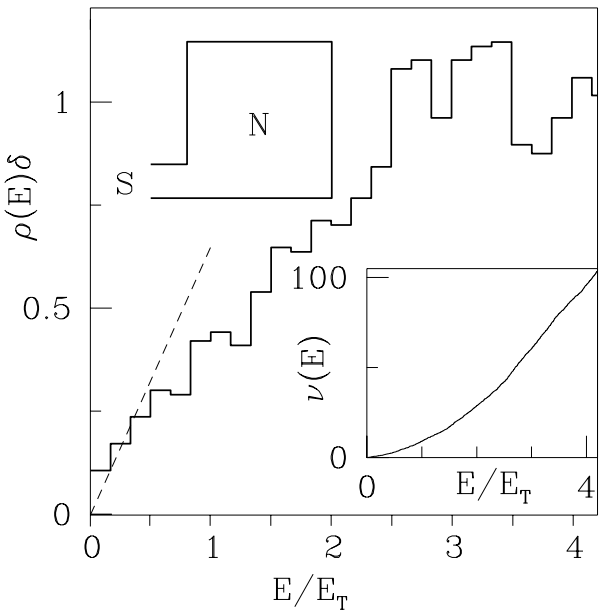

Figure 5-3. Histogram: density of states for a rectangular billiard (shown to scale in the upper left inset), calculated numerically from Eq. (5.1.1). Dashed curve: Bohr-Sommerfeld approximation (5.2.2). The lower right inset shows the integrated density of states, which is the quantity following directly from the numerical computation. The energy $E_T = N\delta/2\pi$, with $N = 200$ modes in the lead to the superconductor.

5.2 Integrable billiards

We now turn to non-chaotic billiards. We consider two types of billiards: rectangular and circular ones.

The rectangular billiard has a lead perpendicular to one of the sides of the rectangle which connects it to a superconductor. (The billiards are drawn to

scale in the insets of Fig. 5-2 and Fig. 5-3). There are no tunnel barriers in the leads. The scattering matrix $S_0(E)$ is computed by matching wave functions in the rectangle to transverse modes in the lead. The density of states then follows from Eq. (5.1.1). To improve the statistics, we averaged over 16 rectangles with small differences in shape but the same area A (and hence the same $\delta = \pi\hbar^2/mA$). The number of modes in the lead (width W) was fixed at $N = m v_F W/\pi\hbar = 200$ (where v_F is the Fermi velocity). In the lower right inset of Fig. 5-3 we show the integrated density of states $\nu(E) = \int_0^E dE' \rho(E')$, which is the quantity following directly from the numerical computation. The density of states $\rho(E)$ itself is shown in the main plot.

We next turn to a circular billiard. The scattering matrix $S_0(E)$ is again determined by matching wave functions at the dotted line (see inset of Fig. 5-2), which also determines the location of the NS interface. A wedge-shaped lead (opening angle θ) is chosen in order not to break the rotational symmetry (which simplifies the calculations). The density of states is averaged over a range of Fermi energies at fixed $N = \mathrm{Int}[m v_F R\theta/\pi\hbar]$. The result for $N = 30$ is the dashed histogram in Fig. 5-2.

The density of states in an integrable billiard can be approximated with a Bohr-Sommerfeld quantization rule,

$$\rho_{\rm BS}(E) = N \int_0^\infty ds\, P(s) \sum_{n=0}^{\infty} \delta\left(E - (n+\tfrac{1}{2})\pi\hbar v_F/s\right). \tag{5.2.1}$$

Here $P(s)$ is the classical probability that an electron entering the billiard will exit after a path length s. Eq. (5.2.1) is the Bohr-Sommerfeld quantization rule for the classical periodic motion with path length $2s$ and phase increment per period of $2Es/\hbar v_F - \pi$. The periodic motion is the result of Andreev reflection at the interface with the superconductor, which causes the electron to retrace its path as a hole. The phase increment consists of a part $2Es/\hbar v_F$ because of the energy difference $2E$ between electron and hole, plus a phase shift of $-\pi$ from two Andreev reflections. In the rectangular billiard we find for $s \to \infty$ $P(s) \to 8(A/W)^2 s^{-3}$, which implies a linear E-dependence of the density of states near the Fermi-level,

$$\rho_{\rm BS}(E) \to \frac{4E}{N\delta^2} = \frac{2E}{\pi E_{\rm T}\delta}, \qquad E \to 0. \tag{5.2.2}$$

In Fig. 5-3 we see that the exact quantum mechanical density of states also has (approximately) a linear E-dependence near $E = 0$, but with a smaller slope than the semi-classical Bohr-Sommerfeld approximation. For the circular billiard, we have calculated $P(s)$ by generating a large number of classical trajectories. The resulting density of states $\rho_{\rm BS}(E)$ is in good agreement with the quantum mechanical result in Fig. 5-2.

We argue that the absence of an excitation gap found in the rectangular and circular billiards is generic for the whole class of integrable billiards. Our argument is based on the Bohr-Sommerfeld approximation. It is known [17,18] that

an integrable billiard has a power-law distribution of path lengths, $P(s) \to s^{-p}$ for $s \to \infty$. Eq. (5.2.1) then implies a power-law density of states, $\rho(E) \propto E^{p-2}$ for $E \to 0$.

5.3 Partially broken time-reversal symmetry

The results in the previous section have been obtained for the case of zero magnetic field. They are a result of the special symmetry of the effective Hamiltonian $H_{\rm eff}$. In this section, we extend the results of the former section to the case of partially broken time-reversal symmetry. The time-reversal symmetry is broken by applying a magnetic flux through the normal dot. We consider a Josephson junction geometry.

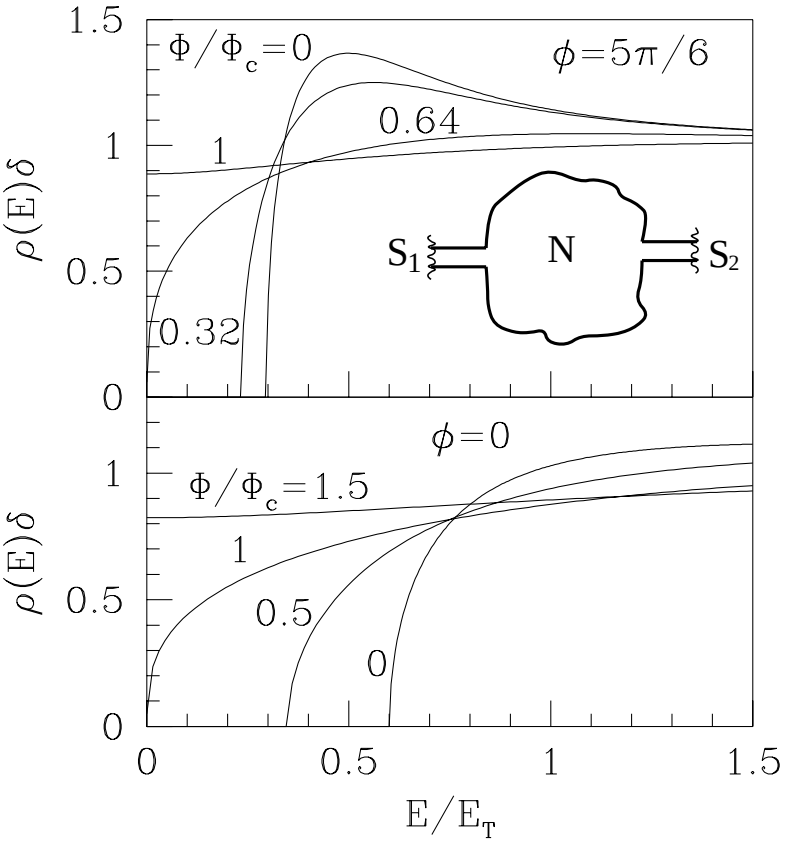

Figure 5-4. Density of states of a chaotic billiard coupled to two superconductors by identical ballistic point contacts, for four values of the magnetic flux Φ through the billiard. The phase difference ϕ between the superconductors equals $5\pi/6$ and 0 in the top and bottom panel, respectively. The curves are computed from Eqs. (5.1.8) and (5.3.5). The Thouless energy is given by $E_{\rm T} = N\delta/2\pi$, and the critical flux $\Phi_{\rm c}$ is defined by Eqs. (5.3.2) and (5.3.6).

The system studied is shown schematically in the inset of Fig. 5-4. A billiard consisting of a normal metal (N) in a perpendicular magnetic field B is connected to two superconductors (S_1, S_2) by narrow leads, each containing $N/2$ transverse modes at the Fermi energy E_F. The order parameters in S_1 and S_2 have a phase difference $\phi \in [0,\pi]$. Mode n couples to a superconductor with phase $\phi_n = \phi/2$ for $1 \le n \le N/2$, $\phi_n = -\phi/2$ for $1 + N/2 \le n \le N$. For simplicity, we assume in this section that there are no tunnel barriers in the leads ($\Gamma = 1$). (The generalization to $\Gamma \neq 1$ is straightforward: the mapping $\{\Gamma, \cos\frac{\phi}{2}\} \to \{1, \frac{\Gamma}{2-\Gamma}\cos\frac{\phi}{2}\}$ produces identical results.)

We assume that the Hamiltonian matrix H has the Pandey-Mehta distribution [6,19]

$$P(H) \propto \exp\left(-\frac{M(1+\alpha^2)}{4\lambda^2}\sum_{i,j=1}^{M}\left[(\mathrm{Re}H_{ij})^2 + \alpha^{-2}(\mathrm{Im}H_{ij})^2\right]\right), \tag{5.3.1}$$

with $\lambda = 2M\delta/\pi$. The parameter $\alpha \in [0,1]$ measures the strength of the time-reversal symmetry breaking. The relation between α and the magnetic flux Φ through a two-dimensional billiard (area A, no impurities, Fermi velocity v_F) is [20,21]

$$M\alpha^2 = c(\Phi e/h)^2 \hbar v_F (A\delta^2)^{-1/2}, \tag{5.3.2}$$

with c a numerical coefficient of order unity. (For example, $c = \frac{2}{3}\sqrt{\pi}$ for a circular billiard which is chaotic because of diffuse boundary scattering [21].) Time-reversal symmetry is effectively broken when $M\alpha^2 \simeq N$, which occurs for $\Phi \ll h/e$. The effect of such weak magnetic fields on the bulk superconductor can be ignored.

In order to determine the density of states, we adopt the Green function technique described in Sec. 5.1, using the slightly modified effective Hamiltonian

$$H_{\rm eff} = \begin{pmatrix} H & -\pi W e^{i\Phi} W^{\rm T} \\ -\pi W e^{-i\Phi} W^{\rm T} & -H^* \end{pmatrix}. \tag{5.3.3}$$

To highest order in $1/M$, the self-consistency equation for G now reads

$$G = \frac{\lambda}{M}\sum_{n=1}^{M}\begin{pmatrix} z-\lambda G_{11} & \pi w_n^2 + x\lambda G_{12} \\ \pi w_n^{*2} + x\lambda G_{21} & z-\lambda G_{22} \end{pmatrix}^{-1}, \tag{5.3.4}$$

where we have abbreviated $w_n^2 = (We^{i\Phi}W^{\rm T})_{nn}$ and $x = (1-\alpha^2)/(1+\alpha^2)$. Eq. (5.3.4) is complemented with the boundary condition $G \to \lambda/z$ for $|z| \to \infty$.

We take the limit $M \to \infty$ at fixed $M\alpha^2$ and δ, and assume in addition that $N \gg 1$. Eq. (5.3.4) then simplifies to

$$\begin{aligned} G_{11} &= [\tfrac{1}{2}(\Phi/\Phi_c)^2 G_{11} - \pi z/N\delta] \times [G_{12}^2 + G_{12}/\cos(\phi/2)], \\ G_{22} &= G_{11},\ G_{21} = G_{12},\ G_{12}^2 = 1 + G_{11}^2, \end{aligned} \tag{5.3.5}$$

where we have defined the critical flux Φ_c by

$$M\alpha^2 = \tfrac{1}{8}N(\Phi/\Phi_c)^2. \tag{5.3.6}$$

The solution of Eq. (5.3.5) for $\phi = 0$ and $\phi = 5\pi/6$ is plotted in Fig. 5-4 for several values of Φ/Φ_c. For $\Phi = 0$ and $\phi = 0$ the excitation gap equals $E_{\rm gap} = aE_T$, with $E_T = N\delta/2\pi$ and $a = 2^{-3/2}(\sqrt{5}-1)^{5/2} \approx 0.6$. The gap decreases with increasing flux Φ or phase difference ϕ. When $\phi = 0$, the gap closes at the critical flux $\Phi_c \simeq (h/e)(N\delta/\hbar v_F)^{1/2}A^{1/4}$. When $\phi = \pi$, there is no gap at any magnetic field. For ϕ between 0 and π, the gap closes at the flux $\Phi_c(\phi)$ given by

$$\Phi_c(\phi) = \left[\frac{2\cos(\phi/2)}{1+\cos(\phi/2)}\right]^{1/2}\Phi_c. \tag{5.3.7}$$

5.4 Conclusion

To conclude, we have shown that the presence of an excitation gap in a billiard connected to a superconductor is a signature of quantum chaos, which is special in two respects: It appears in the spectral density rather than in a spectral correlator, and it manifests itself on the macroscopic energy scale of the Thouless energy rather than on the microscopic scale of the level spacing. Both these characteristics are favorable for experimental observation. The excitation gap closes at a critical flux Φ_c through the billiard. In order of magnitude, $\Phi_c \simeq (h/e)(\tau_{\rm ergodic}/\tau_{\rm dwell})^{1/2}$, where $\tau_{\rm dwell}$ is the mean dwell time of an electron in the billiard and $\tau_{\rm ergodic}$ is the time required to explore the entire available phase space. The precise value of Φ_c depends on the shape of the billiard, but the dependence on the tunnel probability Γ and the phase difference ϕ is universal:

$$\Phi_c(\Gamma,\phi) = \Phi_c(1,0)\left[\frac{2\cos(\phi/2)}{\cos(\phi/2)-1+2/\Gamma}\right]^{1/2}. \tag{5.4.1}$$

The density of states in integrable billiards $\rho(E) \propto E$ for small E. We have presented an argument that the results for the rectangle and the circle are generic for the whole class of integrable billiards, based on the semi-classical Bohr-Sommerfeld approximation. The agreement with the semi-classical Bohr-Sommerfeld approximation is better for the circular than for the rectangular billiard. A rigorous semi-classical theory for this problem remains to be developed.

References

[1] *Chaos and Quantum Physics*, edited by M.-J. Giannoni, A. Voros, and J. Zinn-Justin (North-Holland, Amsterdam, 1991).

[2] M. C. Gutzwiller, *Chaos in Classical and Quantum Mechanics* (Springer, New York, 1990).

[3] O. Bohigas, M.-J. Giannoni, and C. Schmit, Phys. Rev. Lett. **52**, 1 (1984); O. Bohigas, in Ref. [1].

[4] M. V. Berry, Proc. R. Soc. London A **400**, 229 (1985); M. V. Berry, in Ref. [1].

[5] A. V. Andreev, O. Agam, B. D. Simons, and B. L. Altshuler, Phys. Rev. Lett. **76**, 3947 (1996).

[6] M. L. Mehta, *Random Matrices* (Academic, New York, 1991).

[7] For reviews of chaos in quantum dots, see the articles by H. U. Baranger and by R. A. Westervelt, in *Nanotechnology*, edited by G. Timp (AIP Press, 1996).

[8] I. Kosztin, D. L. Maslov, and P. M. Goldbart, Phys. Rev. Lett. **75**, 1735 (1995).

[9] A. Altland and M. R. Zirnbauer, Phys. Rev. Lett. **76**, 3420 (1996).

[10] K. M. Frahm, P. W. Brouwer, J. A. Melsen, and C. W. J. Beenakker, Phys. Rev. Lett. **76**, 2981 (1996).

[11] C. W. J. Beenakker, Phys. Rev. Lett. **67**, 3836 (1991); **68**, 1442(E) (1992). For a review, see C. W. J. Beenakker, in *Transport Phenomena in Mesoscopic Systems*, edited by H. Fukuyama and T. Ando (Springer, Berlin, 1992).

[12] C. Mahaux and H. A. Weidenmüller, *Shell-Model Approach to Nuclear Reactions* (North-Holland, Amsterdam, 1969).

[13] A. Pandey, Ann. Phys. (N.Y.) **134**, 110 (1981).

[14] E. Brézin and A. Zee, Phys. Rev. E **49**, 2588 (1994).

[15] L. A. Pastur, Teoret. Mat. Fiz. **10**, 102 (1972) [Theoret. Math. Phys. **10**, 67 (1972)].

[16] E. Doron, U. Smilansky, and A. Frenkel, Physica D **50**, 367 (1991); E. Doron and U. Smilansky, Phys. Rev. Lett. **68**, 1255 (1992).

[17] W. Bauer and G. F. Bertsch, Phys. Rev. Lett. **65**, 2213 (1990).

[18] H. U. Baranger, R. A. Jalabert, and A. D. Stone, Chaos **3**, 665 (1993).

[19] A. Pandey and M. L. Mehta, Commun. Math. Phys. **87**, 449 (1983).

[20] O. Bohigas, M.-J. Giannoni, A. M. Ozorio de Almeida, and C. Schmit, Nonlinearity **8**, 203 (1995).

[21] K. M. Frahm and J.-L. Pichard, J. Phys. I France **5**, 847 (1995).

[22] E. Brézin and A. Zee, Phys. Rev. E **49**, 2588 (1994).

6 Coulomb blockade threshold in inhomogeneous one-dimensional arrays of tunnel junctions

6.1 Introduction

Since the pioneering work by Gorter in 1951, [1] single charge tunneling effects have been extensively studied in various kinds of geometries. [2] Research on single electronics has led to potential applications in e.g. current standards, [3,4] ultradense integrated digital electronics, [5] thermometry, [6,7] and room-temperature memory. [8] In many of these applications, tunneling occurs through a large number of junctions in series. Most theoretical work has assumed homogeneous arrays. [9–13] The problem is that the number of available states at a finite current rapidly increases with the circuit size, so that one either restricts the analysis to homogeneous arrays or adopts a numerical approach. [14] Using modern techniques, it is possible to fabricate arrays of metallic islands separated by tunnel junctions with almost uniform capacitances. It is however very difficult to avoid non-uniform background charges on the islands. This is relevant, since the charging energy is very sensitive to the background charge.

The aim of this chapter is to provide results for *inhomogeneous* one-dimensional arrays of metallic islands. The inhomogeneity can be both in the junction capacitances and in the background charges on the islands in the array. In particular, we study the threshold voltage for charge transport. The results obtained are exact within the classical (orthodox) model of single electron tunneling, [15] which is accurate when quantum size effects and macroscopic quantum tunneling effects may be ignored.

Using a general expression for the inverse capacitance matrix, we calculate in Section 6.2 the change in the free energy of an N-junction array due to an arbitrary tunneling event. In Section 6.3, we focus on the threshold voltage for transport V_t, which is an observable quantity. We find that inhomogeneity of the junction capacitances C has a small effect on the threshold voltage in large arrays: The expectation value as $N \to \infty$ for the threshold voltage of an array without gate coupling (gate capacitance $C_g = 0$ for each junction) and without background charges is $\langle V_t \rangle = \frac{1}{2} Ne \langle C^{-1} \rangle$, with $\langle C^{-1} \rangle$ being typically not much different from $1/\langle C \rangle$. However, as we show in Section 6.4, a random variation in background charges may change the threshold voltage considerably: In a short array with weak gate coupling ($N^2 C_g / 6.25C < 1$) and random charges

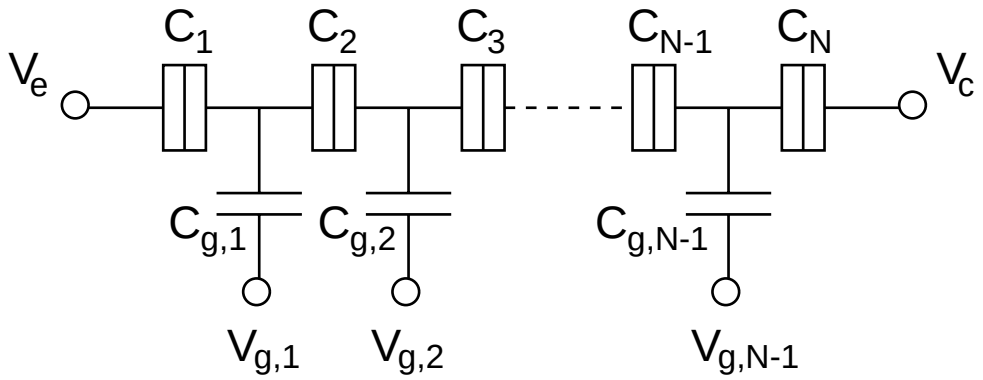

Figure 6-1. Schematic diagram of a one-dimensional array of N tunnel junctions. Island i is coupled to island $i+1$ by a tunnel barrier with capacitance C_{i+1}, and to a gate electrode by an insulating barrier with capacitance $C_{g,i}$. The capacitance C_1 (C_N) denotes the coupling of the first (last) island to the emitter (collector) electrode.

on all N islands, we find $\langle V_t \rangle \propto \sqrt{N}$. In a long array with strong gate coupling ($N^2 C_g / 6.25C \gg 1$, but still $C_g \ll C$), we find $\langle V_t \rangle \propto N$. We compare our results with experiments. [16]

6.2 Free energy

The system under consideration is shown schematically in Fig. 6.2. Within the orthodox model, the state of the system is described by the numbers n_i of electrons on the i-th island, which we combine in a vector: $\vec{n} \equiv (n_1, n_2, \ldots, n_{N-1})$. The tunneling rate, $\Gamma_k(\vec{n})$, corresponding to a single electron tunneling from island $k-1$ to island k is given by [2]

$$\Gamma_k(\vec{n}) = \frac{\Delta G_k(\vec{n})}{e^2 R_k [1 - \exp(-\Delta G_k(\vec{n})/k_B T)]}. \tag{6.2.1}$$

Here R_k is the resistance of the k-th tunnel junction and $\Delta G_k(\vec{n})$ is defined as the difference in free energy of the final and initial states. The free energy comprises the electrostatic energies of the charged capacitors in the system, as well as the potential energies of all electrodes: [9]

$$\begin{aligned} G(\vec{n}) &= \frac{1}{2}\sum_{i=1}^{N-1} C_{g,i}(\phi_i - V_{g,i})^2 + \frac{1}{2}\sum_{i=1}^{N} C_i(\phi_i - \phi_{i-1})^2 \\ &\quad - V_e Q_e - V_c Q_c - \sum_{i=1}^{N-1} V_{g,i} Q_{g,i}. \end{aligned} \tag{6.2.2}$$

We denote by ϕ_i the electrochemical potential of island i ($\phi_0 \equiv V_e$ and $\phi_N \equiv V_c$), and by Q_e, Q_c, and $Q_{g,i}$ the charges on the emitter, collector, and gates,

respectively:

$$\begin{aligned} Q_e &= C_1(V_e - \phi_1) + en_e, && (6.2.3)\\ Q_c &= C_N(V_c - \phi_{N-1}) + en_c, && (6.2.4)\\ Q_{q,i} &= C_{g,i}(V_{g,i} - \phi_i). && (6.2.5) \end{aligned}$$

Here n_e (n_c) is the number of electrons that has tunneled from the emitter (collector) electrode through the first (last) capacitor.

The difficulty in determining the energy difference $\Delta G_k(\vec{n})$ lies in the determination of the electrochemical potentials $\vec{\phi} \equiv (\phi_1, \phi_2, \ldots, \phi_{N-1})$. They follow from the condition that the total capacitive charge on each island i equals en_i plus a background charge $Q_{0,i}$:

$$\begin{aligned} &C_{g,i}(\phi_i - V_{g,i}) + C_i(\phi_i - \phi_{i-1}) + C_{i+1}(\phi_i - \phi_{i+1})\\ &= en_i + Q_{0,i}, \quad i = 1, 2, \ldots, N-1. \end{aligned} \tag{6.2.6}$$

The background charge $Q_{0,i} \in (-e/2, e/2)$ is due to incompletely screened charges in the environment of the island. Eq. (6.2.6) can be written in matrix form as $\boldsymbol{C}\vec{\phi} = \vec{Q}'$, with

$$\boldsymbol{C}_{ij} = \delta_{i,j}(C_i + C_{i+1} + C_{g,i}) - \delta_{i+1,j}C_j - \delta_{i,j+1}C_i, \tag{6.2.7}$$

$$Q_i' = en_i + Q_{0,i} + C_{g,i}V_{g,i} + \delta_{i,1}C_1V_e + \delta_{i,N-1}C_NV_c. \tag{6.2.8}$$

The capacitance matrix $\boldsymbol{C}$ can be inverted exactly. The elements $R_{i,j}$ of the inverse capacitance matrix $\boldsymbol{R} = \boldsymbol{C}^{-1}$ are given by

$$\begin{aligned} R_{i,j} &= C_{i+1}C_{i+2}\cdots C_j D_{i-1}\tilde{D}_{j+1}D_{N-1}^{-1}, \quad i \le j,\\ R_{j,i} &= R_{i,j}. && (6.2.9) \end{aligned}$$

Here we have introduced the subdeterminants D_i ($\tilde{D}_{N-i}$) of the upper left (lower right) capacitance submatrix of dimension i. These can be found recursively from

$$D_i = (C_i + C_{i+1} + C_{g,i})D_{i-1} - C_i^2 D_{i-2}, \tag{6.2.10}$$

$$\tilde{D}_i = (C_i + C_{i+1} + C_{g,i})\tilde{D}_{i+1} - C_{i+1}^2\tilde{D}_{i+2}, \tag{6.2.11}$$

$$D_0 \equiv \tilde{D}_N \equiv 1. \tag{6.2.12}$$

For a homogeneous array with identical capacitances, $C_1 = C_2 = \ldots = C_N$ and $C_{g,1} = C_{g,2} = \ldots = C_{g,N-1}$, we recover the inverse capacitance matrix of Ref. [12].

We now derive a general expression for the difference in free energy $\Delta G_k(\vec{n})$ when an electron tunnels from island $k-1$ to island k. Applying Eq. (6.2) and making use of the orthogonality relation

$$(C_i + C_{i+1} + C_{g,i})R_{i,j} = C_iR_{i-1,j} + C_{i+1}R_{i+1,j} + \delta_{i,j}, \tag{6.2.13}$$

we find that $\Delta G_k(\vec{n})$ takes the form

$$\begin{aligned}\Delta G_k(\vec{n}) &= -\frac{e^2}{2}(R_{k-1,k-1}+R_{k,k}-R_{k-1,k}-R_{k,k-1}) \\ &\quad + e\sum_{i=1}^{N-1} Q_i(R_{i,k-1}-R_{i,k}) + e(V_e - V_{g,1})A_{1,k} \\ &\quad + e\sum_{i=2}^{N-1}(V_{g,i-1}-V_{g,i})A_{i,k} + e(V_{g,N-1}-V_c)A_{N,k}, \qquad (6.2.14)\\ A_{i,k} &= C_i(R_{i-1,k}+R_{i,k-1}-R_{i-1,k-1}-R_{i,k})+\delta_{i,k}. \qquad (6.2.15)\end{aligned}$$

Here, $R_{i,N} = R_{0,i} = 0$ is implied.

Although we are now able to construct all relevant transition rates from expressions (6.2.9) and (6.2.14), the analytic evaluation of the current-voltage characteristic at arbitrary voltage remains a technically involved problem. The threshold voltage, however, is determined by a single transition rate and is therefore easier to evaluate. In the next two sections, we apply our results to this quantity for several characteristic geometries.

6.3 Threshold voltage

Electron transport through a one-dimensional array is realized by a sequence of tunneling events through all junctions between the emitter and the collector (we refer to this as a tunneling sequence). At zero temperature, a specific tunneling sequence contributes to the conductance if the free energy difference of each tunneling event in the sequence is positive. The threshold voltage V_t of the Coulomb blockade is the smallest voltage at which a current can flow through the array at zero temperature. When $|V_e - V_c| < |V_t|$, there exists no conductive tunneling sequence. We first consider the simple case where the system is not gated ($C_{g,i} = 0$ for all i), and then discuss the turnstile configuration, i.e. an array which is coupled to a gate electrode via a single island: $C_{g,i} = C_g\delta_{i,n}$.

6.3.1 No gate coupling

In the absence of gate coupling, the determinants D and $\tilde{D}$, following from Eq. (6.2), have a simple form. For convenience, we introduce the notation

$$S_k^l \equiv \sum_{i=k+1}^{l}\frac{1}{C_i}, \quad S^l \equiv S_0^l, \quad S_k \equiv S_k^N. \qquad (6.3.1)$$

In terms of these quantities,

$$D_k = C_1C_2\cdots C_{k+1}S^{k+1}, \qquad (6.3.2)$$

$$\tilde{D}_k = C_kC_{k+1}\cdots C_NS_{k-1}, \qquad (6.3.3)$$

$$R_{i,j} = S^iS_j/S^N, i \le j. \qquad (6.3.4)$$

We further define $\vec{q} \equiv \vec{n} + \vec{q}_0$, $\vec{q}_0 \equiv e^{-1}(Q_{0,1}, Q_{0,2}, \ldots, Q_{0,N-1})$. From the condition $\Delta G_k(\vec{q}) = 0$, we determine the threshold voltage $V_{t,k}(\vec{q})$ for tunneling through capacitance C_k at arbitrary occupation $\vec{q}$ of the array:

$$V_{t,k}(\vec{q}) = \frac{e}{2}\left(S^N - \frac{1}{C_k}\right) - e\sum_{i=1}^{k-1} q_i S^i + e\sum_{i=k}^{N-1} q_i S_i. \tag{6.3.5}$$

The threshold voltage is determined as follows. For an initial charge state, we determine the minimal activation energy $eV_{t,k}(\vec{q})$ to allow a tunneling event in the array, as well as the corresponding final charge state. The final charge state becomes the initial state in the next step. The minimal activation energy for the new charge state and the corresponding final charge state are again determined, and this procedure is repeated until one electron has been transported from emitter to collector. The largest of the activation energies found equals eV_t. In the special case that all background charges are zero, one has

$$V_t = \tfrac{1}{2}e\left(\sum_{i=1}^{N} 1/C_i - \mathrm{Max}[1/C_1, 1/C_2, \ldots, 1/C_N]\right), \tag{6.3.6}$$

which is an extension of the result $V_t = \frac{1}{2}e\mathrm{Min}[1/C_1, 1/C_2]$ for a double junction. [17] For $N \to \infty$, V_t has a Gaussian distribution with average $\frac{1}{2}Ne\langle C^{-1}\rangle$ and variance $\mathrm{Var}V_t = \frac{1}{4}Ne^2\mathrm{Var}C^{-1}$.

6.3.2 Turnstile configuration

We next consider a turnstile configuration, i.e. an array with a single gate electrode coupled capacitively (capacitance C_g) to island n. The elements of the inverse capacitance matrix are then given by

$$\begin{aligned}
R_{i,j} &= (S^i + C_g S^n S^i_n) S_j (S^N + C_g S^n S_n)^{-1}, \quad n \le i \le j \\
R_{i,j} &= S^i S_j (S^N + C_g S^n S_n)^{-1}, \quad i \le n \le j \\
R_{i,j} &= S^i (S_j + C_g S^n_j S_n)(S^N + C_g S^n S_n)^{-1}, \quad i \le j \le n \\
R_{j,i} &= R_{i,j}.
\end{aligned} \tag{6.3.7}$$

In order to determine the threshold voltage $V_{t,k}(\vec{q})$, we have to distinguish between $k \le n$ and $k > n$. From Eqs. (6.2.14) and (6.3.7) we find that $V_{t,k}(\vec{q})$ now depends on the gate voltage V_g: [18]

$$\begin{aligned}
V_{t,k}(\vec{q}) &= \frac{e}{2}\left(S'^N - \frac{1}{C'_k}\right) - e\sum_{i=1}^{k-1} q_i S'^i + e\sum_{i=k}^{N-1} q_i S'_i \\
&\quad + C_g[V_g - \tfrac{1}{2}(V_e + V_c)] \times \begin{cases} S_n(1 + \frac{1}{2}C_g S_n)^{-1}, & k \le n \\ -S^n(1 + \frac{1}{2}C_g S^n)^{-1}, & k > n \end{cases}
\end{aligned} \tag{6.3.8}$$

where S' is defined as in Eq. (6.3.1) in terms of modified capacitances C':

$$\begin{aligned} C'_l &= C_l(1+\tfrac{1}{2}C_gS_n)(1+C_gS_n)^{-1}, && k \le n, l \le n, \\ C'_l &= C_l(1+\tfrac{1}{2}C_gS_n), && k \le n, l > n, \\ C'_l &= C_l(1+\tfrac{1}{2}C_gS^n), && k > n, l \le n, \\ C'_l &= C_l(1+\tfrac{1}{2}C_gS^n)(1+C_gS^n)^{-1}, && k > n, l > n. \end{aligned} \tag{6.3.9}$$

6.4 Background charge

The background charge in a single-electron tunneling device has a large influence on its properties. For example, by tuning the background charge in a double junction with one gate one can set the threshold voltage to any value between zero and $e/(2C + C_g)$. In this section, we investigate the effect of background charges on the threshold voltage of an array of tunnel junctions. For reasons of clarity, we choose identical junction capacitances in the following ($C_i = C$ for all i). We start by investigating an array with a non-zero background charge on a single island. We then give ensemble-averaged results for random background charges on all islands and compare with the experiments of Delsing et al. [16]

In the absence of gate coupling ($C_{g,i} = 0$ for all i) and for a non-zero background charge $q_{0,m} = Q_{0,m}/e$ on island m, there are three initial tunneling events which may form the bottleneck for conduction:

- transfer of an electron from the emitter to the first island (electron injection through junction $k = 1$);
- tunneling through junction $k = m + 1$ if $q_{0,m} > 0$ or through junction $k = m$ if $q_{0,m} < 0$ (electron-hole creation at island m);
- transfer from the last island to the collector (hole injection through junction $k = N$).

An analysis of the corresponding tunneling sequences results in the threshold voltage

$$\begin{aligned} V_t &= \frac{e}{2C}\left(N - 1 - 2\mathrm{Min}[mq_{0,m}, (N-m)(1-q_{0,m})]\right), \\ &\quad q_{0,m} \ge 0, \end{aligned} \tag{6.4.1}$$

$$\begin{aligned} V_t &= \frac{e}{2C}\left(N - 1 - 2\mathrm{Min}[m(1-|q_{0,m}|), (N-m)|q_{0,m}|]\right), \\ &\quad q_{0,m} < 0. \end{aligned} \tag{6.4.2}$$

For a uniform distribution of $q_{0,m}$ between $\pm\frac{1}{2}$ and a uniform distribution of m between 1 and $N - 1$ its expectation value is $\langle V_t \rangle = (5N - 7)e/12C$, with variance $\mathrm{Var}V_t = (e/2C)^2(N + 1)(3N^2 - 5N + 8)/180N$. The expectation value is slightly smaller than for a homogeneous array without background charges:

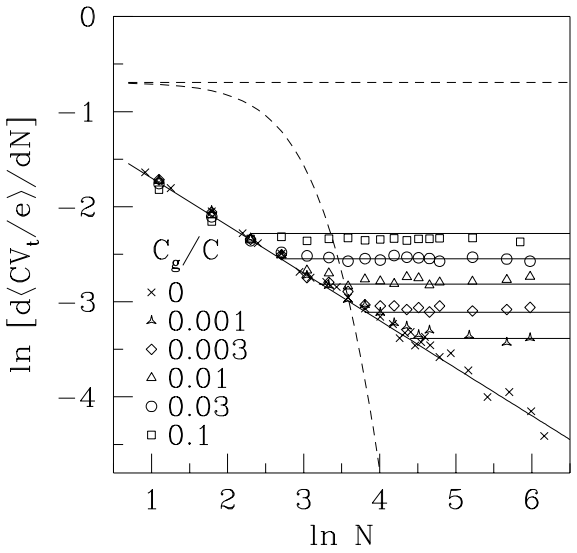

Figure 6-2. Derivative of the average threshold voltage with respect to the array length N, for ensembles of arrays with identical capacitances ($C_i = C$ and $C_{g,i} = C_g$ for all i) and random background charges on all islands, calculated from Eq. (6.4.3). The average is determined numerically from ensembles of 10000 samples for $N \leq 128$ and ensembles of 1000 samples for larger arrays. A cross-over from $\langle V_t \rangle \propto N^{1/2}$ to $\langle V_t \rangle \propto N$ occurs at $N_c \approx 2.5\sqrt{C/C_g}$. Solid lines are the extrapolation formulas (6.4.7) and (6.4.8). The dashed curves are obtained from the result (6.4.5) for zero background charges and $C_g/C = 0$ (upper curve) and $C_g/C = 0.01$ (lower curve).

$V_t = (N-1)e/2C$. In the limit $N \to \infty$ the root-mean-square deviation is $\mathrm{rms}V_t \propto Ne/C$, of the same order as the threshold voltage itself.

We next consider a one-dimensional array of equally gated islands ($C_i = C$, $C_{g,i} = C_g$ for all i). In Refs. [9] and [12] the charge transport in homogeneous arrays by soliton-like excitations was introduced. In terms of the soliton width $\lambda^{-1} = [2\mathrm{arsinh}\sqrt{C_g/4C}]^{-1}$ of Ref. [9], the threshold voltage for an electron tunneling through junction k is given by

$$\begin{aligned} V_{t,k}(\vec{q}) \;=\; \frac{e}{2C}\Bigg(& -2\sum_{i=1}^{k-1}(q_i+q_g)\sinh(i\lambda)\cosh[(N-k+\tfrac{1}{2})\lambda] \\ & +2\sum_{i=k}^{N-1}(q_i+q_g)\sinh[(N-i)\lambda]\cosh[(k-\tfrac{1}{2})\lambda] \\ & +\sinh[(N-\tfrac{1}{2})\lambda]-\cosh[(N-2k+1)\lambda]\sinh\frac{\lambda}{2}\Bigg) \end{aligned}$$

$$\left(\sinh\lambda\cosh\frac{N\lambda}{2}\cosh\frac{(N-2k+1)\lambda}{2}\right)^{-1}. \tag{6.4.3}$$

Here, the gate-induced charge $q_g \equiv C_g[V_g - \frac{1}{2}(V_e + V_c)]$ acts as an offset on the background charge. The average threshold voltage (averaged over the background charge) is therefore independent of V_g. For $N = 2$, we find

$$\langle V_t\rangle = e/(4C + 2C_g). \tag{6.4.4}$$

In the absence of background charges and for $q_g = 0$, we find

$$V_t = \frac{e}{2C}\frac{\sinh[(N-1)\lambda/2]}{\cosh(N\lambda/2)\sinh(\lambda/2)}, \tag{6.4.5}$$

which approaches a constant value as $N \to \infty$, provided $\lambda \neq 0$, i.e. provided $C_g/C \neq 0$. In Figure 6-2 we show the effect of random background charges on all islands in arrays of different lengths for several gate couplings, as calculated from Eq. (6.4.3). The averages are computed numerically by putting a random charge $q_{0,k} \in (-\frac{1}{2}, \frac{1}{2})$ on each island k. The dependence of $\langle V_t\rangle$ on the array length differs drastically from the result (6.4.5) without background charges: Instead of a threshold voltage which exponentially approaches a constant value as $N \to \infty$, we find $\langle V_t\rangle \propto \sqrt{N} - 1$ for small arrays, with a cross-over to a linear N-dependence for large arrays. For $C_g \ll C$, the array length N_c at which the cross-over occurs is found to be 2.5 times the soliton width,

$$N_c \approx 2.5\sqrt{C/C_g} \approx 2.5\lambda^{-1}. \tag{6.4.6}$$

For $N < N_c$ the average threshold voltage is well described by an extrapolation of the result (6.4.4) for $N = 2$:

$$\langle V_t^<\rangle = \frac{e}{4C + 2C_g}\frac{\sqrt{N}-1}{\sqrt{2}-1}. \tag{6.4.7}$$

For $N > N_c$ we can describe the numerical data by

$$\begin{aligned}\langle V_t^>\rangle &= \langle V_t^<\rangle_{N=N_c} + (N - N_c)\left.\frac{\mathrm{d}\langle V_t^<\rangle}{\mathrm{d}N}\right|_{N=N_c} \\ &= \frac{e}{4C + 2C_g}\frac{1}{\sqrt{2}-1}\left(\frac{N+N_c}{2\sqrt{N_c}} - 1\right).\end{aligned} \tag{6.4.8}$$

The cross-over to a linear N-dependence supports the intuitive idea that the background charge in the array is screened beyond N_c. The rms deviation $\mathrm{rms}V_t = 0.31e(\sqrt{N}-1)/(2C + C_g)$ for all N. The rms deviation of the threshold voltage for tunneling through a specific junction k has a much stronger dependence on N than $\mathrm{rms}V_t$ itself: $\mathrm{rms}V_{t,k} \propto N^{3/2}$. Since V_t is chosen as the maximal threshold voltage in a sequence of N minimal values for single tunneling events,

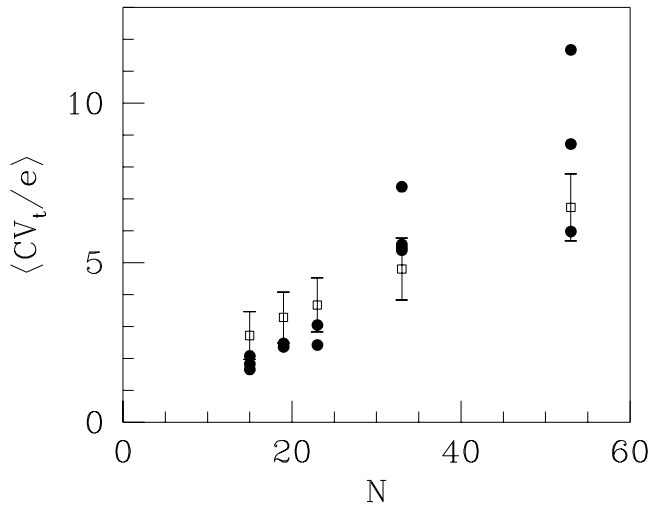

Figure 6-3. Comparison of experimental threshold voltages (taken from Ref. [16], solid dots) with the result of Eq. (6.4.3), averaged over the random background charge (open squares with error bars). We used identical gate and junction capacitances, with $C_g/C = 0.044$ ($N_c = 12$), as estimated in Ref. [16]. There are no adjustable parameters.

the fluctuations in V_t are smaller than those in $V_{t,k}$. In Figure 6-3 we compare the threshold voltage from Eq. (6.4.3), averaged over all background charges, with experimental threshold voltages for arrays of different lengths. [16] We used the values $C = 0.28$ fF and C_g=0.012 fF from Ref. [16], giving $N_c = 12$. Thus, the experimental results are in the regime of a linear dependence of $\langle V_t \rangle$ on N. The qualitative agreement is satisfactory, without any adjustable parameters.

In conclusion, we have derived an exact analytical expression for the threshold voltage $V_{t,k}(\vec{q})$ for tunneling through a junction k in a one-dimensional array of N metallic islands at arbitrary occupation $\vec{q}$ of the islands. We have calculated the average threshold voltage for transport and its fluctuations in a few simple cases. In particular, we have found that including random background charges results in a N^a dependence of $\langle V_t \rangle$, with $a = \frac{1}{2}$ for $N < 2.5\sqrt{C/C_g}$ and $a = 1$ for $N > 2.5\sqrt{C/C_g}$. We have made a comparison with the available experimental data on gated one-dimensional arrays, [16] and found a reasonable agreement.

References

[1] C. J. Gorter, Physica **17**, 777 (1951).

[2] For an introduction, see *Single Charge Tunneling*, edited by H. Grabert and M. H. Devoret (Plenum, New York, 1992); D. V. Averin and K. K. Likharev, in *Mesoscopic Phenomena in Solids*, edited by B. L. Al'tshuler, P. A. Lee, and R. A. Webb (North-Holland, Amsterdam, 1991).

[3] L. J. Geerligs, V. F. Anderegg, P. A. M. Holweg, J. E. Mooij, H. Pothier, D. Esteve, C. Urbina, and M. H. Devoret, Phys. Rev. Lett. **64**, 2691 (1990).

[4] H. Pothier, P. Lafarge, P. F. Orfila, C. Urbina, D. Esteve, and M. H. Devoret, Physica B **169**, 573 (1991); Europhys. Lett. **17**, 249 (1992).

[5] See the recent overview of A. N. Korotkov, in *Molecular Electronics*, edited by J. Jortner and M. A. Ratner (Blackwell, Oxford, to be published).

[6] J. P. Pekola, K. P. Hirvi, J. P. Kauppinen, and M. A. Paalanen, Phys. Rev. Lett. **73**, 2903 (1994).

[7] K. P. Hirvi, J. P. Kauppinen, A. N. Korotkov, M. A. Paalanen, and J. P. Pekola, Appl. Phys. Lett. **67**, 2096 (1995).

[8] K. Yano, T. Ishii, T. Hashimoto, T. Kobayashi, F. Murai, and K. Seki, IEEE Trans. Electron Devices **41**, 1628 (1994).

[9] N. S. Bakhvalov, G. S. Kazacha, K. K. Likharev, and S. I. Serdyukova, Zh. Eksp. Teor. Fiz. **95**, 1010 (1989) [Sov. Phys. JETP **68**, 581 (1989)]; Physica B **173**, 319 (1991).

[10] E. Ben-Jacob, K. Mullen, and M. Amman, Phys. Lett. A **135**, 390 (1989); M. Amman, E. Ben-Jacob, and K. Mullen, Phys. Lett. A **142**, 431 (1989).

[11] D. V. Averin, A. A. Odintsov, S. V. Vyshenskii, J. Appl. Phys. **73**, 1297 (1993).

[12] G. Y. Hu and R. F. O'Connell, Phys. Rev. B **49**, 16773 (1994).

[13] Young Bong Kang, G. Y. Hu, R. F. O'Connell, and Jai Yon Ryu, J. Appl. Phys. **80**, 1526 (1996).

[14] L. R. C. Fonseca, A. N. Korotkov, K. K. Likharev, and A. A. Odintsov, J. Appl. Phys. **78**, 3238 (1995).

[15] D. V. Averin and K. K. Likharev, J. Low Temp. Phys. **62**, 345 (1986); Zh. Eksp. Teor. Fiz. **90**, 733 (1986) [Sov. Phys. JETP **63**, 427 (1986)].

[16] P. Delsing, T. Claeson, K. K. Likharev, and L. S. Kuzmin, Phys. Rev. B **42**, 7439 (1990).

[17] M. Amman, R. Wilkins, E. Ben-Jacob, P. D. Maker, and R. C. Jaklevic, Phys. Rev. B **43**, 1146 (1991).

[18] A similar calculation for the charging energy of a single-electron memory cell has been done by K. Nakazato, R. J. Blaikie, and H. Ahmed, J. Appl. Phys. **75**, 5123 (1994).

Samenvatting

Geïnduceerde supergeleiding in microstructuren

De klassieke theorieën van mechanica en elektromagnetisme voldoen op de schaal van onze macroscopische belevingswereld prima, maar afwijkingen kunnen optreden beneden lengteschalen waarop het golfkarakter van de elektronen zich manifesteert. Zulke afwijkingen worden beschreven door de theorie van de quantummechanica. Mesoscopische fysica richt zich op systemen die zó klein zijn dat elektronen zich merkbaar als golven gedragen, met een ruimtelijke kansverdeling, een amplitude en een fase. Toch zijn de systemen nog zo groot dat een statistische beschrijving mogelijk is. Dit onderscheidt mesoscopische van microscopische systemen.

We onderzoeken in dit proefschrift transporteigenschappen van structuren die bestaan uit metalen of halfgeleiders, en onderzoeken hoe deze eigenschappen veranderen wanneer ze contact maken met supergeleiders. Deze structuren zijn ruwweg een micrometer groot. Een typisch quantummechanisch effect in zulke microstructuren is dat het geleidingsvermogen gequantiseerd is: het transport vindt plaats in modes (zoals in een golfpijp) en elke mode draagt e^2/h bij aan het geleidingsvermogen. Een tweede typisch quantummechanisch effect is tunnelen door een barrière: als een barrière hoger is dan de energie van een elektron, kan het er doorheen tunnelen. Het heeft de kans de barrière "over te slaan" en aan de andere kant te belanden. Op de schaal van macroscopische barrières als muren en deuren is dit moeilijk voorstelbaar. Een resonantie-effect kan optreden als twee tunnelbarrières na elkaar volgen: als de afstand tussen twee barrières een veelvoud is van de halve golflengte heeft het elektron een grote kans gelijk door *beide* barrières te tunnelen.

Het geleidingsvermogen is een veelvoud van e^2/h als alle modes volledig doorgelaten worden. Een mode met transmissiekans kleiner dan 1 draagt slechts gedeeltelijk bij aan het geleidingsvermogen. In een wanordelijke geleider voldoen de transmissiekansen aan een statistische verdeling. We kunnen de transmissiekansen die verdeling laten doorlopen door een variatie van externe grootheden zoals magneetveld of energie. Het blijkt dat de transmissiekansen zó fluctueren, dat de fluctuaties in het geleidingsvermogen onafhankelijk zijn van het gemiddelde geleidingsvermogen, namelijk ongeveer gelijk aan e^2/h. Om deze reden worden deze fluctuaties *universeel* genoemd. In hoofdstuk 2 van dit proefschrift beschouwen we draden die met tunnelbarrières zijn afgesloten. We berekenen de gemiddelde grootte van de fluctuaties in het geleidingsvermogen en vinden dat die slechts afhangt van de verhouding in de hoogte van beide barrières. Voor twee gelijke barrières blijken de fluctuaties twee keer zo groot

te zijn als in afwezigheid van tunnelbarrières.

Wat gebeurt er nu als we de microstructuren koppelen aan supergeleiders? In tegenstelling tot normale geleiders hebben supergeleiders geen weerstand: er kan een stroom in lopen zonder aangelegde spanning. De stroom wordt gedragen door zwak gebonden elektronparen, Cooper-paren geheten. De bindingsenergie die betaald moet worden om een Cooper-paar te ontbinden (te "exciteren") is 2Δ, ofwel Δ per elektron. In normale geleiders mogen excitaties een willekeurig kleine energie hebben, maar in een supergeleider kan een ongepaard elektron alleen voorkomen als het tenminste een excitatie-energie Δ heeft.

De overgang van een normale geleider naar een supergeleider gaat gepaard met een weerstand voor elektrische stroom. Op het eerste gezicht zou deze contactweerstand oneindig groot moeten zijn. Immers, vanwege de minimale excitatie-energie Δ voor een ongepaard elektron in de supergeleider kan bij lage spanningen geen enkel elektron de supergeleider binnendringen, hetgeen een oneindig grote weerstand inhoudt. Gelukkig bestaat er een mechanisme dat voor lage spanningen ladingstransport van een normale geleider naar een supergeleider mogelijk maakt. Aan het grensvlak wordt door toedoen van een inkomend elektron uit de normale geleider een extra elektron uit de omgeving gehaald om een Cooper-paar te kunnen vormen. Dit Cooper-paar wordt probleemloos in de supergeleider geabsorbeerd. Waar het elektron uit de omgeving werd gehaald, blijft een gat over. Net als in een Chinees schuifspelletje kan dit gat zich verplaatsen doordat steeds een elektron in een naburige toestand de lege plek opvult en zelf weer een lege plek achterlaat. Het gevormde gat keert als een echo terug in de normale geleider in de richting van waaruit het inkomende elektron kwam. Dit mechanisme heet Andreev-reflectie. Het komt in dit proefschrift veelvuldig voor.

Het voorbeeld van Andreev-reflectie toont aan dat de koppeling aan een supergeleider de eigenschappen van een normale geleider beïnvloedt. Informatie over de supergeleider wordt meegegeven aan elektronen en gaten die aan het grensvlak reflecteren, zodanig dat de supergeleiding zelf als het ware *geïnduceerd* wordt in de normale geleider. De titel van dit proefschrift verwijst naar de effecten van de koppeling tussen normale geleiders en supergeleiders in mesoscopisch kleine structuren, ofwel: geïnduceerde supergeleiding in microstructuren.

In hoofdstuk 3 koppelen we een normaal geleidende draad met daarin eenzelfde dubbele barrière als in hoofdstuk 2 aan een supergeleidende draad. De geleiding door dit systeem wordt bepaald door de kans op Andreev-reflectie. Als een inkomend elektron resonant tunnelt door beide barrières, doet het Andreev-gereflecteerde gat dat automatisch ook. Door de tunnel-barrières in hoogte van elkaar te laten verschillen neemt de transmissiekans van resonante toestanden af, terwijl die van niet-resonante toestanden toeneemt. Als we alle transmissiekansen sommeren blijkt, dat het geleidingsvermogen van een normaal geleidende draad met een dubbele barrière monotoon daalt als één van

de barrières hoger wordt gemaakt. De koppeling aan een supergeleider zorgt er echter voor, dat er een maximum optreedt als beide barrières ongeveer even hoog zijn. Dit door ons voorspelde maximum is recent waargenomen door een groep in Japan.

Als de normale geleider geen wanorde bevat, volgt het Andreev-gereflecteerd gat precies dezelfde weg als het inkomend elektron. Deze vorm van reflectie wordt wel "retro-reflectie" genoemd. Een bundel elektronen wordt dan als een perfecte echo van gaten tot in de bron weerkaatst. In hoofdstuk 4 laten we zien dat deze echo ook in aanwezigheid van verstrooiing door onzuiverheden waarneembaar blijft, alleen met een kleinere amplitude.

In hoofdstuk 5 richten we ons op het energiespectrum van een metaaldeeltje in contact met een supergeleider. De vraag is of er een laagste excitatie-energie is, net als in een supergeleider (waar de excitatiedrempel Δ is). We vinden dat er in een wanordelijk deeltje inderdaad zo'n excitatiedrempel optreedt, maar veel kleiner dan Δ. In een wanordelijk deeltje is de beweging van de elektronen chaotisch. Het blijkt dat chaotische beweging essentieel is voor de inductie van een excitatiedrempel. Dit is verrassend, omdat het energiespectrum in afwezigheid van supergeleiders hetzelfde is voor chaotische en niet-chaotische systemen.

De elektrostatische energie die nodig is om een elektron op een metaaldeeltje met capaciteit C te plaatsen is $e^2/2C$. Voor zeer kleine deeltjes met lage capaciteiten is dit een belangrijke energieschaal. In hoofdstuk 6 behandelen we transport van elektronen door een keten van kleine metaaldeeltjes. Transport door de keten vindt plaats doordat elektronen van deeltje naar deeltje tunnelen. Het transport is geblokkeerd als de aangelegde spanning te laag is om de benodigde elektrostatische energie te leveren. In hoofdstuk 6 berekenen we de drempelspanning, waarboven een stroom door de keten loopt.

List of publications

- *Prediction of a bcc structure in compressed yttrium*, Joost Melsen, J. M. Wills, Börje Johansson, and Olle Eriksson, Physical Review B **48**, 15 574-15 577 (1993).

- *Calculations of valence stabilities for the lanthanide metals*, Joost Melsen, J.M. Wills, Börje Johansson, and Olle Eriksson, Journal of Alloys and Compounds **209**, 15-24 (1994).

- *Crystallographic phase transitions in actinide metals as a function of pressure*, Olle Eriksson, J.M. Wills, Per Söderlind, Joost Melsen, R. Ahuja, A.M. Boring, and B. Johansson, Journal of Alloys and Compounds, **213/214**, 268-277 (1994).

- *Influence of pseudocore valence-band hybridization on the crystal-structure phase stabilities of transition metals under extreme compressions*, R. Ahuja, P. Söderlind, J. Trygg, J. Melsen, J.M. Wills, Börje Johansson, and Olle Eriksson, Physical Review B **50**, 14690-14693 (1994).

- *Scaling theory of conduction through a normal-superconductor microbridge*, B. Rejaei, C.W.J. Beenakker, and J.A. Melsen, Physical Review Letters **72**, 2470-2473 (1994).

- *Conductance fluctuations, weak localization, and shot noise for a ballistic constriction in a disordered wire*, C.W.J. Beenakker and J.A. Melsen, Physical Review B **50**, 2450-2457 (1994) [Chapter 2].

- *Reflectionless tunneling through a double-barrier NS-junction*, J. A. Melsen and C.W.J. Beenakker, Physica B **203**, 219-225 (1994) [Chapter 3].

- *Conductance fluctuations in a disordered double-barrier junction*, J.A. Melsen and C.W.J. Beenakker, Physical Review B **51**, 14 483-14 489 (1995) [Chapter 2].

- *Giant backscattering peak in angle-resolved Andreev reflection*, C.W.J. Beenakker, J.A. Melsen, and P.W. Brouwer, Physical Review B **51**, 13 883-13 886 (1995) [Chapter 4].

- *Effect of the coupling to a superconductor on the level statistics of a metal grain in a magnetic field*, K.M. Frahm, P.W. Brouwer, J.A. Melsen, and C.W.J. Beenakker, Physical Review Letters **76**, 2981 (1996).

- *Induced superconductivity distinguishes chaotic from integrable billiards*, J.A. Melsen, P.W. Brouwer, K.M. Frahm, and C.W.J. Beenakker, Europhys. Lett. **35**, 7 (1996) [Chapter 5].

- *Superconductor-proximity effect in chaotic and integrable billiards*, J. A. Melsen, P. W. Brouwer, K. M. Frahm, and C. W. J. Beenakker, Physica Scripta **T69**, 223-225 (1997) [Chapter 5].

- *The use of parallel arrays of ultra–small double tunnel-junctions as thermometers*, Heinz-Olaf Müller, Ulrik Hanke, K.-A. Chao, and Joost Melsen, Nanotechnology **7**, 1 (1996).

- *Coulomb blockade threshold in inhomogeneous one-dimensional arrays of tunnel junctions*, J. A. Melsen, Ulrik Hanke, H.-O. Müller, and K.-A. Chao, to be published in Phys. Rev. B [Chapter 6].

Curriculum Vitæ

Op 19 januari 1970 ben ik geboren te Ossendrecht. Van 1982 tot 1988 genoot ik voorbereidend wetenschappelijk onderwijs aan het Christelijk Gymnasium te Utrecht en het Stedelijk Gymnasium te 's Hertogenbosch. In 1988 nam ik deel aan de Nederlandse Natuurkunde- en Chemie-Olympiades. In datzelfde jaar begon ik mijn studie Technische Natuurkunde aan de Technische Universiteit Eindhoven. In juni 1989 behaalde ik de propædeuse. Tijdens mijn studie heb ik twee student-assistentschappen bekleed en deelgenomen aan een studiereis naar Japan. Tevens ben ik twee jaar student-vertegenwoordiger in de faculteitsraad geweest. Mijn afstudeeronderzoek naar cohesie-eigenschappen en kristalstructuren van zeldzame-aardmetalen heb ik verricht in de vakgroep Theorie van de Gecondenseerde Materie aan de Universiteit van Uppsala, Zweden, onder begeleiding van dr. Olle Eriksson en prof. dr. Börje Johansson. In juni 1993 slaagde ik voor het Ingenieursexamen.

In september 1993 trad ik in dienst van de Nederlandse organisatie voor Wetenschappelijk Onderzoek om als Onderzoeker in Opleiding promotieonderzoek te verrichten bij prof. dr. C. W. J. Beenakker. De belangrijkste resultaten van het onderzoek zijn beschreven in dit proefschrift. Een deel van het onderzoek is uitgevoerd in samenwerking met prof. dr. Koung-An Chao aan de Universiteit van Trondheim, Noorwegen. Mijn onderwijstaak bestond uit het geven van werkcolleges bij het college Elektromagnetisme II. Ik heb mijn onderzoeksresultaten gepresenteerd op nationale en internationale conferenties.

STELLINGEN

behorend bij het proefschrift
Induced Superconductivity in Microstructures
van Joost Melsen

1. In afwezigheid van tijdomkeersymmetrie volgt de verdeling van energieniveaus van een metaalkorrel in contact met een supergeleider uit het Laguerre ensemble van de toevalsmatrixtheorie.

   K. M. Frahm, P. W. Brouwer, J. A. Melsen en C. W. J. Beenakker, Phys. Rev. Lett. ***76****, 2981 (1996).*

2. Door matrices te kiezen volgens een parameterisatie in Eulerhoeken kan het circulaire unitaire ensemble van de toevalsmatrixtheorie worden gereproduceerd, indien de door Życzkowski en Kuś voorgestelde invariante maat $\mathrm{d}\mu$ wordt vervangen door

$$\mathrm{d}\mu = \mathrm{d}\alpha \prod_{s=1}^{N} \prod_{r=1}^{s} \mathrm{d}\chi_{1s} \mathrm{d}\psi_{rs} \mathrm{d}(\cos^{2r} \phi_{rs}).$$

   K. Życzkowski en M. Kuś, Phys. Rev. E ***53****, 319 (1996).*

3. Het is niet gerechtvaardigd om de NMR-lijnvorm in kleine metaalkorrels te identificeren met de verdeling van de lokale toestandsdichtheid.

   K. B. Efetov en V. N. Prigodin, Phys. Rev. Lett. ***70****, 1315 (1993).*

4. Het temperatuurbereik van een thermometer gebaseerd op de temperatuurafhankelijke tunnelstroom door een dubbele potentiaalbarrière kan drastisch worden vergroot door parallelle schakeling van verscheidene dubbele potentiaalbarrières met verschillende elektrostatische capaciteiten.

   H.-O. Müller, U. Hanke, K.-A. Chao en J. A. Melsen, Nanotechnology ***8****, 29 (1997).*

5. Polarisatiebijdragen tot de energie van de $4f$-elektronen, vergelijkbaar met die in atomen, verklaren de divalentie van de metalen Europium en Ytterbium in hun grondtoestand, in tegenstelling tot de trivalentie van de overige Lanthanide metalen.

   J. A. Melsen, J. M. Wills, B. Johansson en O. Eriksson, J. Alloys and Compounds ***209****, 15 (1994).*

6. Onder compressie zijn open kristalstructuren in Scandium stabiel.

   O. Eriksson, J. M. Wills, P. Söderlind, J. A. Melsen, R. Ahuja, A. M. Boring en B. Johansson, J. Alloys and Compounds ***213****, 268 (1994).*

7. De golflengte van licht geëmitteerd door Silicium nanokristallen verandert door oxidatie.

8. Parallaxmetingen door de satelliet Hipparcos aan Cepheïden maken een aanpassing van 10 % in astronomische lengteschalen noodzakelijk.

   M. W. Feast en R. M. Catchpole, Monthly Notices of the Royal Astronomical Society, ***286****, L1 (1997).*

9. Kunst is schaars.

Joost Melsen
Leiden, 18 juni 1997